CNRS
Centre National de la Recherche Scientifique

INFN
Istituto Nazionale di Fisica Nucleare

VIRGO

Real-time simulation of interferometric gravitational wave detectors involving moving mirrors

Biplab BHAWAL

Groupe VIRGO, Laboratoire de l'Accélérateur Linéaire, CNRS-IN2P3, Batiment 208, Orsay Cedex, 91405, France.

VIR-NOT-LAL-1390-070
Issue: 1
Date : 09 December; 1996

VIRGO * A joint CNRS-INFN Project
Project Office: INFN-Sezione di Pisa * Via Livornese, 1291-56010 San Piero a Grado, Pisa Italia.
Secretariat: Telephone (39) 50 880 327 or 880 352 * FAX (39) 50 880 350 * e-mail virgo@pisa.infn.it

Abstract

A method of real-time dynamical simulation for laser interferometric gravitational wave detectors and various physical effects related to these are presented here. The method is based on a digital filtering approach and is applied with success for the dynamical simulation of 2-mirror cavities (both low and high finesse), 3-mirror coupled cavity and a full length power-recycled interferometer with mirrors having longitudinal motion. The details of the simulation procedure vary in different cases and sometimes new ways are developed to perform analytical calculations describing field evolution in various coupled or uncoupled cavities. Computer experiments performed with the fast simulation code for 3-mirror cavities also establish a rule for the appearance of resonance peaks in coupled cavities. Details related to the appearance of the dynamical peaks are also investigated and the related physical points are discussed. The final analytical representation used for the fast simulation of a full length power-recycled interferometer is analogous to a 2-mirror dynamical cavity with time-dependent reflectivities, when intra-cavity fields of the interferometer are expressed together in a state-vector representation. A detailed discussion establishes relationship among physical effects pertaining to field evolution in 2-mirror cavities and coupled cavities or the full interferometer. A proposal is made for a relatively easier *start-up* procedure for a dynamical power-recycled interferometer to bring it near to the operating condition from time zero.

1 Introduction

Gravitational wave detectors based on laser interferometry are currently being developed by various collaborating groups [1, 2, 3, 4]. Some common features to the long baseline facilities (as shown in Fig.1) are these: (a) To increase the storage time of light, Fabry Perot (FP) cavities to be used in the arms, (b) To maximise signal to noise ratio, the arm length difference to be so adjusted that the output port remains on the dark fringe, (c) To reduce the shot noise, high power laser to be used, in conjunction with power recycling technique[5], in which, at a dark fringe operation, the outgoing light is recycled back into the interferometer by putting a mirror in front of the source, thus enhancing the laser power, (d) To isolate mirrors from the seismic noise, all of the six mirrors to be suspended as pendulums.

The full interferometer is thus a system of coupled cavities. In addition to maintaining the dark fringe condition, all of these cavities are to be kept on resonance with the laser source. This is a difficult job since the suspended mirrors, by getting excited by the residual seismic noise, may oscillate around their equilibrium points at low frequency with an amplitude of some tens of wavelength.

All these features provide newer dimensions to the interferometry of the gravitational wave detectors. It should be noted that the physical effects related to dynamical single or coupled cavities and interferometers have been hardly discussed in the literature because of the simple reason that prior to the time the gravitational wave detectors got conceived, people could not even imagine designing such a system for some useful purpose.

A detailed investigation of these effects is necessary for a complete understanding of the operation of interferometric detectors. At this point of time, it is, therefore, extremely important to develop numerical simulation programmes that may predict the behaviour of the detector with sufficient level of accuracy. The need of this also arises in order to evaluate and optimize parameters of different components of the interferometer. We need to know how fields at various locations of the interferometer change as the mirrors move, so that we can utilize those informations to detect any variation in the required operating condition. An automatic length control system can then be developed based on these dynamical parameters.

It is straight-forward to write a simulation programme using exact equations of field evolution, but it takes too long computational time as compared to the real time to perform its calculation and so does not come to be of much/any use for either the control system or investigation of the

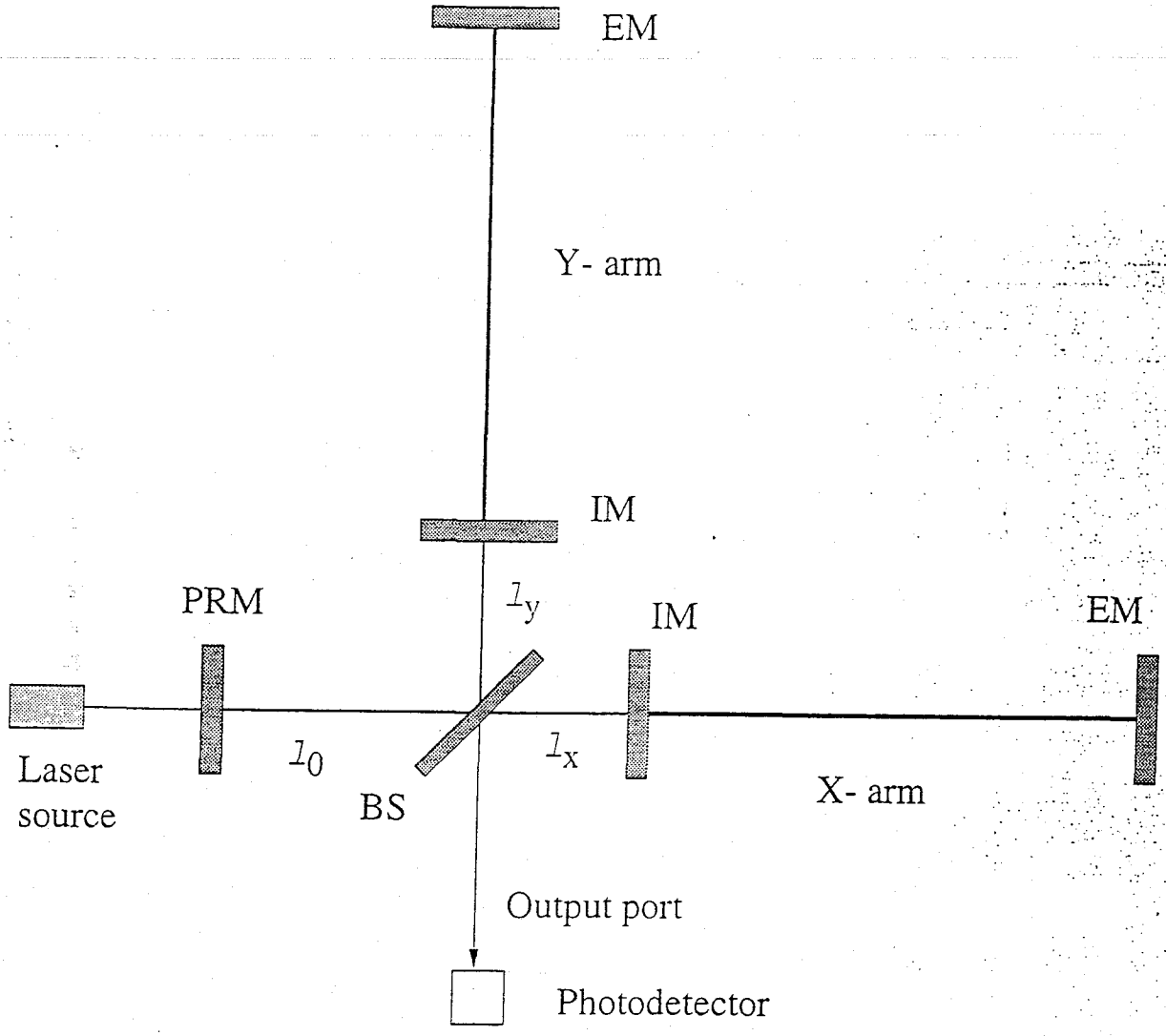

Figure 1: Configuration of a power recycled interferometer. BS - Beam Splitter EM - End Mirror, IM - Input Mirror, PRM - Power Recycling Mirror.

physical effects. This demands the requirement of fast simulation codes for a part or the whole of the interferometer which we can utilize for this purpose. If the behaviour of various servo responses can be properly ascertained, we can also compare performances of the real interferometer with the one running in computer (provided the latter is fast enough) and initiate proper action if anything goes wrong during operation. Such a complete simulation incorporating both signal generated by moving mirrors in a high finesse 2-mirror cavity and the response of the servo control system has been reported by the LIGO team[6].

With these objectives in mind, in this paper, I develop a method of dynamical simulation for a power-recycled interferometer, which is able to perform real-time calculations for various levels of accuracy. The method is based on a digital filtering approach and a number of important physical points understood by a step-by-step investigation process. This investigation finally establishes relationship among characteristics of dynamical field evolution in a long-baseline interferometer with those in 2-mirror and 3-mirror coupled cavities. Therefore, in sections 2, 3, 4, I introduce various aspects of this method and discuss the characteristics of dynamical response in low finesse 2-mirror cavity, high finesse 2-mirror cavity and a 3-mirror coupled cavity respectively. The special features of coupling between recycling cavity and arm cavity are discussed in sec. 5 with the help of the results obtained by performing computer experiments using the fast code developed for 3-mirror coupled cavity. Finally, in sec. 6, I use all the understandings arrived at through this step-by-step process along with the techniques developed thereby to write the fast numerical code for power-recycled interferometer. The physical effects related to the coupling of fields in-between two arm cavities of an interferometer are also discussed and on the basis of these points, in the same section, I propose a relatively easier method for solving the *start-up* problem of such interferometers, i.e., to bring all the coupled cavities near to the resonant condition starting from time zero. Section 7 summarizes important conclusions on the physical effects in a dynamical power-recycled interferometer as well as considerations about the computational speed of the codes developed.

2 Fast simulation of low finesse 2-mirror cavities : Digital filtering approach based on *Perturbation method*

In this section, I study the simplest case of simulation, i.e., that of a 2-mirror cavity of low finesse. Such a cavity of finesse about 50 will be used in the arms of the VIRGO interferometer. We may note in advance that a direct analogy can be established between the response of a power-recycled interferometer and that of a 2-mirror cavity under general dynamical conditions, as will be shown in sec.6. The dynamical response may show low or high finesse characteristics depending on the operating condition of a light beam. Results of the investigation in this section are, therefore, very important and will be applied in writing the simulation programme of the whole interferometer in sec.6.

An analogy is established here between a digital filter and the linear response of a cavity towards small motion of mirrors. A fast simulation procedure based on this is developed thereafter [7]. The analytical calculation presented here for the response of a low finesse cavity is based on the perturbative technique. I investigate how well such a perturbative calculation can describe the evolution of fields when used in the fast dynamical simulation procedure based on digital filtering approach (DFA). The numerical results and comparison with other methods are also presented.

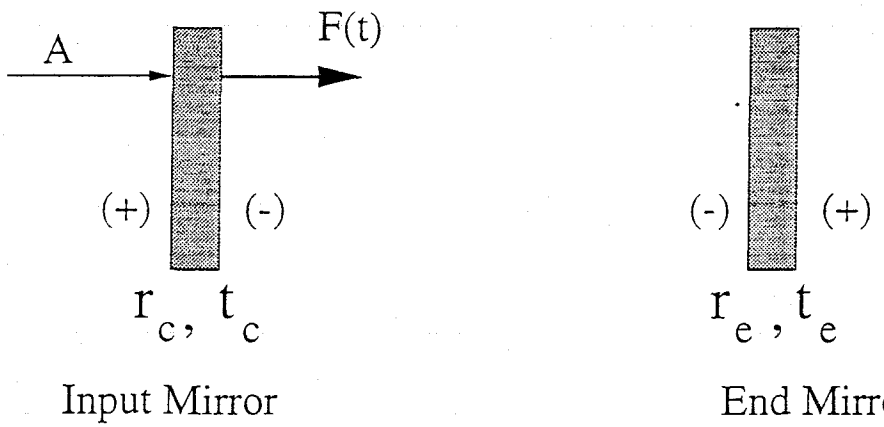

Figure 2: Notation for a 2-mirror cavity; r_c (r_e) and t_c (t_e) are amplitude reflectivity and transmittivity respectively for the input (end) mirror. The sign (+) or (−) indicates the phase acquired on reflection from that side of the mirror.

2.1 Cavity linearized equation

Let us first write down the exact equation for the intra-cavity field, F based on the notation of Fig.2 by taking the laser source to be the reference point for the motion of the mirrors:

$$F(t) = t_c A \exp j[\frac{2\pi}{\lambda} x_c(t)] + r_c r_e \exp j[\theta(t-\tau/2)] F(t-\tau), \quad (1)$$

where $\tau = 2L/c = 2 \times 10^{-5}$ sec. is the round-trip time for VIRGO 3-Km cavities and λ is the wavelength of the laser light, 1.064μmeter: t_c is the amplitude transmittivity of the input mirror, whereas r_c and r_e are the amplitude-reflectivities of the input and end mirror respectively. The quantity, $\theta(t)$ represents round-trip phase offset in the cavity at any time t:

$$\theta(t-\tau/2) = \phi + \frac{2\pi}{\lambda} 2x(t-\tau/2), \quad (2)$$

where ϕ is the initial (comnstant) round-trip phase offset and $x(t-\tau/2)$ is variation in the length of the cavity as experienced by the light at time t due to the movement of the mirrors:

$$2x(t-\tau/2) = -x_c(t-\tau) + 2x_e(t-\tau/2) - x_c(t), \quad (3)$$

where $x_c(t)$ and $x_e(t)$ are displacements of the input and the end mirror respectively.

If we assume that both the variation. $x(t)$ of the length, L of the cavity and the frequency of such variation are small enough, we can reasonably predict that the field amplitudes will also vary slowly around some stationary point (an elaborate and nicer treatment can be found in Ref.[8]). The Eq.(1) can, therefore, be written in the following form for small x :

$$F(t) = t_1 A \exp j[\frac{2\pi}{\lambda} x_c(t)] + R[1 + j\frac{2\pi}{\lambda} 2x(t-\frac{\tau}{2})] F(t-\tau), \quad (4)$$

where

$$R = r_c r_e \exp j[\phi]. \quad (5)$$

Note that we make a simplifying assumption that the input light, A is constant. The stationary point of the intracavity field can thus be written from the zeroth order equation:

$$F_0 = \frac{t_c A}{1-R}. \quad (6)$$

which just represents the quasi-static field, i.e., when mirrors do not move at all or moves so slowly that it does not affect anything for a long time. The variation of the intra-cavity light from this can be obtained from the first order equation:

$$\delta F(t) = R[\delta F(t-\tau) + j\frac{4\pi}{\lambda}F_0 x(t-\frac{\tau}{2})]. \tag{7}$$

This leads to the following transfer function for the cavity in the s-domain of the Laplace transformation:

$$H_c(s) = \frac{\delta F(s)}{x(s)} = jPF_0\frac{\exp(-\frac{\tau}{2}s)}{1-R\exp(-\tau s)}x(s), \tag{8}$$

where

$$P = (\frac{2\pi}{\lambda})R. \tag{9}$$

The Eq.(8), as such, is not of much use for the time domain simulation, since we need to know $x(t)$ in the full time domain ($t \to +\infty$) for the calculation of $\delta B(s)$. However, as is discussed in the next subsection, the technique of digital filtering can be appropriately applied to take advantage of the linear equation (7) with the objective of developing a fast computational method for the variation in the intracavity light.

2.2 Cavity as a digital filter

A number of standard texts [9, 10] on digital filters are available. However, it is worthwhile introducing a few important concepts here to understand the domain of validity of the analogy between a cavity and a digital filter, which I am going to describe.

Let us consider a transfer function of the following form corresponding to the input, X and output, Y in the s-domain :

$$H(s) = \frac{Y(s)}{X(s)} = \frac{\sum_{k=0}^{K} C_k \exp(-ks\Delta)}{1-\sum_{m=1}^{M} D_m \exp(-ms\Delta)}, \tag{10}$$

where k and m are integers and Δ is some fixed time interval.

The correspondence between this transfer function and its own discrete form in the Z-transform domain can be established by a conformal transformation, $z = \exp(s\Delta)$:

$$\bar{H}(n) = \frac{\bar{Y}(n)}{\bar{X}(n)} = \frac{\sum_{k=0}^{K} C_k z^{-k}}{1-\sum_{m=1}^{M} D_m z^{-m}}. \tag{11}$$

where n represents the sampled points with a time period, Δ.

So, one can now arrive at the following equation describing the output function in its discrete form :

$$\bar{Y}(n) = \sum_{k=0}^{K} C_k \bar{X}(n-k) + \sum_{m=2}^{M} D_m \bar{Y}(n-m). \tag{12}$$

This is known as the *infinite impulse response* (IIR) filter which is actually a series of feedback loops as is obvious from the equation above.

Let us now look back at Eq.(7) and compare it with Eqs.(11,12). We can easily see that Eq.(7), as such, can provide only two nonzero coefficients ($C_1 = PB_0$ and $D_2 = re^{j\phi}$) for the evaluation of

the output,i.e., the variation in the intracavity light, δB in the discrete time domain with a sampling period of $\tau/2$. However, if we wish, we can always increase the number of the coefficients, C_k simply by explicitly evolving the recursive relation, Eq.(7), in N steps for time $N\tau$. In optical language, this is equivalent to tracing the path of the light for N number of bounces on the moving end-mirror.

It should be noted that such a procedure, however, does not increase the number of nonzero D_m coefficients and, in fact, reduces the numerical importance of the only available coefficient (which is D_m for $m = 2n$ at any stage, n) at every step of this evolution by a factor R. So, if we are able to take a sufficiently large value of N, we can reasonably neglect the contribution of previous outputs in the present value of the output in a low finesse cavity. Such a filter which does not receive any input in the form of a feedback is called *finite impulse response* (FIR) filter and for such filters, the coefficients, C_k represent the unity impulse response of the filter. It should be noted that by going through this step, the concept of the cavity as a filter got converted from an IIR one to a FIR one.

In the context of a two-mirror cavity, we can thus write down the following equation for the intra-cavity light directly from Eq.(7):

$$F(t + N\tau) = \frac{t_1 A \exp j[x_c(t)]}{1 - R}(1 + jP \ \text{Sum}) \tag{13}$$

where

$$\text{Sum} = \sum_{n=1}^{N} R^{N-n} x(t + (n - \frac{1}{2})\tau). \tag{14}$$

The structure of the correction term shows that it is nothing but the time-convolution of the input, $x(n)$ with the unity-impulse response-function represented by the coefficients,

$$C_k = jPF_0R^{k-1}, \quad \text{where} \quad k = 1, 2, 3, \ldots \tag{15}$$

Before we go to the next section we should keep in mind that the usefulness of the analysis presented here depends strongly on the validity of the assumption that the mirror movement is very slow which enables us to use the linear equation for the cavity. So, the validity of the analysis depends on how we make a suitable choice for the number of bounces, N. The value of N is to be ascertained numerically in the next subsection by taking error considerations into account.

2.3 Simulation and results

The numerical investigation shows that the phase factor which depends on $x_c(t)$ in Eq.(13) has almost no influence on the evolution of fields in a low finesse cavity (note that it will not be so in the next section, when we discuss about high finesse cavities). So, while developing the following simulation technique, we can safely ignore this factor. This also means that for a low finesse cavity, it does not matter whether we take the laser source or the input mirror to be our reference point of mirror motion, provided the speed of the input mirror is of the order of 1 μm/sec or less than that.

The procedure of the numerical simulation is as follows:

- **step 1**: Time is sliced into equal intervals of width $\Delta = N\tau$, so that any time $t_i = iN\tau$, where i is an integer.

- **step 2**: The phase, ϕ is fixed to the following value during any time interval (t_i, t_{i+1})

$$\phi_i = \phi_0 + \frac{4\pi}{\lambda} x(i\Delta). \tag{16}$$

where ϕ_0 is a small initial phase offset at time $t = 0$.

•**step 3**: During the time interval (t_i, t_{i+1}), the rate of change of the cavity length is also assumed to be constant

$$w_i = \frac{x_{i+1} - x_i}{N\tau} \tag{17}$$

This is a valid assumption, as long as the frequency of mirror oscillation is small and we choose a reasonable value of N. For example, for a frequency of, say, 200mHz, we can reasonably talk about a value of N up to, say, 200 without making much error.

•**step 4**: The assumption in step 3 enables us to arrive at a very simple expression for the convolution-sum in Eq.(13). This sum now turns out to be an *arithmetico-geometric* series which can be easily converted into its compact form [11]. So,

$$\text{Sum} = \frac{(N - \frac{1}{2}) - (N + \frac{1}{2}) r_e r_c \exp j[\phi_i]}{(1 - r_c r_e \exp j[\phi_i])^2} w_i \tau + \mathcal{O}(R^N) \tag{18}$$

The $\mathcal{O}(R^N)$ terms can be neglected for sufficiently large values of N.

•**step 5**: Substituting $i \leftarrow i + 1$, the same procedure is repeated again,i.e., the values of ϕ_i and w_i are changed in the next step and B_{i+1} is calculated.

As one can see, this method makes a slope-by-slope approximation of the actual mirror movement, where each slope (velocity, w_i) lasts for a short time. The span of this short time (represented by N) can be decided by numerical investigation of the error level introduced by slope-by-slope approximation.

The above method based on a digital filtering approach (DFA) can now be compared with other methods[12] of simulation which have been tried in order to get a fast simulation of low-finesse cavity: (a) *the sequential method* (SM), which computes the intracavity beam at each round-trip and so is accurate but very slow, (b) *the quasi-static method* (QSM) that just computes a stationary value from the cavity Airy function (Eq.6) for the intracavity light on the assumption of constancy of all quantites over a sufficiently long time and thus its error is independent of the time-step used in the computation, (c) *the differential equation method* (DEM) [12] which under the assumption of constancy of x (and thus of the phase offset) over an interval $\Delta = N\tau$, solves the cavity differential equation in that interval, sets the initial condition for the next step with that solution, changes the phase by another step and solves the differential equation again. As a result, for smaller values of N, the DEM approaches the accurate SM and for higher values of N, it approaches the QSM.

An important difference between the DEM method and the present method is that while the former makes a step-by-step approximation (i.e. x is constant over the interval Δ) for the mirror displacement, $x(t)$, the present method takes a slope-by-slope approach (i.e., x changes with constant velocity during Δ) for the same. As a result, a comparison between either DEM or QSM and the present method can only be made for small values of N. For large values of N, such a comparison is meaningless since, in that case, only in the limit $w \to 0$, the present method can be expected to be similar to either QSM or DEM.

The simulation program as described in the last section is run for two values of mirror velocity (which, for the sake of simplicity, has been assumed to be constant throughout the time of simulation), 1μm/sec and 0.5μm/sec. The values of r_c and r_e are chosen to be 94.0% and 99.99% respectively, which corresponds to a finesse of approximately 50[2]. A power-loss of 10 ppm has been considered for both mirrors.

A typical resonance curve generated by the exact SM method for such a cavity with $w = 1\mu$m/sec is shown in Fig.3. The resonance curve generated by either QSM or DFA method under similar

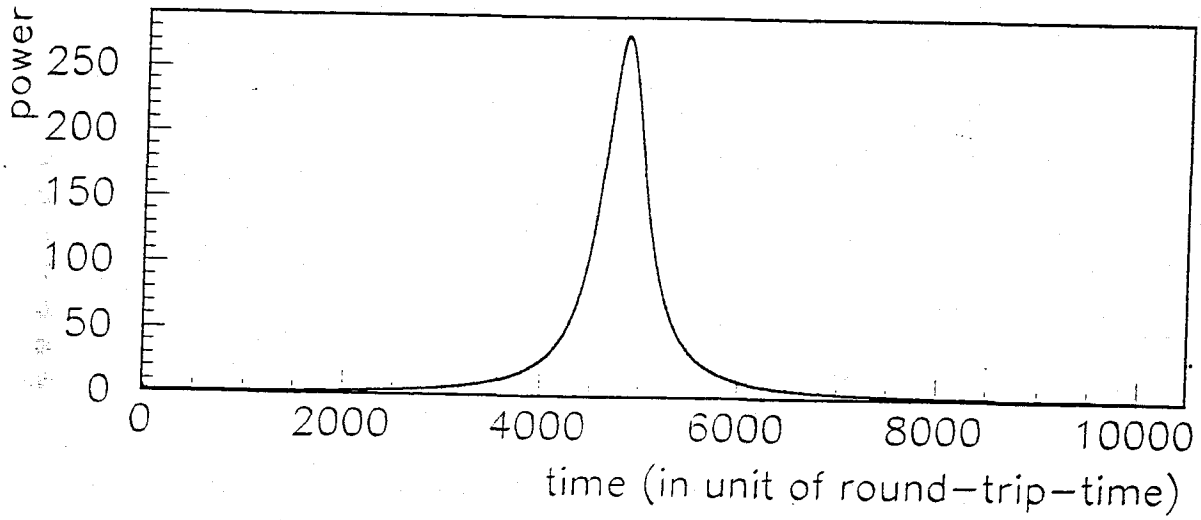

Figure 3: A typical resonance curve for a low finesse cavity that can be drawn by using SM or QSM or DEM or DFA method (with reasonable values of N in the last two cases), while the cavity length changes at a rate $w = 1\mu$m/sec. Input power, $|A|^2$ is assumed to be one unit. Note that the resolution of the plot can not make difference among curves obtained from these methods. The error levels of QSM and DFA are shown in the next figure.

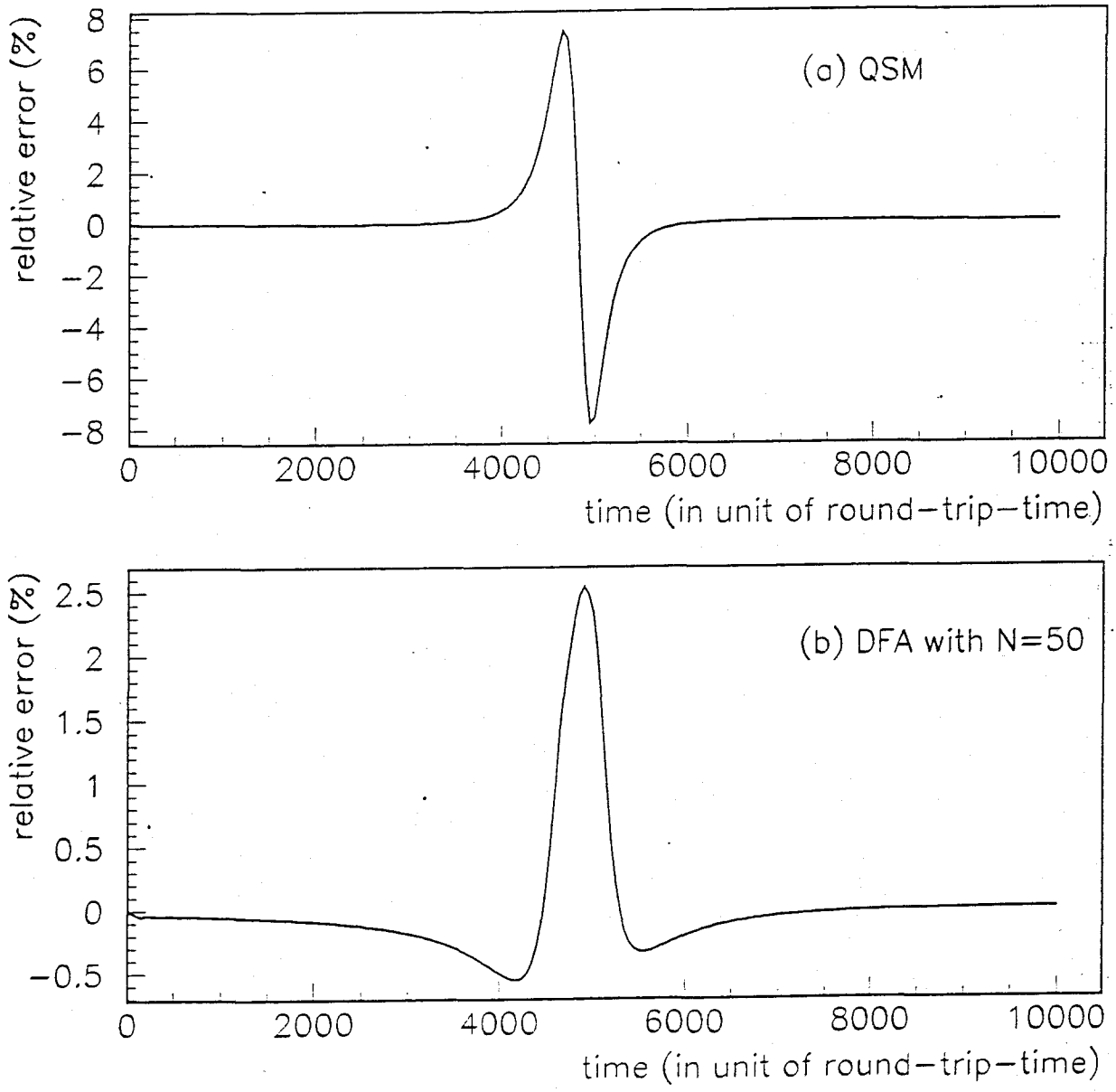

Figure 4: Relative error (%) of (a) QSM and (b) DFA based on perturbative calculation as compared to the exact SM in computing the resonance curve of Fig.3. Note that the error level of QSM is independent of the choice of the number of steps, N (provided N is not so large that the sampling of values becomes meaningless).

conditions looks to be similar to the above curve, but any of these methods actually makes some error (wrt the SM), which remains to be invisible by the resolution of the plot.

The 'relative error' made by either QSM or DFA with respect to (wrt) the accurate SM method in drawing the same resonance curve is plotted in Fig.4. The *relative error of some method Y wrt some other method X*, is defined as follows:

$$\text{Relative error}(\%) \;=\; \frac{\text{value predicted by Y} - \text{value given by X}}{\text{value given by X}} \times 100. \qquad (19)$$

The nature of the error curve for DFA as shown in Fig.4(b) is more or less similar for various values of N and w, but is quite different from those for either QSM (Fig.4a) or DEM. The error curves generated by QSM and DEM are similar looking, but the level of error is less in DEM as compared to QSM[12]).

The maximum values of the error curves of the DFA as a function of N have been plotted in Fig.5. One can see that the simulation performs quite satisfactorily even for large values of N (= say 60 for $w = 1\mu$m/sec or say 100 for $w = 0.5\mu$m/sec, if we take an arbitrary value of about 4% to be an upper limit). I neglected $\mathcal{O}(r^N)$ terms in Eq.(18) for simulation and thus for sufficiently low value of N, the maximum value of error increases again, as can be seen in Fig.5.

The relative error increases not only for higher values of N and/or mirror-velocity, but also for higher values of the cavity finesse. The finesse of a cavity can as well be expressed by the product of the amplitude-reflectivities of the two mirrors. Since we always keep the value of r_e equal to a constant, 99.99%, from now onwards I always refer to the finesse of a cavity in terms of the reflectivity of the input mirror, r_c.

Now we fix $N = 50$ and tabulate the maximum values of error curves generated by DFA for increasing values of r_c in Table 1. As we can see, the error increases too fast just after crossing the value $r_c = 0.975$. A validity domain for this method based on perturbative calculations may be ascertained in terms of an upper limit of about 0.975 on r_c for a mirror velocity of ≤ 1 μmeter/sec; This limit, however, depends on what trade-off one would like to make between computational speed and error in its application and should be mentioned in that spirit. But whatever be the trade-off, the perturbative calculation of cavity response is certainly not applicable in the digital filtering approach of fast simulation for a value of finesse corresponding to $r_c \geq 0.99$. So, we need to replace the perturbative calculation by some other method in the framework of the digital filtering approach of fast simulation when we intend to apply the same to high finesse cavities.

From now onwards, we refer to cavities with $r_c \leq 0.975$ as *low finesse cavities* and those with $r_c \geq 0.985$ as *high finesse cavities*. The cavities with $0.975 < r_c < 0.985$ correspond to the intermediate range for which a perturbative approach of simulation leads to too much of error for high values of mirror velocities (i.e.$\approx$ 1 μm/sec.), but, on the other hand, for which the high-finesse characteristics of the cavity response (as I discuss in the next section) are not so prominent. In any case, the fast simulation methods to be developed in the next section for high finesse cavities can always be applied to lower finesse cavities. I am making this division in the range of finesse just to make a clear-cut distinction between the high finesse and low finesse characteristics, which 1allows us a convenient basis of our discussion.

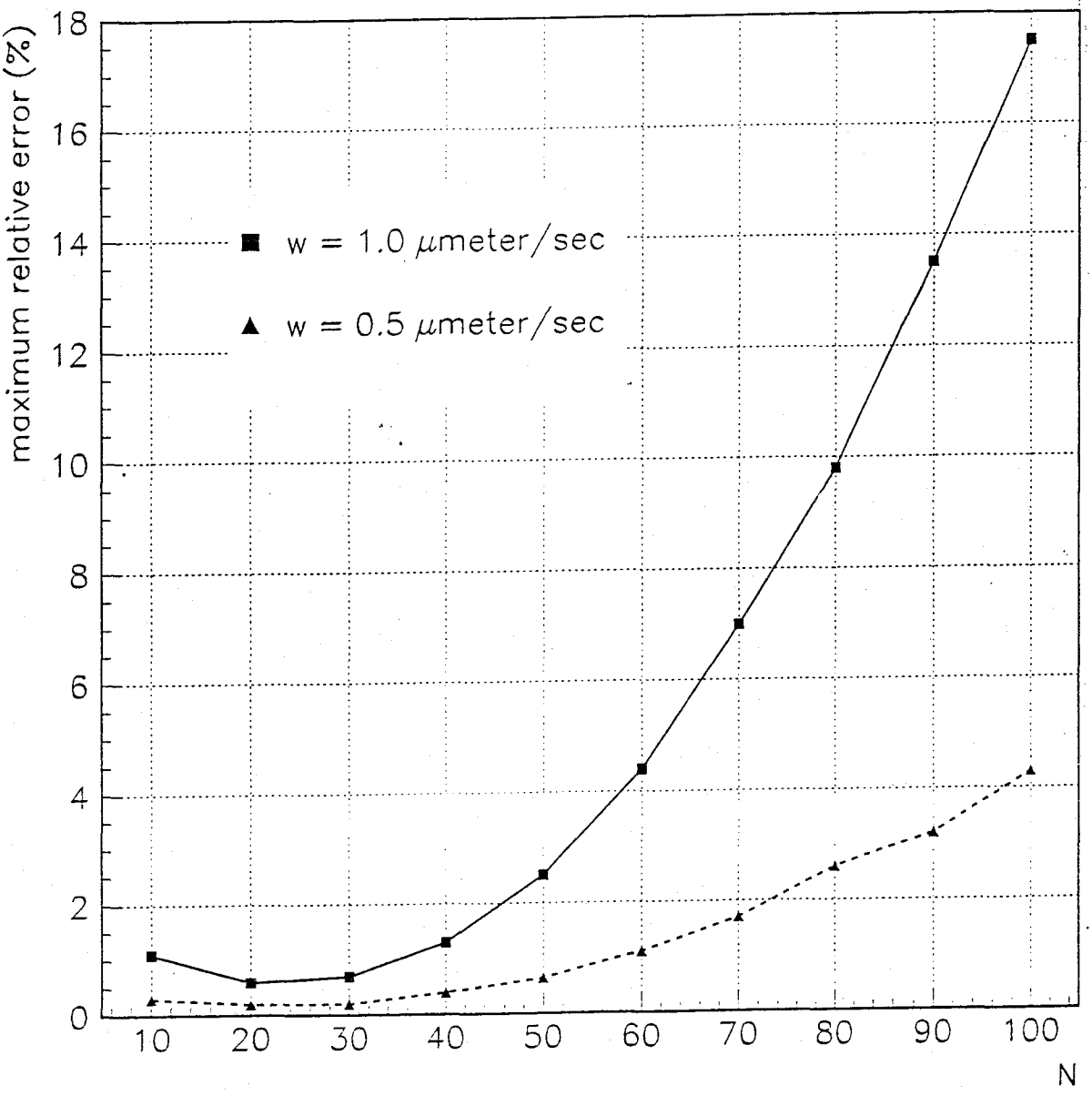

Figure 5: Maximum values of the relative error (%) of DFA based on perturbative calculation as compared to the exact SM (in computing the resonance curve of Fig.3) is plotted against N, the number of steps for two rates of change in the cavity length.

Table 1: Approximate values of the peaks of the relative error curves for cavities with various values of the finesse, keeping N fixed to 50. Note that for $r_c > 0.96$, the error curves are characterised by lot of oscillations, but one can always find a maximum value of the error near the resonance point. This table shows how DFA based on perturbative calculation breaks down for high values of finesse.

r_c	Max. rel. error(%) ($v = 0.5\mu$m/s)	Max. rel. error(%) ($v = 1\mu$m/s)
0.94	0.65	2.5
0.95	0.80	3.2
0.96	1.0	4.2
0.97	2.0	8.0
0.975	4.0	14.5
0.98	10.0	32.0
0.985	30.0	90.0
0.99	175.0	325.0

3 Simulation of High finesse 2-mirror cavities : Digital filtering approach based on *Jump-and-Sump method*

We may note again in advance that there exists a direct analogy between the dynamical response of a power-recycled interferometer and that of a 2-mirror cavity. We will also see in sec.6 that most of the time in a general dynamical situation and especially at the desired operating condition of the laser light, the response of the interferometer shows high finesse characteristics.

In the last section, we found that the perturbative calculation of cavity response, when utilized in DFA method of fast simulation, fails to describe the evolution of the fields as we increase the finesse of the cavity. This just indicates that the perturbative approach of performing cavity calculations is not suitable for describing the enhanced sensitivity of the high finesse dynamical cavities towards small perturbations in the form of mirror movement. In this section, I introduce a method[13] replacing the perturbative calculation in the framework of DFA and apply the same for the simulation of high finesse 2-mirror cavities.

The enhanced sensitivity of the cavity in its dynamical response to the mirror movement can be illustrated here by drawing a resonance curve for the intra-cavity field by using the Eq.(1) of the SM method in Fig.6(a) when only the end mirror moves at a speed 1μm/sec. The value of r_c is chosen to be 0.998733 (A question like 'why such a value' will get answered in section IV where we will see that this choice will cut short the number of figures of this paper).

When the mirror movement is very slow or zero, the corresponding resonance curve, as generated by QSM method is shown in Fig.6(b). A comparison of Figures 6(a) and 6(b) and all those generated for the low finesse cavity in section2 brings forth certain special characteristics of the dynamical response of high finesse cavities:

(a) *Failure to achieve maximum peak value :* One can see that the peak value of the dynamical curve fails to reach the maximum value of power (the quasi-static value, Fig.6b) that can be achieved on resonance from such a system. The reason is the fast motion of mirror which does not allow partial beams to stick to the resonance or near-resonance value for a long time.

(b) *Displacement of the peak from the resonance point :* The peak value of the dynamical resonance

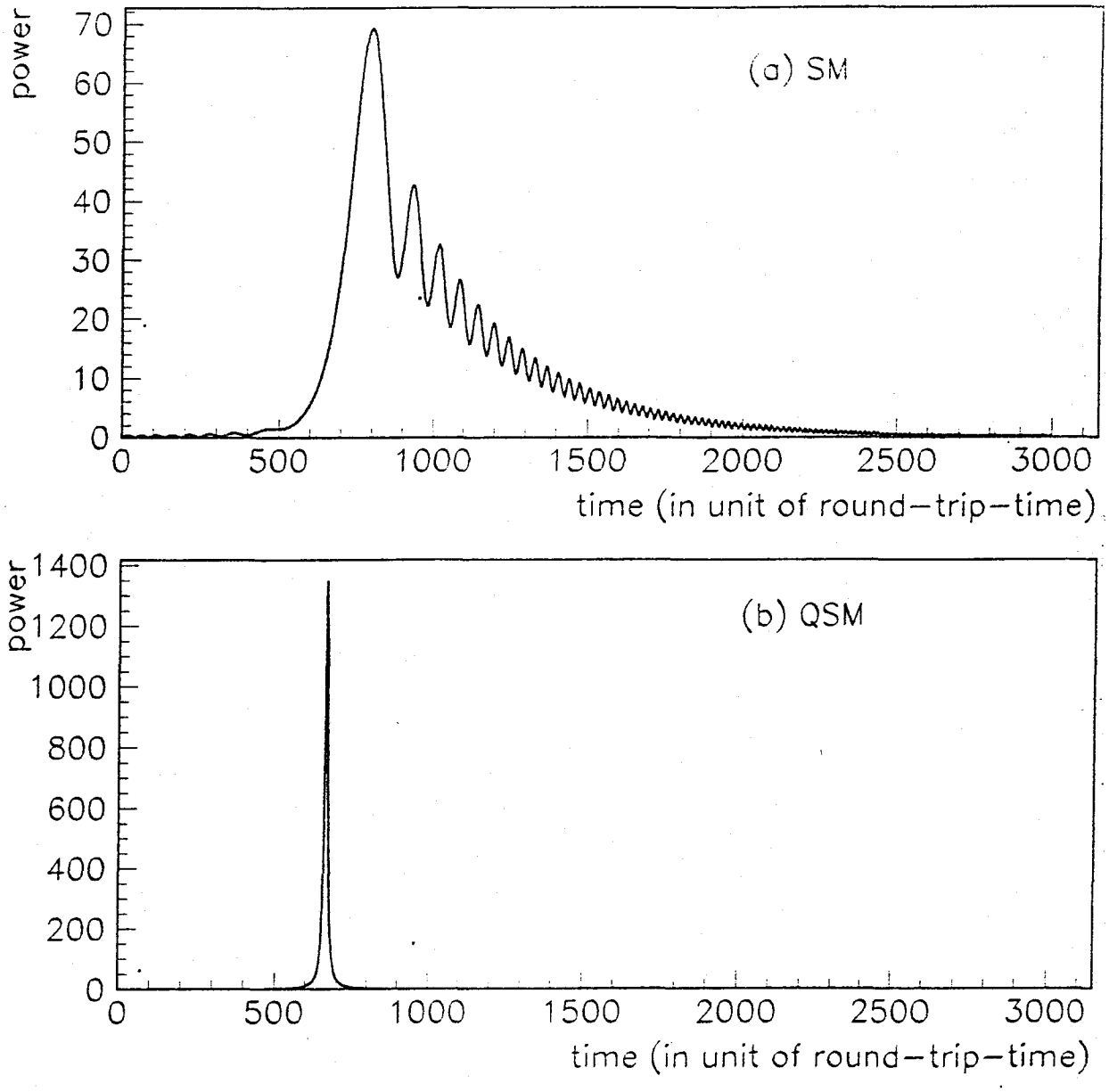

Figure 6: (a) Dynamical resonance curve for a high finesse ($r_c = 0.998733$) 2-mirror cavity while only the end mirror moves and so the cavity length changes at a rate of $w = 1\mu$m/sec. Input power is assumed to be one unit. (b) Quasi-static resonance curve for the same cavity.

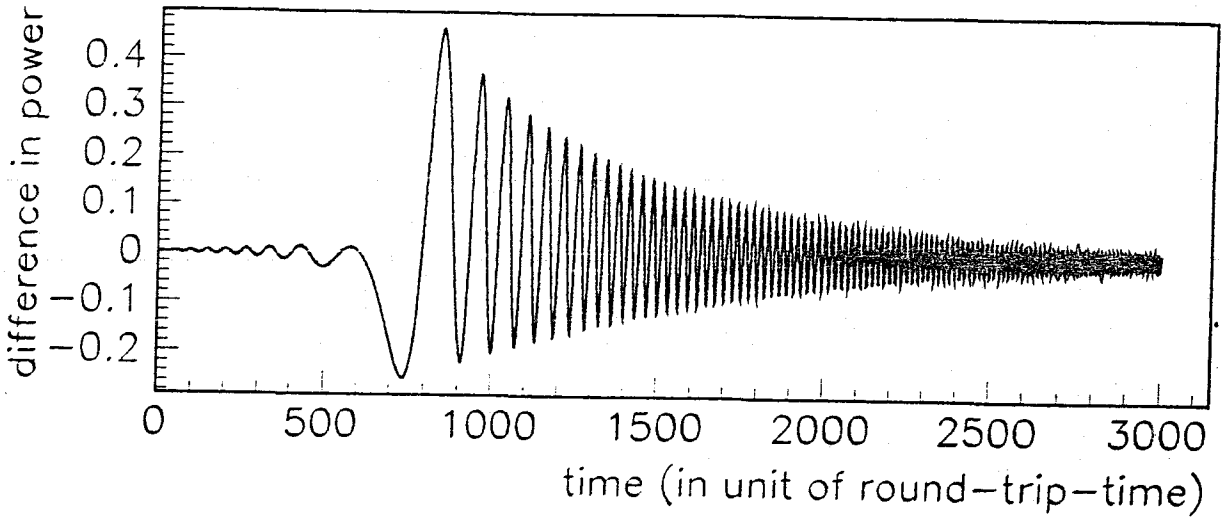

Figure 7: Difference in power between the case when the input mirror moves (at a speed of 1μm/sec) and when it does not, but the rate of change in cavity length, w is same in both cases (= 1μm/sec). The latter case corresponds to Fig. 6(a).

curve appears a few round-trips after the actual point of resonance (i.e., $\theta = 2\pi$). Due to high finesse, a large number of partial beams get stored for a long time, each of them bearing different phase information about the moving cavity and a combination of all these beams find a maximum point of their combined power at a point somewhat displaced in time from their quasistatic resonance point.

(c) *Oscillations after crossing the peak :* The oscillation of power just after crossing the peak is due to the generation of beats by the interference of the Doppler-shifted beams which were there for long time (as a result of high finesse) and those beams which are relatively newcomers. The frequency of this oscillation increases for a short time and then again decreases down to zero as the interferometer goes farther away from resonance and the contribution of long-lasting beams becomes less and less (the last point can be shown in a frequency-domain simulation. It will also be evident when we'll study the relative error in the resonance curves generated by some non-exact equations at the end of this section).

(d) *Enhanced sensitivity towards the movement of the input mirror :* Unlike in the low finesse case, the field evolution now gets affected by the Doppler shift that is experienced by the input light wrt source due to the movement of the input mirror. Fig. 7 shows the difference in power of the field, F between a case when both mirrors move and when only the end mirror moves, but the rate of change of the cavity length, w is kept to be same (= 1μm/sec) in both cases. The resonance curve corresponding to the latter case is already shown in Fig.6(a). The numerical investigation and Fig. 7 show that if the mirror velocity is restricted to $\leq$ 1μm/sec, there will be little and insignificant effect on the field evolution near resonance. We can, thus, neglect this phase factor in the input light again for the case of high finesse cavities without committing much error.

To describe this enhanced sensitivity with a faster simulation, the following analytical calculation is incorporated in DFA method of fast simulation, replacing the perturbative method :

step 1 : Let us start with the following equation of the intra-cavity field,F :

$$F(t+\tau) = t_c A + R \exp j[\frac{4\pi}{\lambda} x(t+\tau/2) F(t) \tag{20}$$

written for a small variation x in the length of the cavity. This equation is then recursively evolved in time for N steps, where one step is equivalent to the round-trip time, τ of the cavity and thus obtain:

$$F(t+N\tau) = t_c A[1 + \sum_{n=2}^{N} R^{n-1} \prod_{k=N-n+2}^{N} \exp_k] + F(t) R^N \prod_{k=1}^{N} \exp_k, \tag{21}$$

where

$$\exp_k = \exp[j\frac{4\pi}{\lambda} x_k], \tag{22}$$

and

$$x_k \equiv x(t + (k-1/2)\tau) \tag{23}$$

and is described by Eq.3.

step 2 : Let us assume that for a reasonable number of steps, N, the mirror motion can be approximated by a constant velocity,v, which enables me to write Eq.(22) as

$$\exp_k = \exp[\xi(k-1/2)] \tag{24}$$

where $\xi = j4\pi v\tau/\lambda$.

step 3 : It is also assumed that the mirror displacement that takes place within the interval $N\tau$ is very small, so that I can linearize all the exponentials in Eq.(21), thus obtaining

$$F(t+N\tau) = \frac{t_c A(1-R^N)}{1-R} + t_c A \xi R \sum_{i=1}^{N-1} R^{i-1} \sum_{k=N-i-1}^{N} (k - \frac{1}{2}) + F(t) R^N \exp[\xi \frac{N^2}{2}] \tag{25}$$

Note that the first and third terms in the above equation have been obtained by summing the series (geometric in the first term and arithmatic in the second term) of terms in Eq.(21). In fact the series in the second term in the above equation can also be shown to be a combination of an *arithmetico-geometric series* [11] and an arithmetic series:

$$\frac{t_c A \xi R}{1-R} \sum_{k=2}^{N} (k - \frac{1}{2}) R^{N-k} - \frac{t_c A \xi R^N}{1-R} \sum_{k=2}^{N} (k - \frac{1}{2}) \tag{26}$$

Both these series can be summed over easily, so that the final equation can be written down as

$$F(t+N\tau) = \frac{t_c A(1-R^N)}{1-R} - \frac{t_c A \xi R}{1-R} S - \frac{t_c A \xi R^N}{2(1-R)}(N^2 - 1) + F(t) R^N \exp[\xi \frac{1}{2}] \tag{27}$$

where

$$S = \frac{N - 0.5 - 1.5R^{N-1}}{1-R} - \frac{R - R^{N-1}}{(1-R)^2} \tag{28}$$

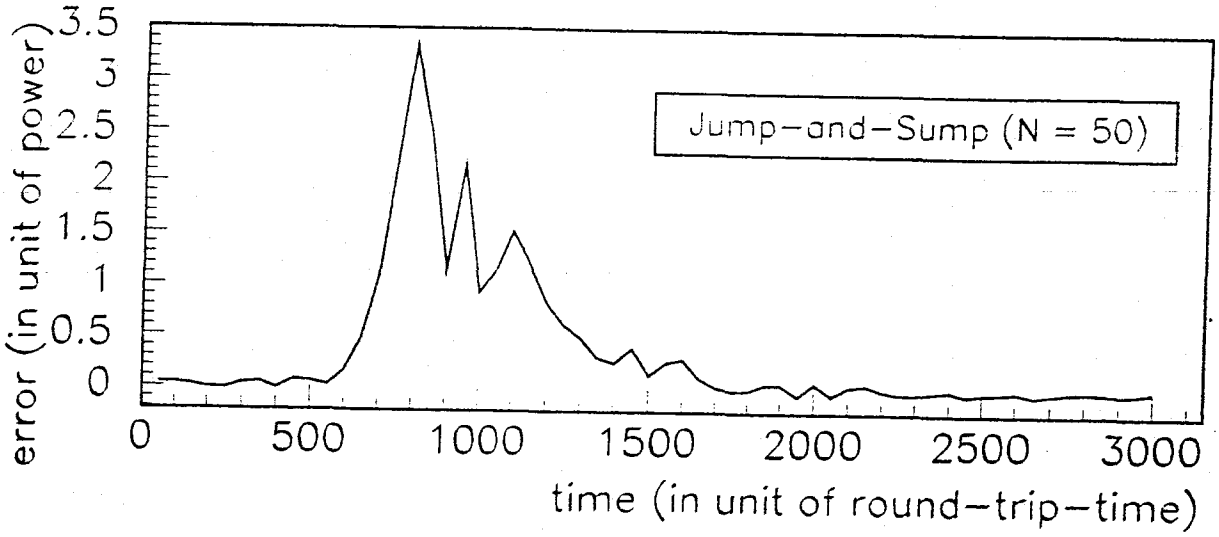

Figure 8: Error made by DFA based on JAS as compared to SM for $N = 50$ in calculating the resonance curve of Fig.6(a)

One may note that, unlike the low-finesse case in sec.II, the last term in Eq.27 representing the feedback is not neglected in this case. The first reason is that the terms of order $\mathcal{O}(R^N)$ are not really negligible now because of high value of R. Speaking in the language of digital filters with an argument related to the same reason, we can say that feedbacks are really important in this case since partial beams get stored for a long time in such cavities. The equivalent IIR filters cannot be converted into FIR ones, as long as we intend to apply the linear Eq.27 by restricting N within a suitable upper limit. This limit is to be determined numerically.

The simulation procedure is same as that described for low finesse cavity in section 2, except that, in step 4, Eq.27 is to be used instead of Eq.13. Since this method involves *jumping* a few steps of field-evolution and then *summing up* the contribution of various partial beams, I call this method - the *Jump-and-Sump* (JAS) method. It should be noted that JAS is *not* a replacement for DFA. Rather it is a replacement for the perturbative calculation that the low-finesse version of DFA is based upon.

The error in unit of power (i.e., just the difference) made by DFA based on JAS as compared to SM is shown in Fig.8 for $N = 50$. The relative error as given by Eq.19 is also plotted in Fig.9. We see the relative error is quite small near the resonance but it shoots up as the field starts oscillating with higher and higher frequency. This is simply due to the fact that the frequency resolution of the method is worse than that of the exact method due to an increase by a factor of N in its sampling interval. However, since the field-amplitudes at those points are exceedingly small, this relative error is irrelevant for the simulation programme. As this oscillation starts decreasing soon, the relative error also gets reduced and soon becomes almost zero - much before the next resonance point comes (Gap between two resonance points for $w = 1$ μm/sec is 26600 round trip times).

One may note that although relative error is a better measure than simple error, in the case of high finesse response of the cavities, it may lead to some confusion because of its sudden shoot-off after crossing a resonance peak. *From the next section onwards* only relative error in a certain important

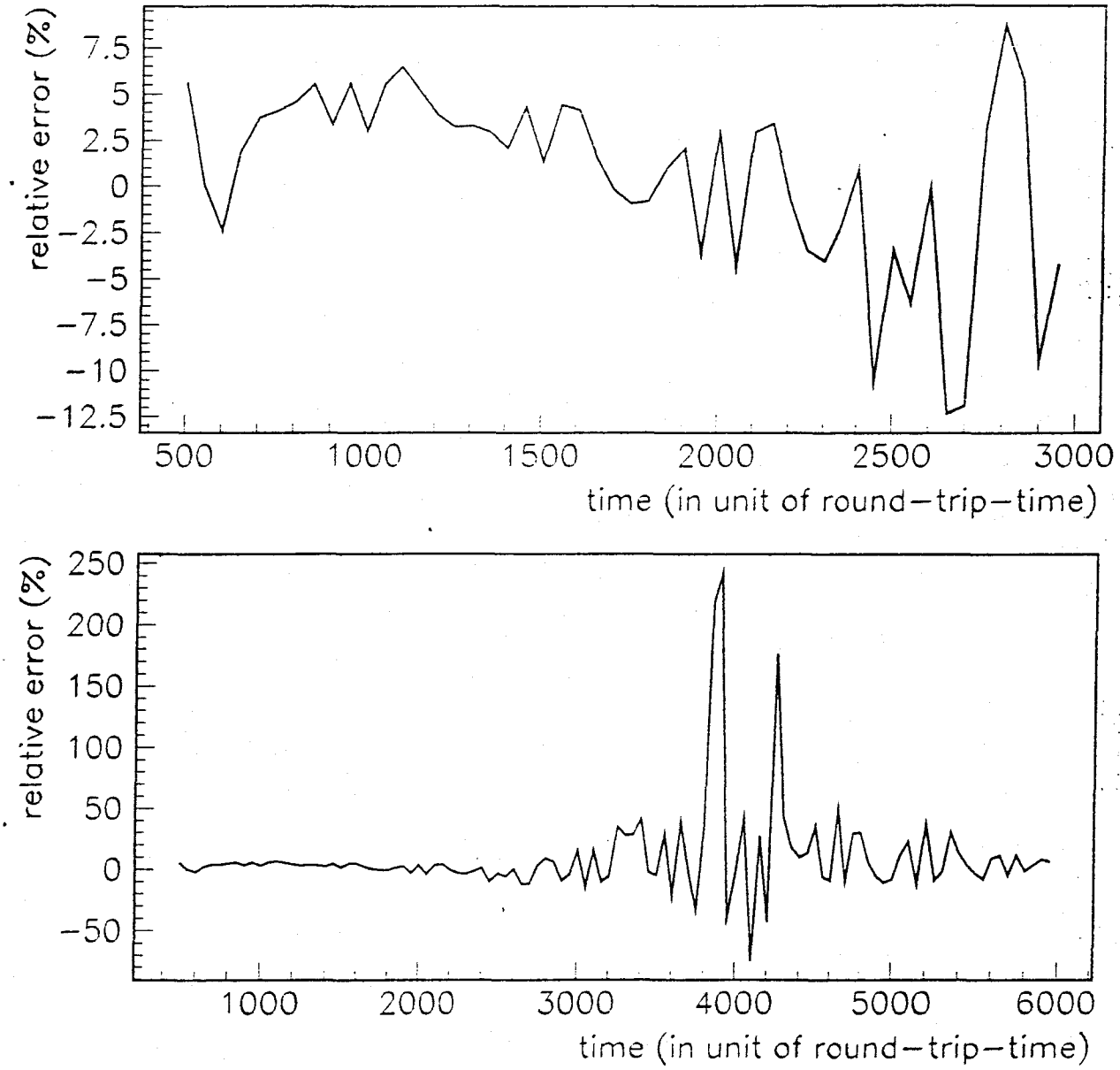

Figure 9: Relative error (%) made by DFA based on JAS as compared to SM for $N = 50$ in calculating the resonance curve of Fig.6(a). Plot (a) is nothing but a zoomed-in part of plot (b). The relative error increases for a short time while the field amplitude is very small: This 'increase' is thus unimportant.

range of time around the resonance point will be plotted, as in Fig. 9(b). One should keep in mind that the increasing level of relative error for a short time due to the reduced frequency resolutions of the methods to be described are actually unimportant because of the reasons explained above.

Numerical investigation shows that DFA based on JAS works quite well (with moderate values of N, say, 50) even for higher values of cavity finesse. As may be obvious, when applied to low finesse cavities, this commits same level of error as that of DFA based on perturbative calculation.

4 Simulation of 3-mirror coupled cavity

A power-recycled interferometer with a FP cavity in each arm, which is constituted by static mirrors, can be thought to be equivalent to a 3-mirror cavity. Study of such a simpler geometry of the optical arrangement can thus provide us answers to some of the issues which are in common with a complete FP-type power recycled interferometer, e.g., coupling of intra-cavity fields, sensitivity to misalignment etc. The resonance properties of such a cavity are, in general, quite complex, in which the mode losses may depend on the distribution of the optical field between the two cavities and the behaviour of this distribution may again depend on, among other parameters, the relative sizes of the cavities[14]. The static properties of such coupled cavities have been discussed in Ref.[15, 16]. Some table-top experiments were also performed to study the frequency response of such a coupled cavity [17, 18].

In the dynamical case, however, such an equivalence between the full power-recycled interferometer with FP arm cavities and a 3-mirror cavity can be established only under some simplifying assumptions, i.e., that the beam-splitter is static and that the movement of the input mirror or the end mirror of one arm cavity exactly mimic the movement of the corresponding mirror in the other arm cavity (the movement we mention in the present context is measured wrt the beam-splitter).

On the other hand, such an interferometer can also be thought to be equivalent to two dynamical 3-mirror cavity systems coupled with each other through a shared part of their recycling cavities. The nature of this coupling is investigated in sec.6. So, one important step towards the final goal of understanding and simulating the dynamical response of a power-recycled interferometer would be to investigate physical effects and test the applicability of the numerical methods developed for 2-mirror cavities in a 3-mirror coupled cavity.

In this section, it is shown that the evolution of fields in a 3-mirror cavity is just like that in a 2-mirror cavity whose input mirror reflectivity is changing with time. Under a general dynamical condition, most of the time, this reflectivity is quite high. Utilizing this idea, I apply the method of DFA based on JAS introduced in case of high finesse cavities in sec.3 and also incorporate a special technique, called *Freezing-the-Finesse* which takes care of the changing reflectivity, to write the fast DFA code for 3-mirror cavity.

4.1 Field equations in a dynamical 3-mirror cavity

The notation to be used for the calculation of fields in a 3-mirror coupled cavity is shown in Fig.10. The amplitude-reflectivities of the input mirror (the recycling mirror for a dynamically equivalent interferometer), the middle mirror (the input mirror of arm-cavities of a dynamically equivalent interferometer) and the end mirror are represented by r_1, r_2 and r_3 respectively. The numerical values chosen for them for the simulation to be described below are 0.96, 0.94 and 0.9999 respectively which are same as those to be used for corresponding mirrors in VIRGO interferometer[2].

The exact equations for the intra-cavity fields in a 3-mirror coupled cavity when all mirrors move

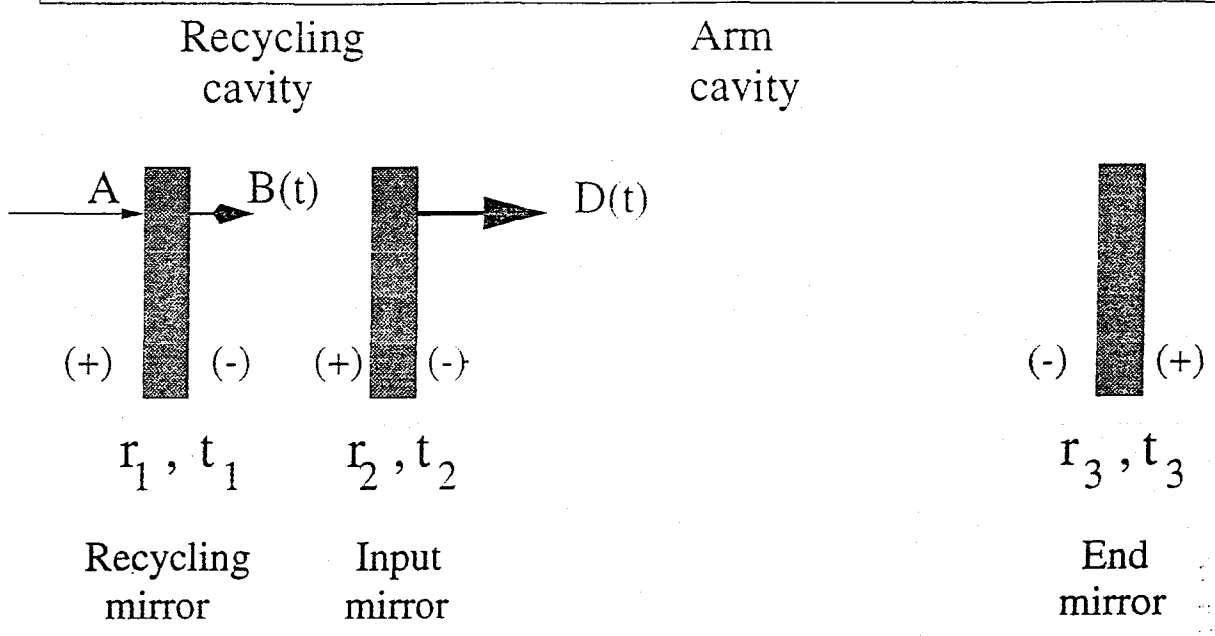

Figure 10: Notation used for 3-mirror coupled cavity; The (+) or (−) sign on two sides of a mirror indicates the phase (i.e., either zero or π) that a light beam acquires on reflection from that particular side of the mirror.

can now be written as follows :

$$\begin{aligned} B(t) &= t_1 A \exp j[p_1(t)] \\ &\quad -r_1 r_2 B(t-2\tau_r)\exp j[\phi_r - p_1(t-2\tau_r) + 2p_2(t-\tau_r) - p_1(t)] \\ &\quad +t_2 r_1 r_3 D(t-2\tau_c-\tau_r) \\ &\quad \times \exp j[\phi_c + \phi_r/2 - p_2(t-2\tau_c-\tau_r) + 2p_3(t-\tau_c-\tau_r) - p_1(t)], \end{aligned} \tag{29}$$

$$\begin{aligned} D(t) &= t_2 B(t-\tau_r)\exp j[\frac{1}{2}\phi_r - p_1(t-\tau_r) + p_2(t)] \\ &\quad +r_2 r_3 D(t-2\tau_c)\exp j[\phi_c - p_2(t-2\tau_c) + 2p_3(t-\tau_c) - p_2(t)] \end{aligned} \tag{30}$$

where ϕ_r and ϕ_c are initial (constant) round-trip phase offsets in recycling and arm cavities respectively; τ_r and τ_c are one-trip time in recycling and arm cavities respectively; $p_i(t)$ are changing phase offsets(one-trip) due to the motion of mirror i. i.e., $p_i(t) = (2\pi/\lambda)x_i$, x_i representing displacement; The positive direction of motion is set to be from 1st (recycling) mirror towards the 3rd (end) and the reference point for the mirror movement is taken to be the laser source.

If we assume that mirrors are not moving at all or are moving so slowly that their motion does not affect any field for a long time, then we can arrive at the following quasi-static expressions for B and D:

$$B_0 = At_1(1 - r_2 r_3 \exp[j\phi_c])/\chi_0 \tag{31}$$

$$D_0 = At_1 t_2 \exp[j\phi_r/2]/\chi_0 \tag{32}$$

where

$$\chi_0 = 1 + r_1 r_2 \exp[j\phi_r] - r_2 r_3 \exp[j\phi_c] - r_1 r_3 (r_2^2 + t_2^2)\exp[j\phi_r + j\phi_c]. \tag{33}$$

The *Double-resonance* condition is achieved when $\phi_c = 2n\pi$ and $\phi_r = 2m\pi$, where n and m are integers. The numerical values for $|B_0|^2$ and $|D_0|^2$ at double-resonance condition are ≈ 49.0W and ≈ 1584.0W respectively for $|A|^2 = 1.0$W and the values of reflectivities as chosen above for VIRGO. In the static case, the power transmitted through the system is maximum at this point [15]; However, in general, a maximum point of transmission may occur at a value, $\phi_c \neq 2n\pi$ for a value of $\phi_r \neq 2m\pi$. The rules of the occurence of these resonance peaks will be discussed in the next section for both the static and dynamical cases.

The exact numerical code for the 3-mirror cavity is written on the basis of Eqs. (29) and (30) as shown in Fig.11. It should be noted that this code is really exact only if the ratio of the lengths of the arm cavity and the recycling cavity is an integer, ρ. It is, however, not a very important consideration because, in case ρ is not an integer, a code like this based on the nearest integer value of ρ would make only negligible error wrt one which may take into account the real value of ρ. The reason is that in almost all cases of interest, we need *not* study the system with a very fine level of frequency resolution (i.e., with a sampling period smaller than the round-trip-time in recycling cavity).

A dynamical double resonance curve for the field B, while only the end mirror moves with a velocity of 1 μm/sec. and ϕ_r is set to a value of $2m\pi$ is shown in Fig.12. It so turns out that the corresponding resonance curve for the field, D looks exactly like what we plotted in Fig.6(a) for a 2-mirror high finesse cavity with $r_c = 0.998733$ whose length was also changing at the same rate. The following discussion explains this.

The exact code as represented in Fig.11 takes a very long time to compute the field evolution. We, therefore, need to develop a faster way of doing this by finding some ways of writing non-exact equations for 3-mirror coupled cavities. One way of doing this is to replace the recycling cavity by an equivalent mirror whose reflectivity, $r_{\rm rec}$ depends on the dynamical phase offset denoted by θ_r in the recycling cavity, and then to write down the equation for D in the resulting 2-mirror cavity constituted by the end mirror and the equivalent mirror for the recycling cavity:

$$D(t) = t_{\rm rec}(t)A + r_{\rm rec}(t)r_3 \exp[j\theta_c(t-\tau_c)]D(t-2\tau_c), \tag{34}$$

where

$$r_{\rm rec}(t) = \frac{r_2 + r_1(r_2^2 + t_2^2)\exp[j\theta_r(t)]}{1 + r_1 r_2 \exp[j\theta_r(t)]} \tag{35}$$

$$t_{\rm rec}(t) = \frac{t_1 t_2 \exp[j\theta_r(t)/2 + p_1(t)]}{1 + r_1 r_2 \exp[j\theta_r(t)]} \tag{36}$$

The field B can then be easily calculated using this equation. Simulation programme based on these equations now runs about 270 times faster since the time-sampling rate is much smaller now (i.e, $1/\tau_c$ instead of $1/\tau_r$) and also it needs to perform much less expensive algebraic calculations without memorizing any data in a buffer.

We find that this equation makes negligible (in fact zero upto several decimal points near the peak) relative error as compared to the exact code. However, in this case also, the relative error shoots up for some time after crossing the resonance peak, as the fields start oscillating with higher and higher frequencies. This is due to a reduced frequency resolution of the method which effectively increases the sampling period by a factor of ρ. As already explained in section 3 for the case of DFA based on JAS, this error is unimportant since the absolute value of the field is very low in that range. Obviously, this level increases as the ratio of lengths of the arm cavity and recycling cavity is reduced and vice versa.

The reason that the above equation can work so accurately is that the missing information in the equation, τ_r is only 40 nanosec as compared to τ_c which is about 10 microsec. So, any extra information

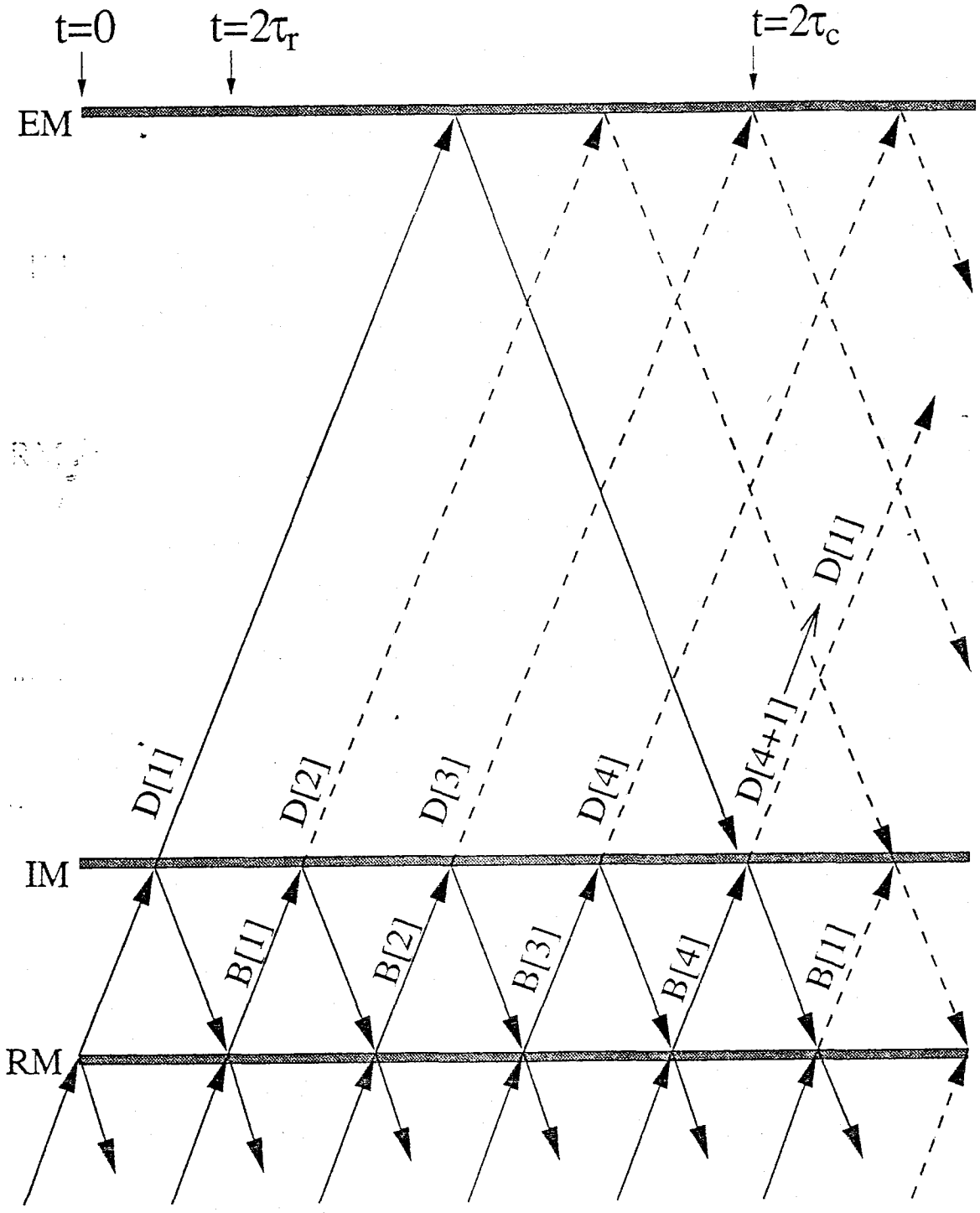

Figure 11: Exact dynamical code written for a 3-mirror cavity for which the ratio of lengths of the arm cavity and the recycling cavity is an integer, ρ. The figure shows the case for $\rho = 4$; For the equivalent case of the VIRGO interferometer, ρ has been assumed to be 250 (= 3000/12). Note that at any moment of time the code needs to memorize 2ρ number of data for the evolution of phases in two cavities and ρ number of past values for the field D. RM - Recycling Mirror, IM - Input Mirror, EM - End Mirror.

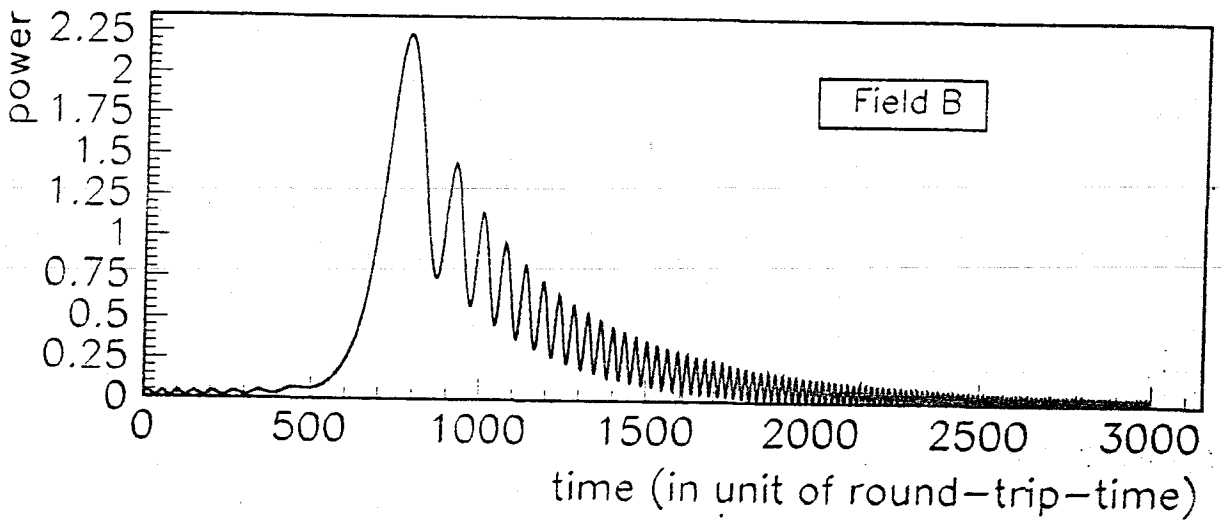

Figure 12: A dynamical double resonance curve for the field B in a 3-mirror cavity, while only the end mirror moves with a velocity 1 $\mu m/sec$ and the round-trip phase in the recycling cavity, θ_r is set to an integral multiple of 2π. Input power is one unit.

into the dynamical response that τ_r could have contributed amounts to a negligible time-gap between cause and effect as compared to the evolution of fields during one-trip time in the arm cavity. For same reasons, if we had tried the other way round by playing a similar trick by replacing arm cavity by an equivalent mirror, we would have written completely wrong equations for the dynamical evolution of fields.

On the basis of the above observation, we may thus make an assumption that τ_r can be neglected with respect to τ_c in the exact set of equations. This approximation was first used by Redding[19] and has also been applied by others [20] to study the responses of a 3-mirror cavity. From now onwards, we refer to this as small recycling cavity (*small-rec-cav*) approximation.

Using this approximation, the full dynamical Eqs. 29 and 30 can now be written as

$$B(t+\tau) = \frac{1}{\chi(t+\tau)}\left[t_1 A \exp j[p_1(t+\tau)] + t_2 r_1 r_3 D(t) \exp j[\frac{\theta_r(t+\tau)}{2} + \theta_c(t+\tau/2)]\right] \quad (37)$$

$$D(t+\tau) = t_{\rm rec}(t+\tau)A + r_{\rm rec}(t+\tau) r_3 D(t) \exp j[\theta_c(t+\tau/2)], \quad (38)$$

where $\tau = 2\tau_c$ and

$$t_{\rm rec}(t) = \frac{1}{\chi(t)} t_1 t_2 \exp j[\frac{1}{2}\theta_r(t) + p_1(t)] \quad (39)$$

$$r_{\rm rec}(t) = r_2 + \frac{t_2^2 r_1 \exp j[\theta_r(t)]}{\chi(t)}. \quad (40)$$

$$\theta_r(t) = \phi_r - 2p_1(t) + 2p_2(t). \quad (41)$$

$$\theta_c(t-\tau_c) = \phi_c - p_2(t-2\tau_c) + 2p_3(t-\tau_c) - p_2(t). \quad (42)$$

$$\chi(t) = 1 + r_1 r_2 \exp j[\theta_r(t)] \quad (43)$$

4.2 Simulation by *Jump-and-sump* while *freezing-the-finesse*

We may now ask ourselves if it would be possible to compute even faster than what the ***short-rec-cav*** approximation can allow us. To get a reply of this question, we note that the evolution of field D as represented by Eq.(38) is just like that of the intra-cavity field, F of a 2-mirror cavity whose input mirror reflectivity $r_c \equiv r_{\rm rec}$ is changing with time.

$$F(t+\tau) = t_c(t+\tau)A + F(t+\tau)R(t+\tau)\exp[j\theta(t+\tau/2)] \quad (44)$$

where $R(t) = r_e r_c(t) e^{j\phi_i}$ is the product of the amplitude-reflectivities of the end mirror, r_e, the input mirror, r_c and a very small constant phase offset ϕ_i in a round-trip of the cavity when mirrors are not moving. The evolution of field B represented by Eq.(37) is completely dependent on that of D, which means that if we can compute D faster, we can compute B also at the same speed. Let us plot the reflectivity, $r_{\rm rec}$ as a function of $\Delta\theta_r = \theta_r - (2m+1)\pi$ in Fig.13. One can see that except for values very near to $(2m+1)\pi$ for θ_r, the value of $r_{\rm rec}$ is always quite high and very near to ≈ 0.998733 - the value at $\theta_r = 2m\pi$. This explains why the dynamical double resonance curve for the field D in a 3-mirror cavity has an exactly similar behaviour like that of a high finesse 2-mirror cavity with $r_c = 0.998733$ (as in Fig.6a), when we assume that only the end mirror is moving and set $\theta_r = 2m\pi$.

So, we now have a ready answer to the above question in our hand. If we consider the simplest case of constant $r_{\rm rec}$ by assuming 'only end mirror moving', we just need to apply the method of DFA based on JAS to Eqs.38 to develop a code much faster than what *small-rec-cav* approximation can ensure us. For example, the error level for JAS as compared to the equations approximated by *small-rec-cav* for the field D in this simplest case, when we allow only end mirror to move and set $\theta_r = 2m\pi$, is same as what is shown in Fig.8.

However, to have a complete simulation, we need also to consider the dynamics of the recycling cavity and thus the changing values of $r_{\rm rec}$. By making a comparison of Eq.(44) with Eq.(38), we note that in the equivalent expressions for $r_c(t)$ and $t_c(t)$,i.e., $r_{\rm rec}$ and $t_{\rm rec}$ respectively, the time-dependence arises only through the dependence of θ_r on time. We noted that except for a small range of values of θ_r near $2m\pi$, the equivalent reflectivity, $r_{\rm rec}(t)$ does not change much from unity. This leads me to incorporate a special technique named as *Freezing the Finesse* (FTF)[21]. As the name suggests and as is explained below, I set the values of θ_r and so of r_c and t_c to suitable constants before each step of the *Jump-and-Sump* method, thus effectively *freezing* the equivalent finesse of the 3-mirror cavity during each interval of jumping.

So, the procedure of simulation for 3-mirror cavities when all mirrors move is as follows:

- **step 1**: Time is sliced into equal intervals of width $\Delta = N\tau$, so that any time $t_i = iN\tau$, where i is an integer.

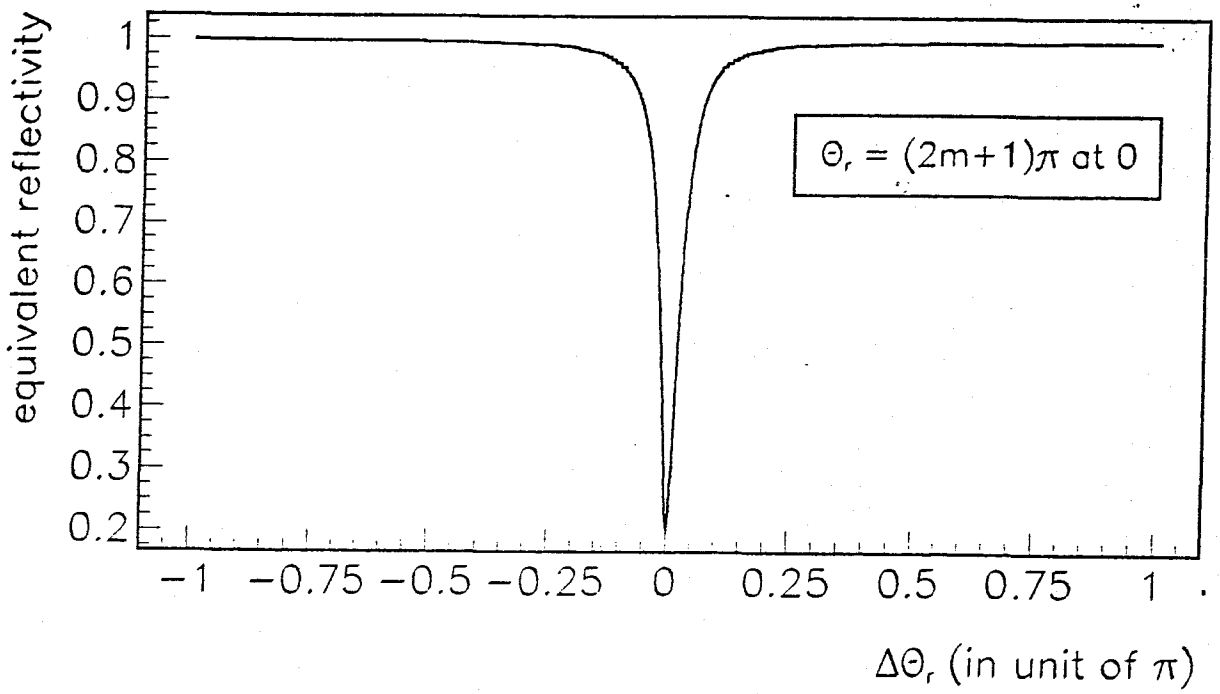

Figure 13: The equivalent amplitude reflectivity of the recycling mirror, r_{rec} is plotted as a function of round-trip phase offset, $\Delta\theta_r$ in the recycling cavity.

- **step 2**: If we assume that for the short time interval, (t_i, t_{i+1}), the mirrors move with constant velocities, then by defining the rates of change of the phase offsets in the recycling and arm cavity respectively as

$$w_r = v_2 - v_1, \tag{45}$$
$$w_c = v_3 - v_2. \tag{46}$$

we can write

$$\theta_r(t) = \phi_r + \frac{4\pi}{\lambda} w_r t, \tag{47}$$
$$\theta_c(t) = \phi_c + \frac{4\pi}{\lambda} w_c (t - \tau_c). \tag{48}$$

- **step 3**: The phase, ϕ_i and reflectivity, r_c in the expression for R and t_c in Eq.44 are fixed to the following values during any time interval (t_i, t_{i+1})

$$\phi_i = \theta_c(t_i) \tag{49}$$
$$r_{ci} = \frac{1}{2}[r_{\rm rec}(t_i) + r_{\rm rec}(t_{i+1})] \tag{50}$$
$$t_{ci} = t_{\rm rec}(t_{i+1}). \tag{51}$$

- **step 4** (*Jump-and-sump*) : The Eq.27 of the is then applied to compute the field, D inside the arm cavity of the 3-mirror coupled cavity. The field at t_{i+1}, $D(t + N\tau)$ is obtained from the value of the field at t_i, $D(t)$ by simply substituting $D \to F$, $r_3 \to r_e$, $r_c \to r_{ci}$, $t_c \to t_{ci}$ and $v_i \to w_c$ in Eq.27.

- **step 5**: The values of ϕ_{i+1} and v_{i+1} are changed in the next step and D_{i+2} is calculated.

Before we discuss about the error levels of such a simulation, we note that if p_1 were a constant, that would not have affected the intra-cavity field-amplitudes in any way, since it would have acted as an overall phase. The variation in p_1, i.e. the velocity, v_1, however, affects the field amplitudes whenever the operating condition of the beam corresponds to a high value of effective finesse (i.e., whenever $r_{\rm rec}$ is high) for the 3-mirror system. So, if we completely neglect p_1 in Eqs.(37) and (38), it leads to almost no error if the beam is on exact antiresonance in the arm-cavity and on resonance in the recycling cavity (i.e., $\theta_c = (2n+1)\pi$ and $\theta_r = (2m+1)\pi$: Effective finesse is the lowest). However, it leads to the same level of error as shown in Fig.7 when the beam is on or near double resonance (i.e., $\theta_c = 2n\pi$ and $\theta_r = 2m\pi$: Effective finesse is the highest). Throughout the following discussion on error levels, we neglect this phase factor arising out of the Doppler-shift of the incoming light wrt the source.

As we can expect, the error made by the technique of FTF strongly depends on the first derivative of $r_{\rm rec}$ with respect to time. So, we can guess that the error will be less as long as $r_{\rm rec}$ varies slowly, which it does almost throughout the range of θ_r except for a small range (i.e.,about $\pm 0.2\pi$) around $\theta_r = \pi$.

In Fig.14(a), I plot a double resonance curve for the field D using Eq.38 while phases change with rates: $w_r = w_c = 1\mu$m/sec. The same resonance curve, when drawn by using faster method of DFA based on JAS and FTF for $N = 30$ gives relative error with respect to the equations based on *small-rec-cavity* as shown in Fig. 14(b). As has been explained, the error is quite small near resonance and increases for some time when the field oscillates rapidly with very small amplitude. For $N = 40$, the error near resonance vary between $\pm 3\%$, whereas for $N = 50$ the same figures increases to about $\pm 5\%$.

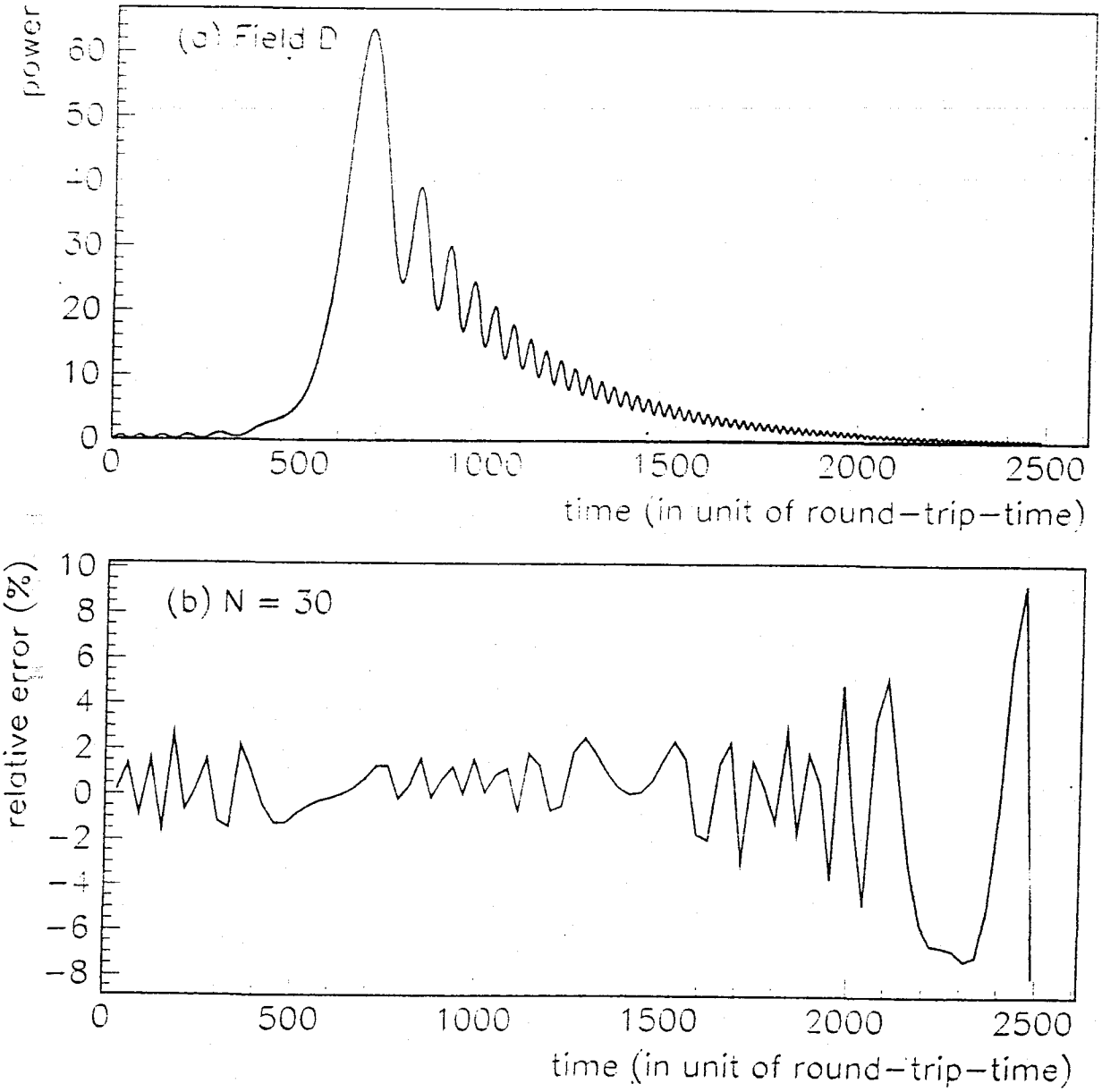

Figure 14: (a) A dynamical double resonance curve for field D in a 3-mirror cavity drawn by using equations based on only small-rec-cav assumption for $w_r = w_c = 1\mu$m/sec. Input power is one unit. (b) the relative error by DFA based on JAS and FTF wrt only small-rec-cav in calculating the same curve for $N = 30$. The relative error increases [illegible] while the field amplitude is very [illegible]. This 'increase' is thus unimportant.

For other combinations of w_r and w_c, the error levels vary, but in all cases for same N, it remains to have the same order of magnitude, provided, of course, that the velocities do not become too high compared to 1μm/sec.

Now we discuss the error consideration when the effective finesse of the system is near the lowest,i.e., when the beam is on exact antiresonance ($\theta_r = 2\pi - 1\mu$rad) in arm cavity, but on resonance ($\theta_c = (2m+1)\pi$) in the recycling cavity, while the phases change as : $w_r = w_c = 1\mu$m/ sec. The peak for this condition is drawn in Fig.15(a) by using Eq.38. The relative error in drawing the same curve using DFA based on JAS and FTF for $N = 30$ with respect to the curve in Fig.15 a is plotted in Fig.15(b). As expected, the error now is more than the case of double resonance. The peak of the error increases to about 8% for $N = 40$ and about 10% for $N = 50$. For other combinations of w_r and w_c, unlike the previous case, the error levels do not change much due to lower values of effective finnesse in this region.

So, we see that for any value of N, the simulation error is the least for a beam on double resonance. While the operating condition of the beam is anywhere else, the error in simulation increases. When the operating condition gets to the exact antiresonance point in the arm cavity but individual resonance point in the recycling cavity, the simulation for DFA based on JAS and FTF runs with its highest level of error.

Even the highest level of error is quite tolerable for (say) $N = 50$ for which the programme runs at a speed about 30 times faster than a code based only on the approximation of *small-rec-cav* (Eqs.37 and 38).

5 Three-mirror coupled cavity : *What happens when all mirrors move*

Now that we have a fast simulation code in our hand, we can use it to perform some experiments[22] with the aim of obtaining some physical insights into the coupling of the intra-cavity fields in a 3-mirror cavity. Specifically, I study how and when the peaks for the intra-cavity fields of a 3-mirror cavity appear in both static and dynamical cases. This will also come to use for writing an algorithm for starting up a power-recycled interferometer to bring all its constituent cavities near to the operating condition.

In subsection 5.1, I describe how various curves are drawn to bring out physical issues related to the field-distribution in the two cavities and tabulate some values after introducing various important parameters. In subsection 5.2 all these physical points are discussed. It should be noted here that although these discussions are regarding 3-mirror coupled cavities, the conclusions drawn here are, however, very important and come to great use when we start discussing about the full power-recycled interferometer, as is shown in the next section.

5.1 Dynamical curves and the corresponding Quasi-static curves

Dynamical Curves

As shown in Eqs.(37) and (38), intra-cavity fields are functions of two parameters, the round-trip phase offsets, θ_r and θ_c. However, if we assume constancy of velocities of mirrors for a short time, we can express these phases in the unit of those acquired due to mirror motion in one round-trip-time (rtt) of the arm cavity. Such a unit provides an advantage in terms of plotting the power of the fields as a function of only one parameter, the number of round-trips, instead of two, θ_r and θ_c, as shown in figures 16 to 23. So, phases acquired in one rtt by θ_r and θ_c are given by $K_r j$ and $K_c j$ respectively.

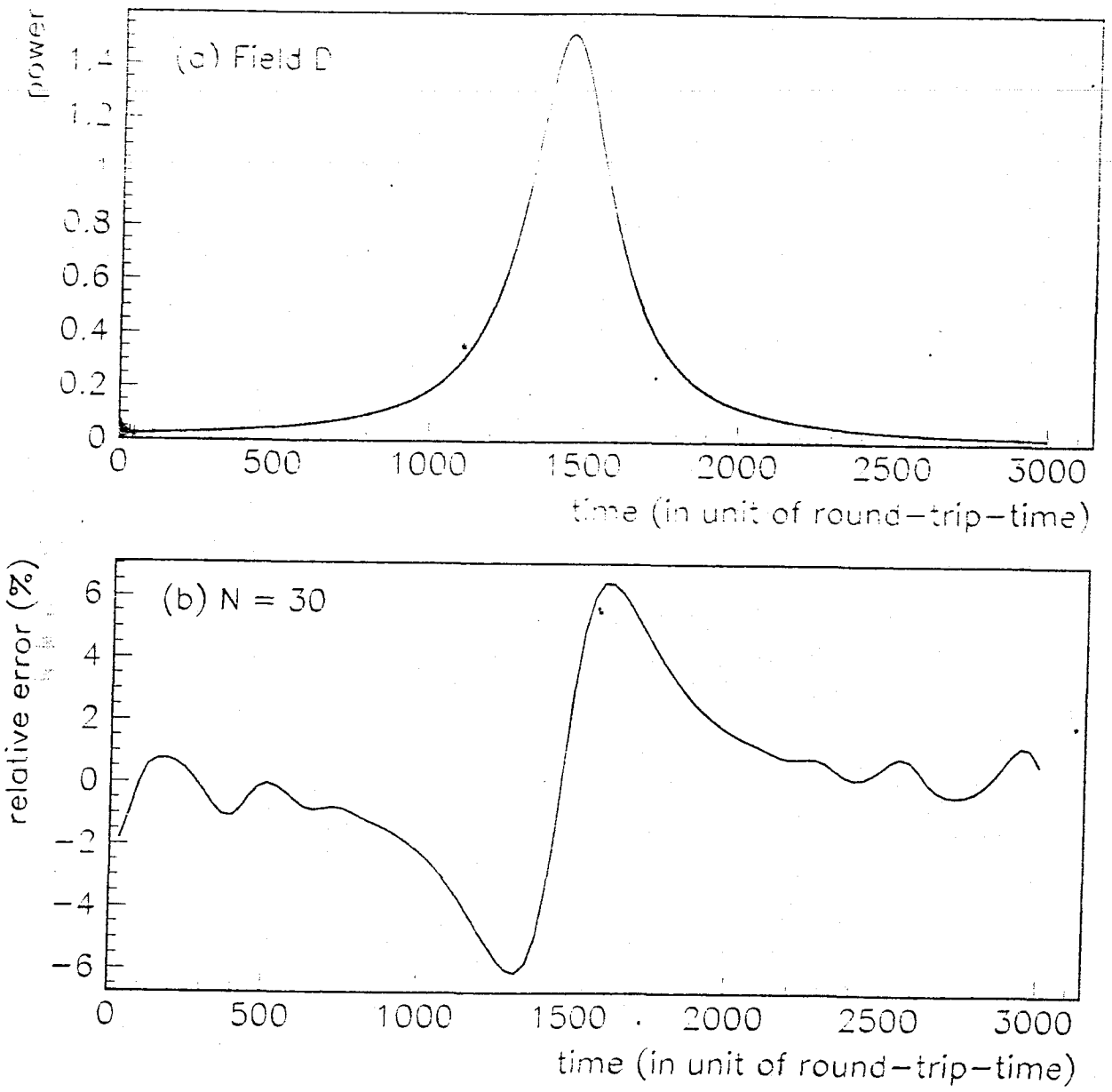

Figure 15: (a) A resonance peak of field D in a 3-mirror cavity when the beam is on exact antiresonance in the arm and on resonance in the recycling cavity, as drawn by equations based on only small-rec-cav assumption for $w_a = w_r = 1$ m-sec. Input power is one unit. (b) The relative error by DF, JAS and FTF wrt only small-rec-cav in calculating the same curve for $N = 30$.

where $\jmath$ is the number of rtt and so

$$\theta_r(\jmath) = K_r\jmath + \phi_r \quad (52)$$

$$\theta_c(\jmath) = K_c\jmath + \phi_c \quad (53)$$

$$K_r = (\frac{2\pi}{\lambda})2\tau w_r, \quad (54)$$

$$K_c = (\frac{2\pi}{\lambda})2\tau w_c. \quad (55)$$

$$(56)$$

How to follow Figures 16-23 :

Figures 16 to 23 are generated for various cases pertaining to the dynamical condition of the 3-mirror cavity. In all these figures, the rates of change of the lengths of the recycling and arm cavities, w_r and w_c have been chosen respectively to be 1.7 μm/sec and 1.0μm/sec and the input power is assumed to be 1.0 unit. Notice that different values for velocities have been chosen to keep our discussion at a general level. Assumption of the same rates of change might have made our discussion much simpler but at the cost of generality and reality.

Throughout our discussion, we express θ_r and θ_c in terms of the nearest integer values of rtt. The small fractional difference between the actual (real) and the quoted value (integer) does not affect the main physical points that we are going to describe here.

Note : In all of these figures, the points $\theta_r = 2m\pi$ (n is any integer) and $\theta_r = (2m+1)\pi$ have been fixed at points $\jmath = 324$ and $\jmath = 8147$ respectively (Notice: θ_r acquires a phase of π in $8147 - 324 = 7823$ rtt, whereas θ_c acquires the same in 13300 rtt, since the chosen value of w_r is greater than that of w_c).

In the first figure, the phase offset in the arm cavity is chosen to be such that the $\theta_c = 2\pi n$ (n is any integer) point coincides with $\theta_r = 2m\pi$ at $\jmath = 324$, thus generating the double-resonance curve (dynamical). In the same figure, when θ_r is equal to $(2m+1)\pi$ (at $\jmath = 8147$), the value of θ_c is $+0.588235\pi$ and so this corresponds to an *individual resonance point* of the recycling cavity and some light leaks into the arm cavity.

In the next successive figures, the initial phase offset in the arm cavity is changed in such a way that $\theta_c = 2\pi n$ point gets shifted towards $\theta_r = (2m+1)\pi$ before getting coincident with it in Fig. 21 (*Case ii*) and then crosses the point to the other side.

Some of the interesting numerical values for these figures as well as those corresponding to the intermediate situations are shown in Table 3. There are two peaks in each figure. The quantities, P_i(DY) and $\jmath_i$(DY) represent the power and location of the i-th peak ($i = 1, 2$) for the field D, whereas $\jmath_0$ represents location of the point $\theta_c = 2n\pi$. The value of θ_c when $\theta_r = (2m+1)\pi$ (at $\jmath = 8147$) is represented by ∇.

The figures are different from each other just because the $\theta_c = 2n\pi$ point appears at a different location in each case. So, each of these figures can as well be represented by the values of ∇ and/or $\jmath_0$.

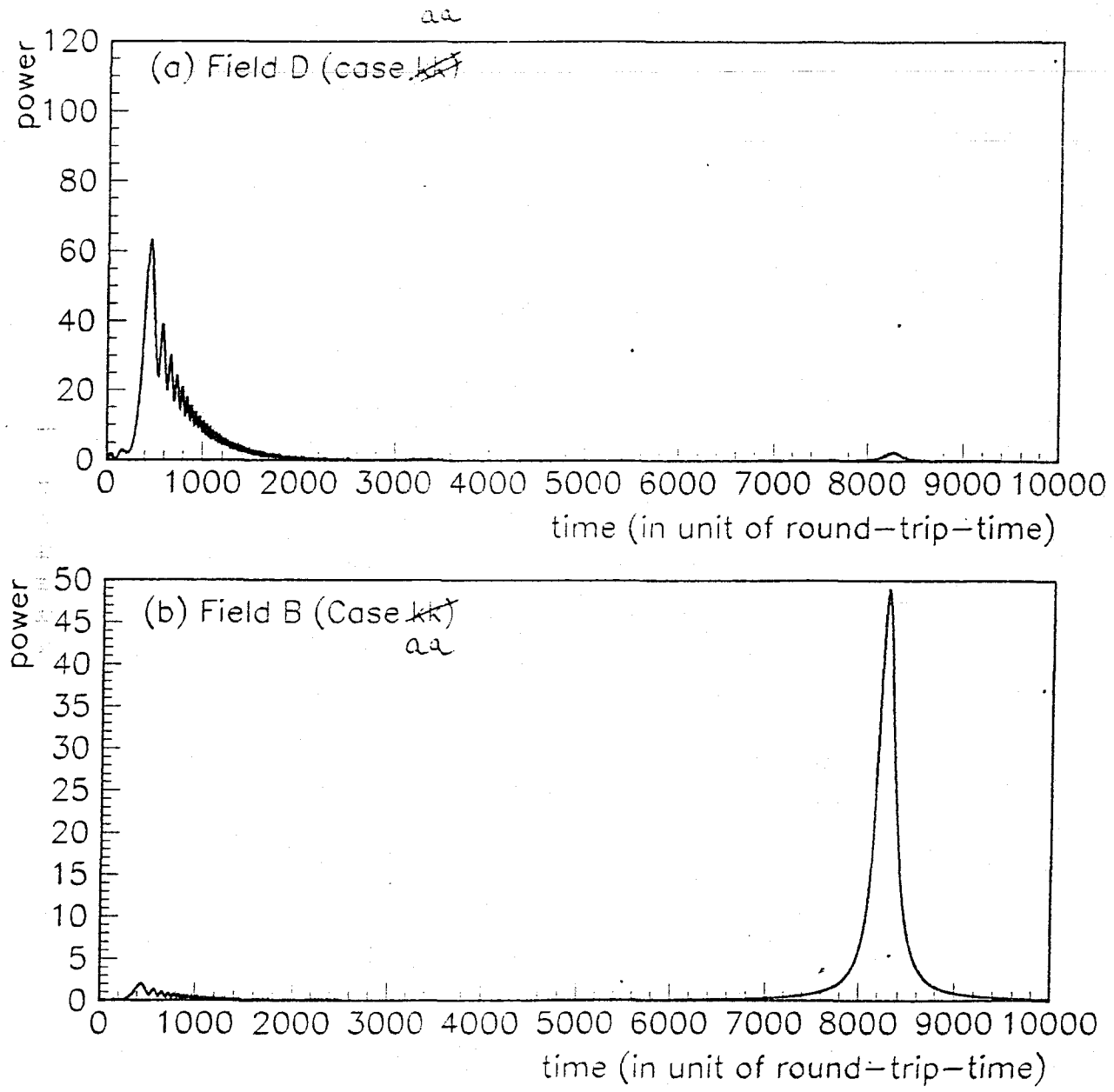

Figure 16: Evolution of fields (a) D and (b) B in case aa which corresponds to double-resonance condition for first peaks.

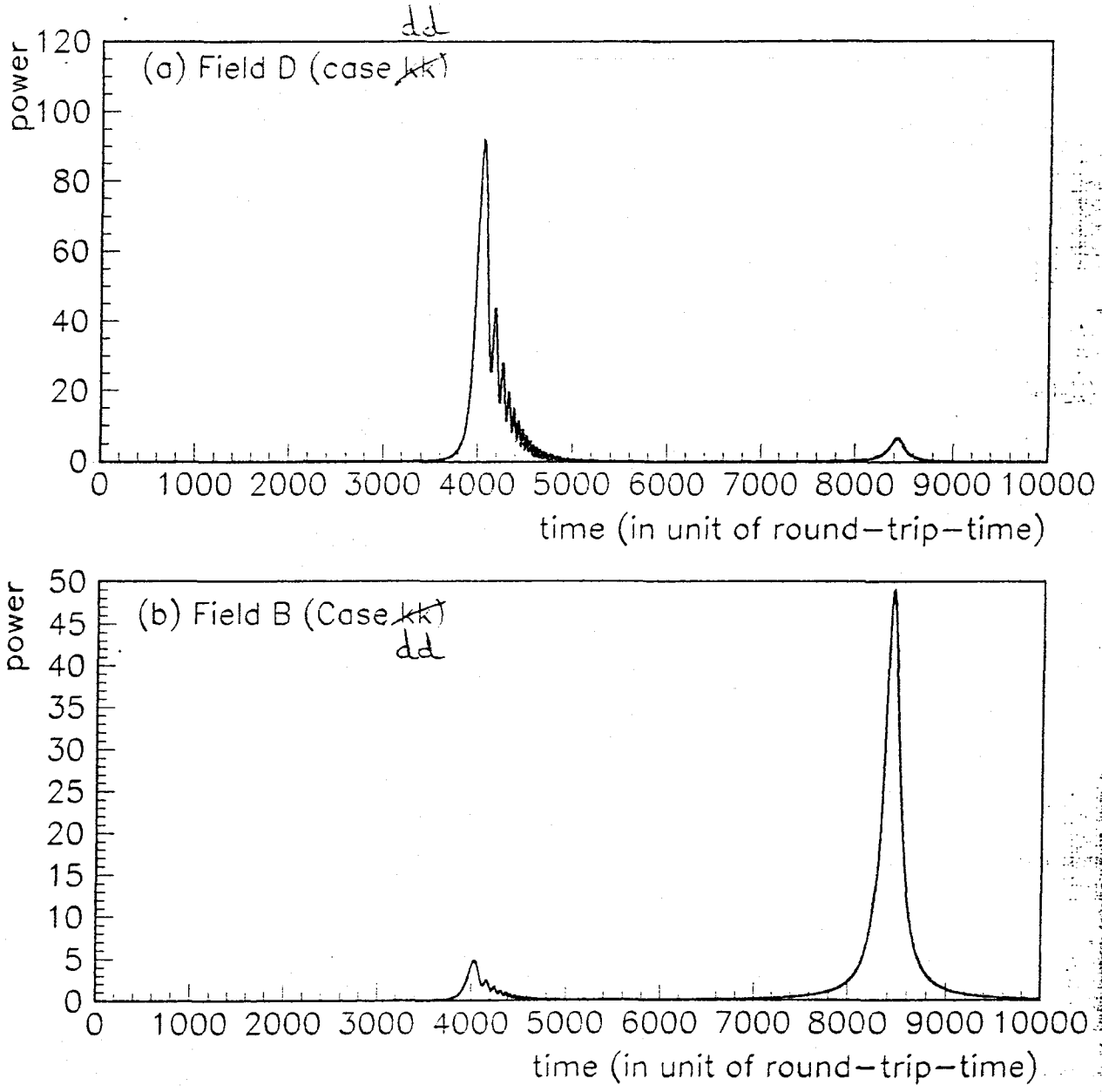

Figure 17: Evolution of fields (a) D and (b) B in case dd.

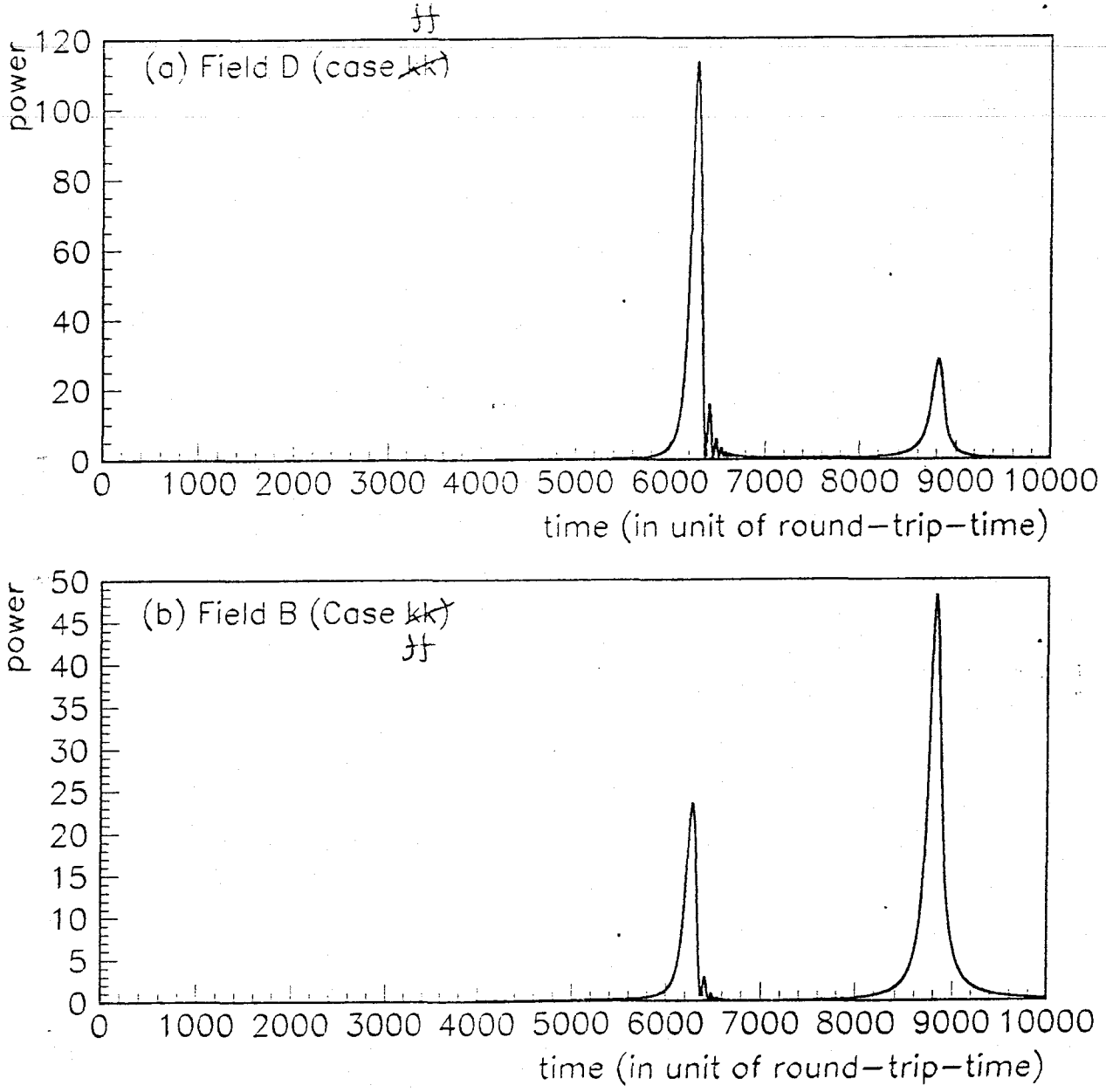

Figure 18: Evolution of fields (a) D and (b) B in case ff.

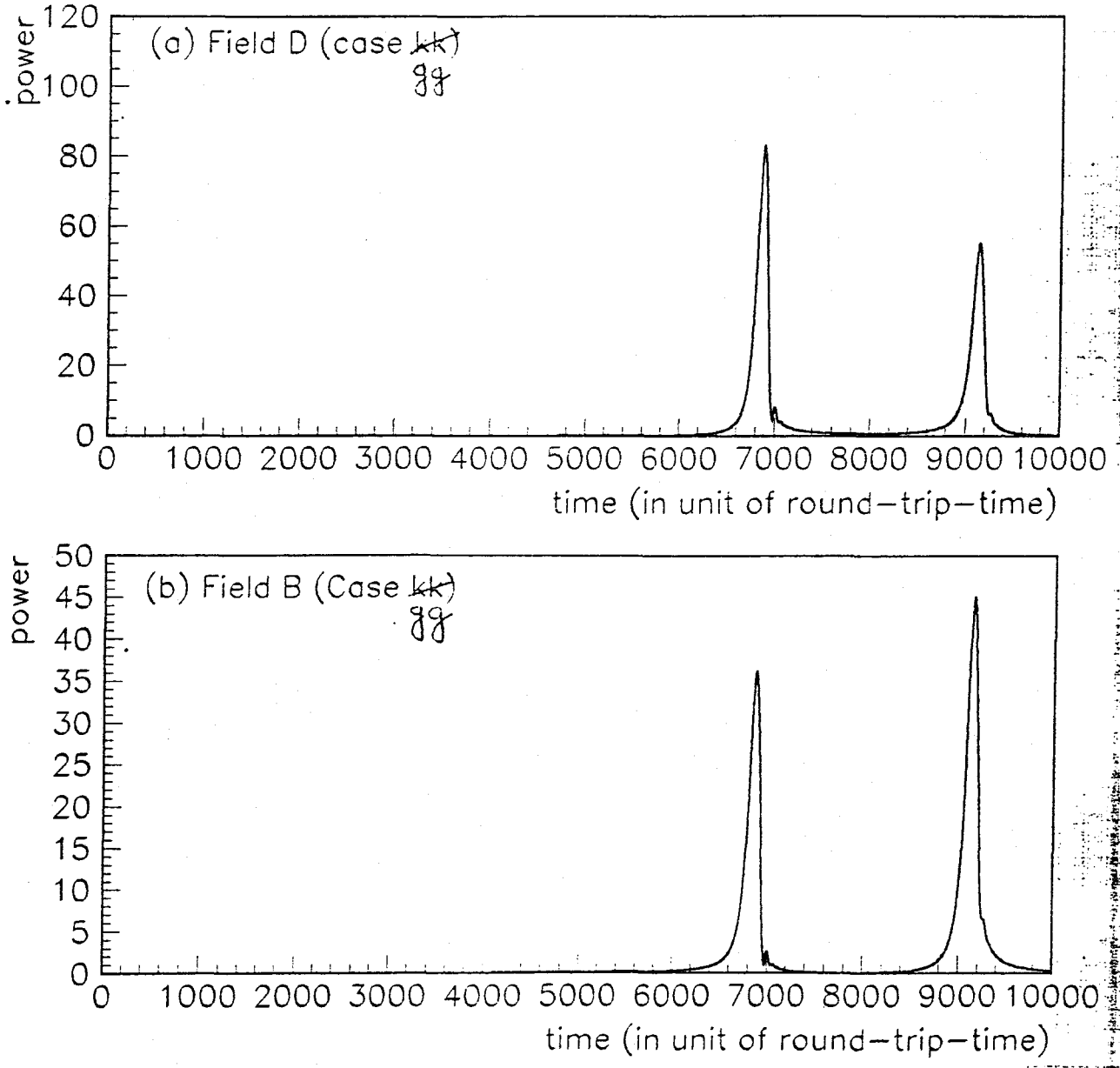

Figure 19: Evolution of fields (a) D and (b) B in case gg

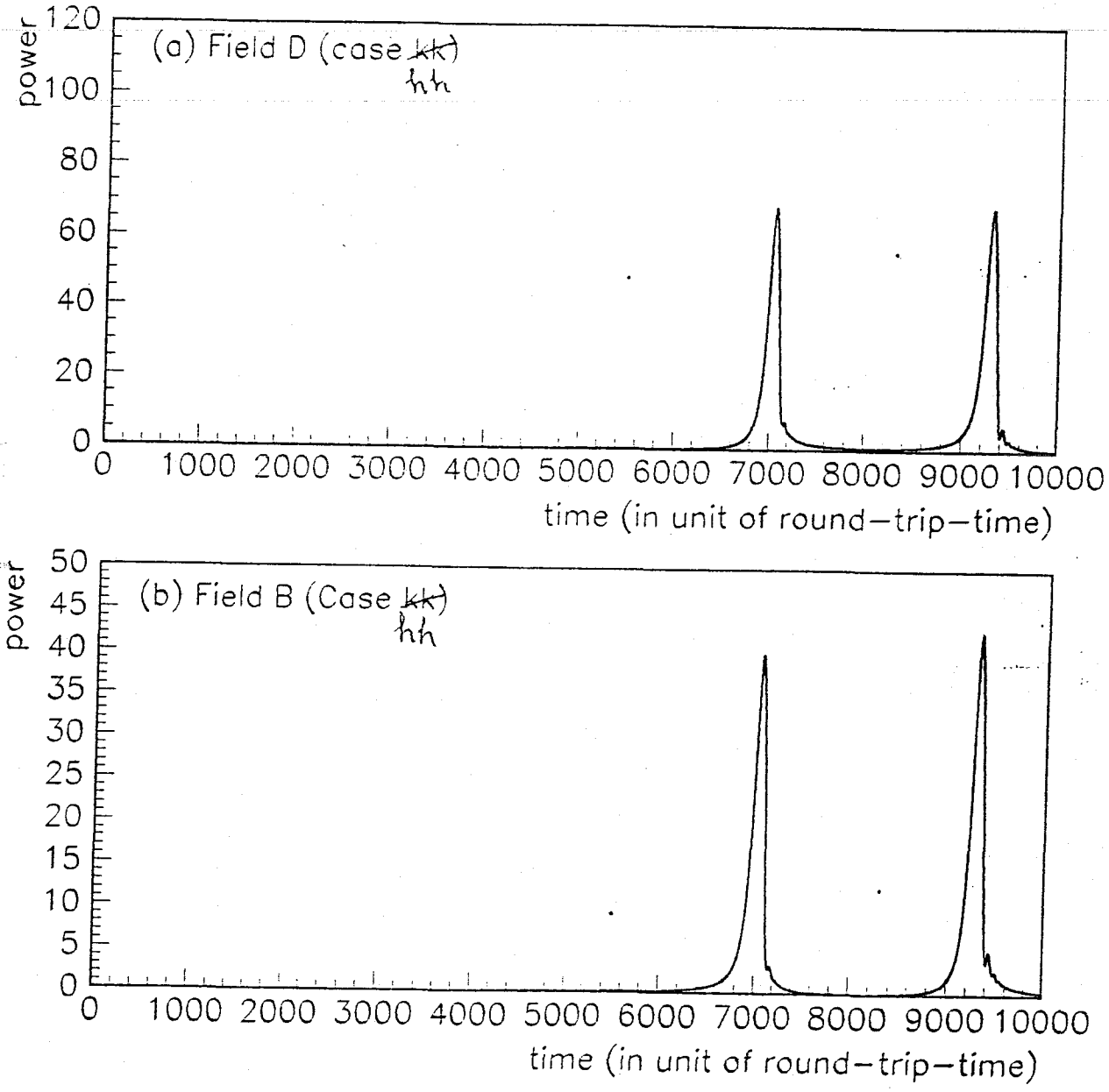

Figure 20: Evolution of fields (a) D and (b) B in case hh

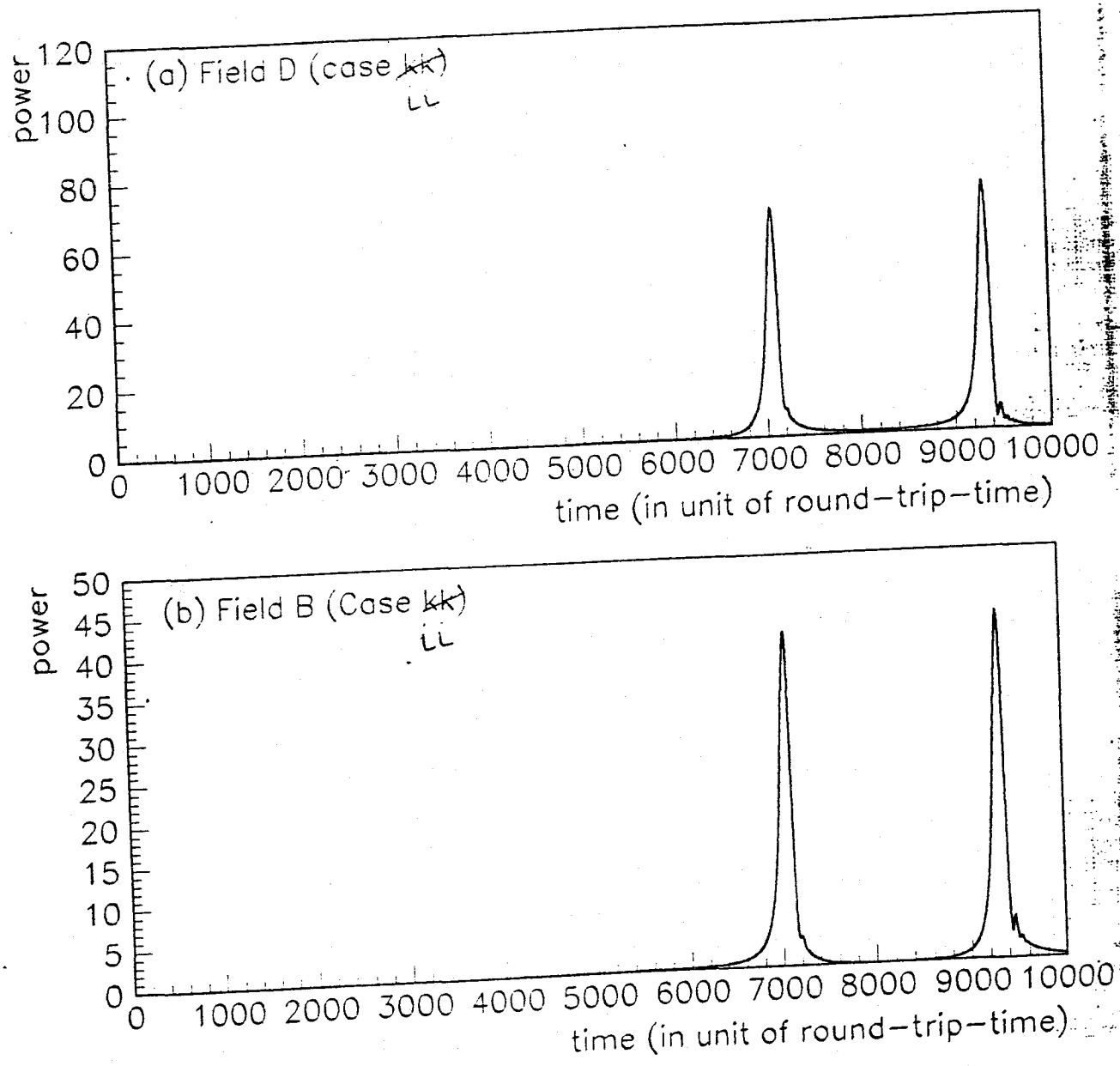

Figure 21: Evolution of fields (a) D and (b) B in case ii

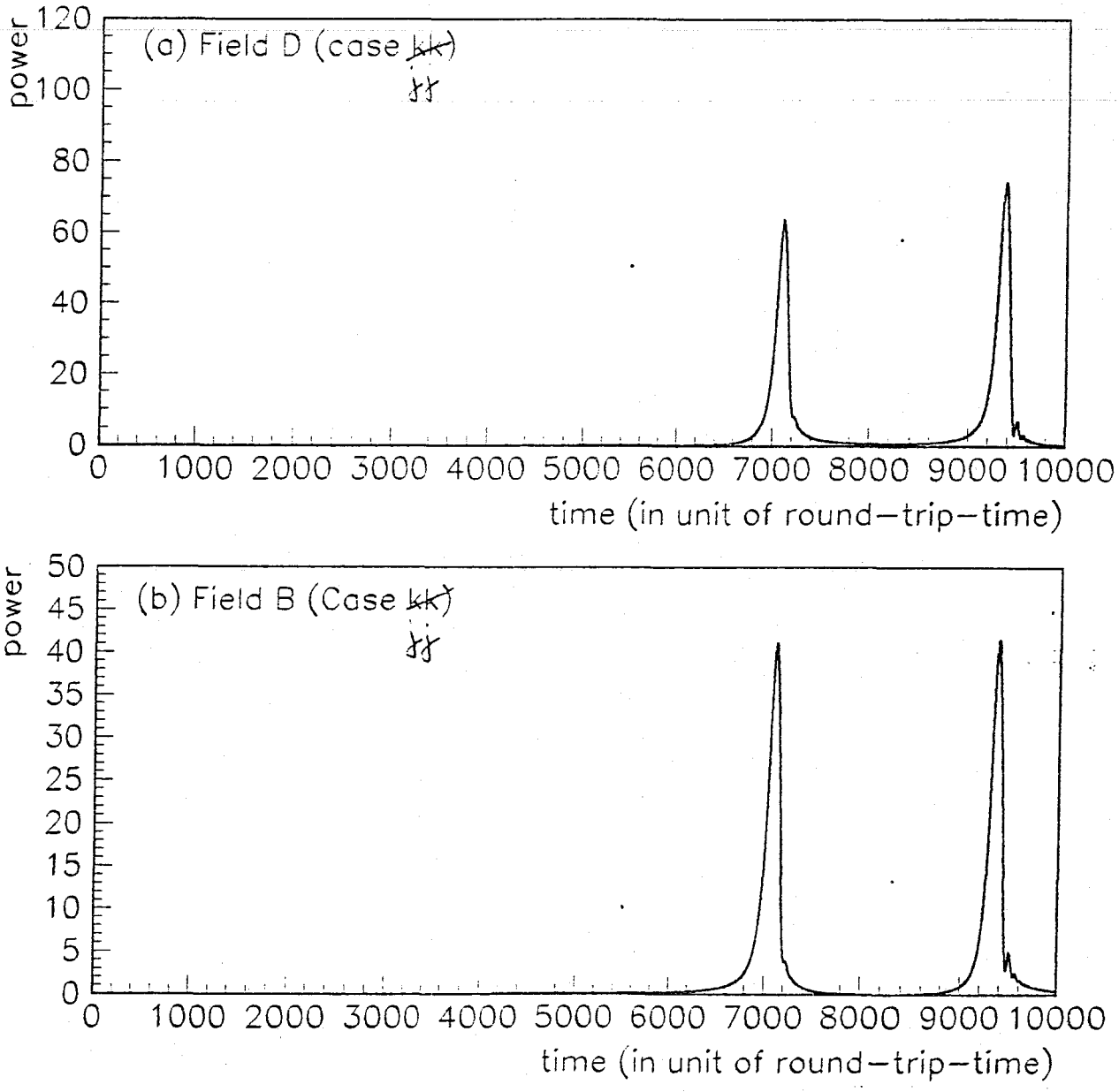

Figure 22: Evolution of fields (a) D and (b) B in case jj

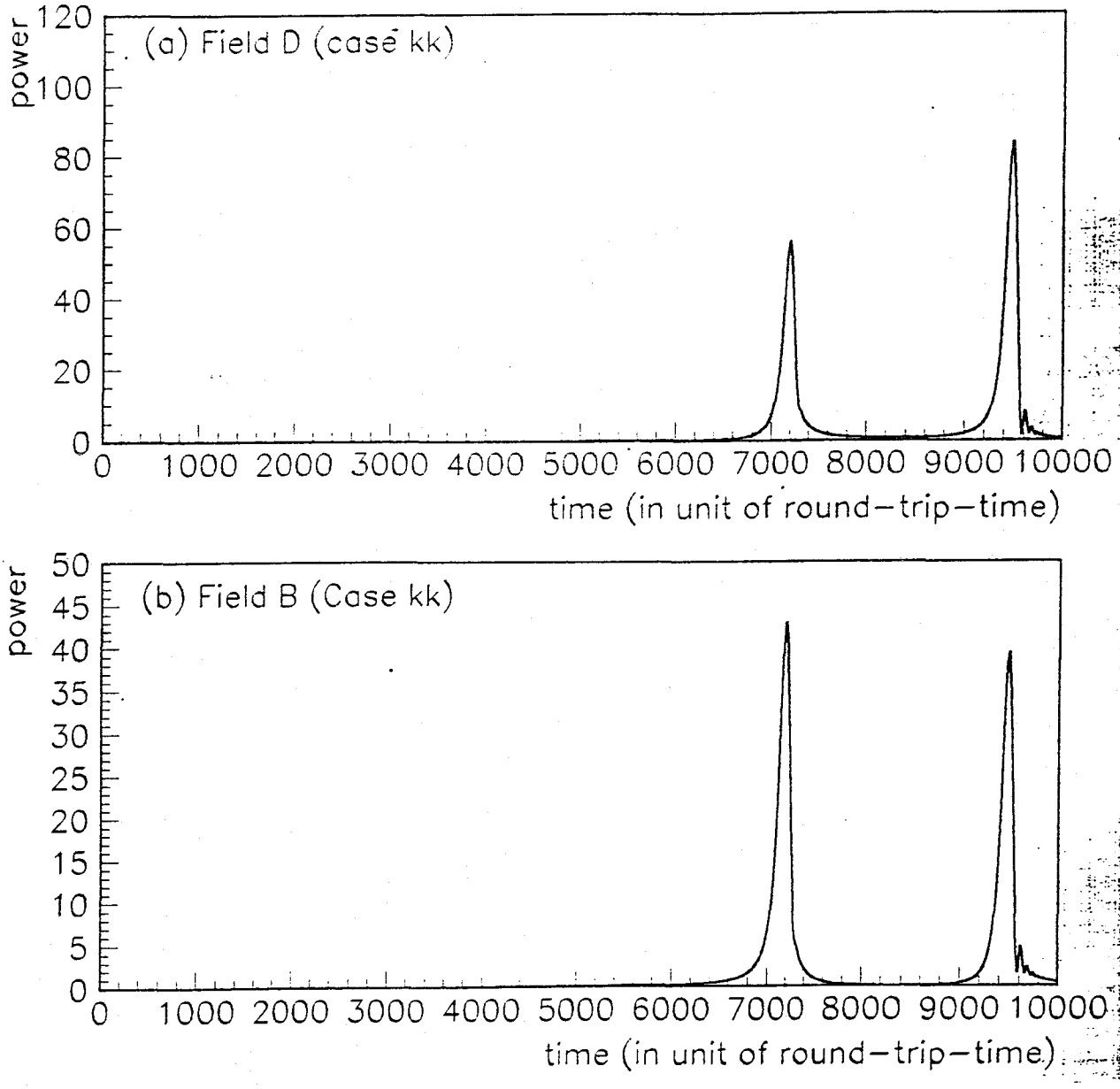

Figure 23: Evolution of fields (a) D and (b) B in case kk

Table 2: This shows numerical values of some important quantities for the dynamical simulation of 3-mirror coupled cavities under different situations. The *-marked cases aa,dd,ff-kk correspond to figures 2-9 respectively.

Case	$\jmath_0$	∇	P_1(DY)	$\jmath_1$(DY)	P_2(DY)	$\jmath_2$(DY)
aa*	324	$+0.588235\pi$	63	450	2.3	8262
bb	1497	$+0.5\pi$	66	1565	3	8298
cc	2827	$+0.4\pi$	76	2817	4.2	8351
dd*	4157	$+0.3\pi$	90	4046	6.5	8430
ee	5487	$+0.2\pi$	114	5222	13	8563
ff*	6817	$+0.1\pi$	115	6278	28	8815
gg*	7748	$+0.03\pi$	83	6870	55.1	9139
hh*	8083	$+0.0048\pi$	68.8	7042	68.8	9297
ii*	8147	$+0.0$	65	7073	72	9330
jj*	8211	-0.0048π	63.5	7102	74.5	9363
kk*	8419	-0.0204π	55.4	7192	83.5	9480

Quasistatic Curves for the corresponding dynamical case :

For a closer study of the physical nature of these curves, here I introduce what I call *Quasistatic curve* corresponding to each of the dynamical case described above. In the quasistatic (QS) expressions for the intra-cavity fields in Eqs.31 and 32, phases θ_r and θ_c are expressed in terms of the parameter $\jmath$ and thus in units of phases which could be acquired in a dynamical case in one rtt with $w_r = 1.7\mu$m/sec and $w_c = 1.0\mu$m/sec respectively. Then the power of each of these fields is plotted as a function of $\jmath$.

For example, the quasistatic curve for field D corresponding to the dynamical Cases gg and ii are plotted in Figures 24(a) and 24(b) respectively. Table 3 gives numerical values for some important quantities for the quasistatic curves corresponding to the dynamical cases described in Table 2.

In quasistatic curves, we plot something static in a *seemingly dynamical way*. These curves just represent how the intra-cavity fields in a static 3-mirror cavity vary if these are measured step-by-step by changing the phase offsets in the two cavities at each step in such a way that these changes exactly mimic the corresponding dynamical case.

So, these curves provide us the actual values of the phases for the resonance points,i.e., a static 3-mirror cavity shows resonance peaks for exactly these values of the phases. However, as also noted in case of high finesse cavities in sec.3, in dynamical cases, the peaks appear a few rtt after crossing these resonance points. For example, the quasi-static expressions above find their maximum values when $\theta_r = 2m\pi$ and $\theta_c = 2n\pi$ (*Double-resonance point*). According to the QS expressions the double-resonance peak should appear at $\jmath_0 = 324$, but dynamical equations give the peak value at $\jmath = 450$ (see Table 2 and Fig.16). Also the dynamical resonance curve has a peak value much less than the corresponding quasistatic value and it is characterised by lot of oscillations after crossing the peak, as explained in sec.3.

5.2 Analysis of results

We noted in sec. 4 that the effective finesse of a 3-mirror system is the highest while the beam operates in the double resonance condition (which happens in Case aa here) and is the lowest when the beam is on exact antiresonance in the arm cavity but on resonance in the recycling cavity (which happens

Table 3: This shows numerical values of some important quantities for the *quasistatic curves* of 3-mirror coupled cavities under different situations.

Case	y_0	P_1(QS)	y_1(QS)	P_2(QS)	y_2(QS)
aa	324	1350	324	2.3	8260
bb	1497	1290	1438	3	8295
cc	2827	1100	2693	4.2	8347
dd	4157	810	3927	6.5	8424
ee	5487	500	5113	12	8550
ff	6817	230	6188	28	8790
gg	7748	114	6807	58	9092
hh	8083	85.4	6988	76.8	9242
ii	8147	81	7020	81	9274
jj	8211	76.7	7052	85.3	9306
kk	8419	64.4	7148	102	9417

Table 4:

	$\Delta_1^c(DY)$	$\Delta_1^r(DY)$	$\Delta_2^c(DY)$	$\Delta_2^r(DY)$	$\Delta_1^c(QS)$	$\Delta_1^r(QS)$	$\Delta_2^c(QS)$	$\Delta_2^r(QS)$
aa	126	126	7938	−7708	0	0	7936	−7710
bb	68	1241	6801	−7672	−59	1114	6798	−7675
cc	−10	2493	5524	−7619	−134	2369	5520	−7623
dd	−111	3722	4273	−7540	−230	3603	4267	−7546
ee	−265	4898	3076	−7407	−374	4789	3063	−7420
ff	−539	5954	1998	−7155	−629	5864	1973	−7180
gg	−878	6546	1391	−6830	−941	6483	1344	−6878
hh	−1041	6718	1214	−6673	−1095	6664	1159	−6728
ii	−1074	6749	1183	−6640	−1127	6696	1127	−6696
jj	−1109	6778	1152	−6607	−1159	6728	1095	−6664
kk	−1227	6868	1061	−6490	−1271	6824	998	−6553

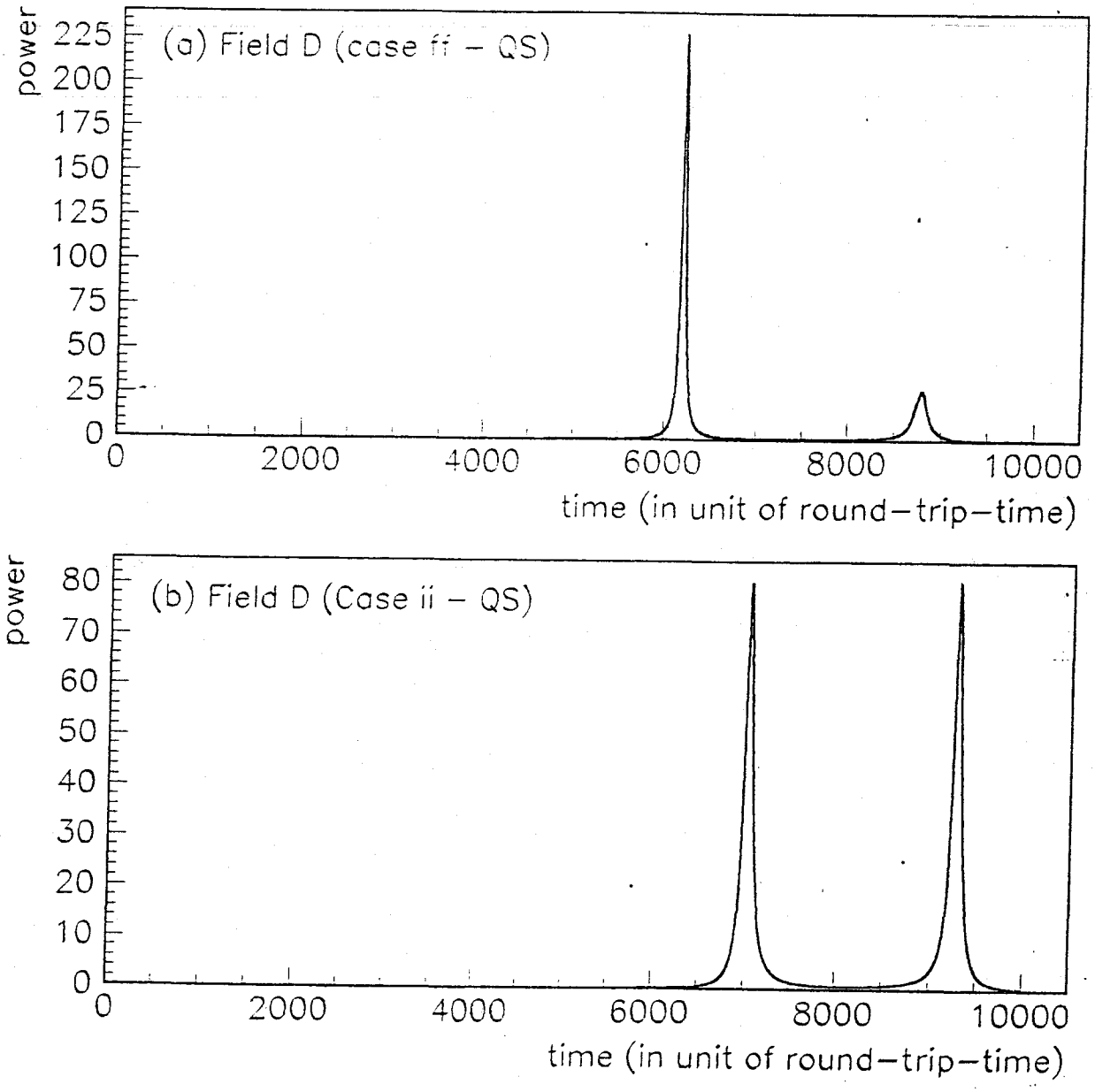

Figure 24: Quasistatic curves for the field D for (a) case aa and (b) case ii.

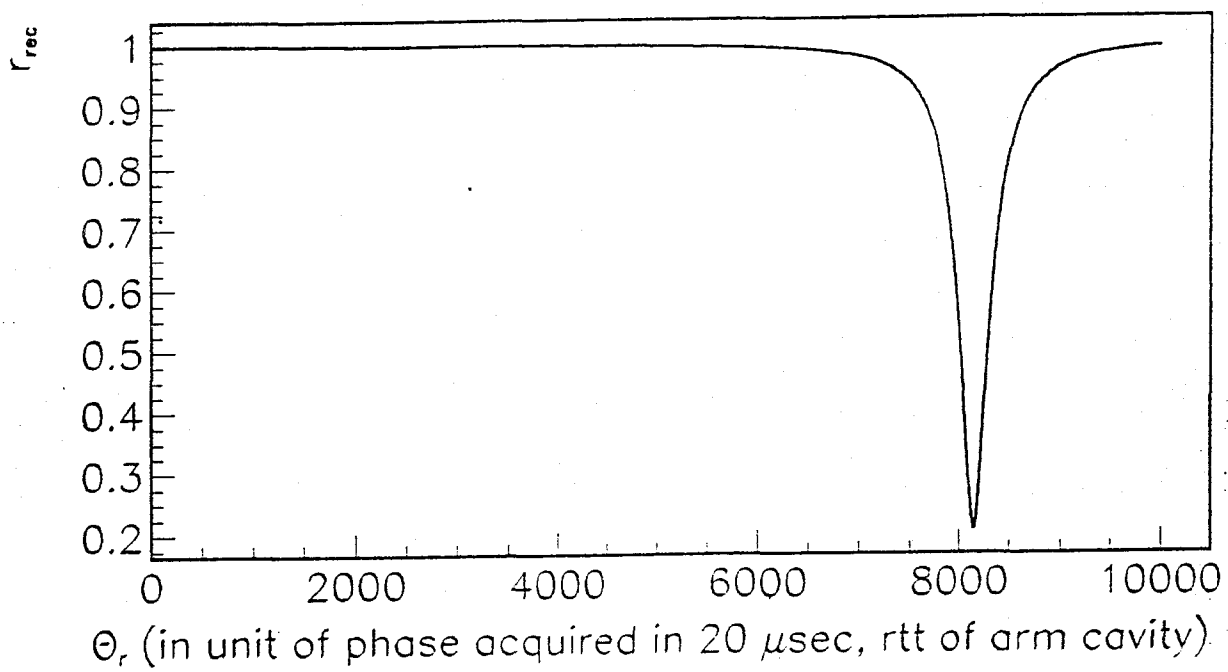

Figure 25: Equivalent reflectivity of the recycling cavity as a function of the phase offset in the same cavity. The points ($\jmath =$) 324 and 8147 for the phase offset correspond to $\theta_r = 2m\pi$ and $\theta_r = (2m+1)\pi$ respectively, as in Figures 16-23.

in case ii). In the following discussion, we refer to these two operating conditions as *highest finesse condition* and *lowest finesse condition* respectively.

The effective finesse as expressed in terms of $r_{\rm rec}$ can be plotted as a function of θ_r expressed in terms of $\jmath$ (for the same range covered in any of figures 16-23), as shown in Fig.25. As can be seen, the effective finesse is quite high except for a small range around $\jmath = 8147$ (where $\theta_r = (2m+1)\pi$).

On the basis of these observations, we can explain a few physical effects related to what we observe in figures 16-23:

- *first peak for the field, D*: We observe that as we go from Fig.16 to Fig.20 (i.e., from the highest to a lower finesse condition for the peak), the resonance power of the first peak for the field D increases initially (cases aa to ff) and then decreases again (cases ff to ii). As we go from the case aa to ff, the effective finesse decreases slowly, the sensitivity towards mirror movement reduces and thus the first peak grows up. However, for the cases gg to kk, the effective finesse is quite low and although the system is now much less sensitive towards the mirror movement, the maximum achievable power (quasistatic) itself can have a low value again because of the same reason of having low effective finesse.

- *second peak for the field, B*: For case aa (Fig.16), the B field is on its *individual resonance* at its second peak. Since the recycling cavity itself has a low finesse, the field achieves its quasistatic power (about 49.0) and show a typical resonance curve of a low-finesse 2-mirror cavity without

any oscillation after the resonance point is crossed. It remains to be so in the next few cases, but then start decreasing again, when its coupling with the D field becomes very important as the point $\theta_c = 2n\pi$ comes nearer to $\theta_r = (2m+1)\pi$.

- *second peak for the field, D*: For case aa and a few of the next cases, this peak is just the part that leaked into the arm cavity from the *individual resonance* power of the recycling cavity. This has a typical low-finesse shape and grows up as the corresponding peak for the field B decreases from its quasistatic value because of more coupling between two cavities at the operating condition of the second peak.

- *first peak for the field, B*: In case aa, it is just the double resonance curve and experiences the high value of effective finesse of the system with its own oscillations and by its failure to achieve the quasistatic power. It slowly grows up in power and sheds its high finesse like outlook as it approaches the $\theta_r = (2m+1)\pi$ point, the individual resonance point of the recycling cavity.

- *A Symmetry*: As can be expected, the arrangement of the curves are symmetrical about case hh, when the value of ∇ (the value of θ_c when $\theta_r = \pi$) is $+0.0048\pi$. That is why case kk ($\nabla = -0.0204$) is symmetrical with case gg ($\nabla = +0.03\pi$). From this symmetry one can easily guess what would happen if the point $\theta_c = 2n\pi$ is moved in between $\theta_r = (2m+1)\pi$ and $\theta_r = 2m\pi$.

  The only question is why the symmetry is about the case represented by $\nabla = +0.0048$(case hh) and *not* about that represented by $\nabla = 0.0$ (case ii). This is because of some assymetery introduced by the dynamical response of the system.i.e., due to the shifting of resonance curve from the actual resonance point. However, as can be seen from the corresponding quasistatic curve for the case ii (Fig.21), the symmetry could have been actually observed to be about case ii, in case the experiments were done in a static 3-mirror cavity by a step-by-step change in the phase offset. For similar reasons, this symmetry for the field B is about the case jj which corresponds to $\nabla = -0.0048$.

- *Reflected light*: Every resonance point is characterised by lot of oscillations in the reflected beam from the 3-mirror cavity as shown in Fig.26. The oscillations are most prominent when the beam is on double-resonance (first peak of case aa) and are much less as the operating condition shifts to a state of lower effective finesse (second peak of case aa and peaks of case ii).

- *Transmitted light*: As can be expected from analytical expressions, the evolution of peaks of the transmitted beams in the successive figures follow the same kind of description as those of the field D. Fig.27 shows peaks in the transmitted field for two cases, aa and ii. One may note that unlike the static case, the maximum transmission (among all other peaks) does not occur at the double resonance condition when the mirrors move.

- *Positioning of peaks in the quasistatic cases*: Here I discuss about the positions of occurrence of these peaks, which brings out an important physical point regarding the coupling of fields between the two cavities.

  Let us denote the values of θ_r and θ_c at the first and second peaks respectively by

$$\theta_r = 2\pi m + K_r \Delta_i^r \tag{57}$$

$$\theta_c = 2\pi n + K_c \Delta_i^c. \tag{58}$$

  where $i = 1, 2$ representing the first and second peaks respectively. The values of these Δs for both static and dynamic cases are presented in Table 4.

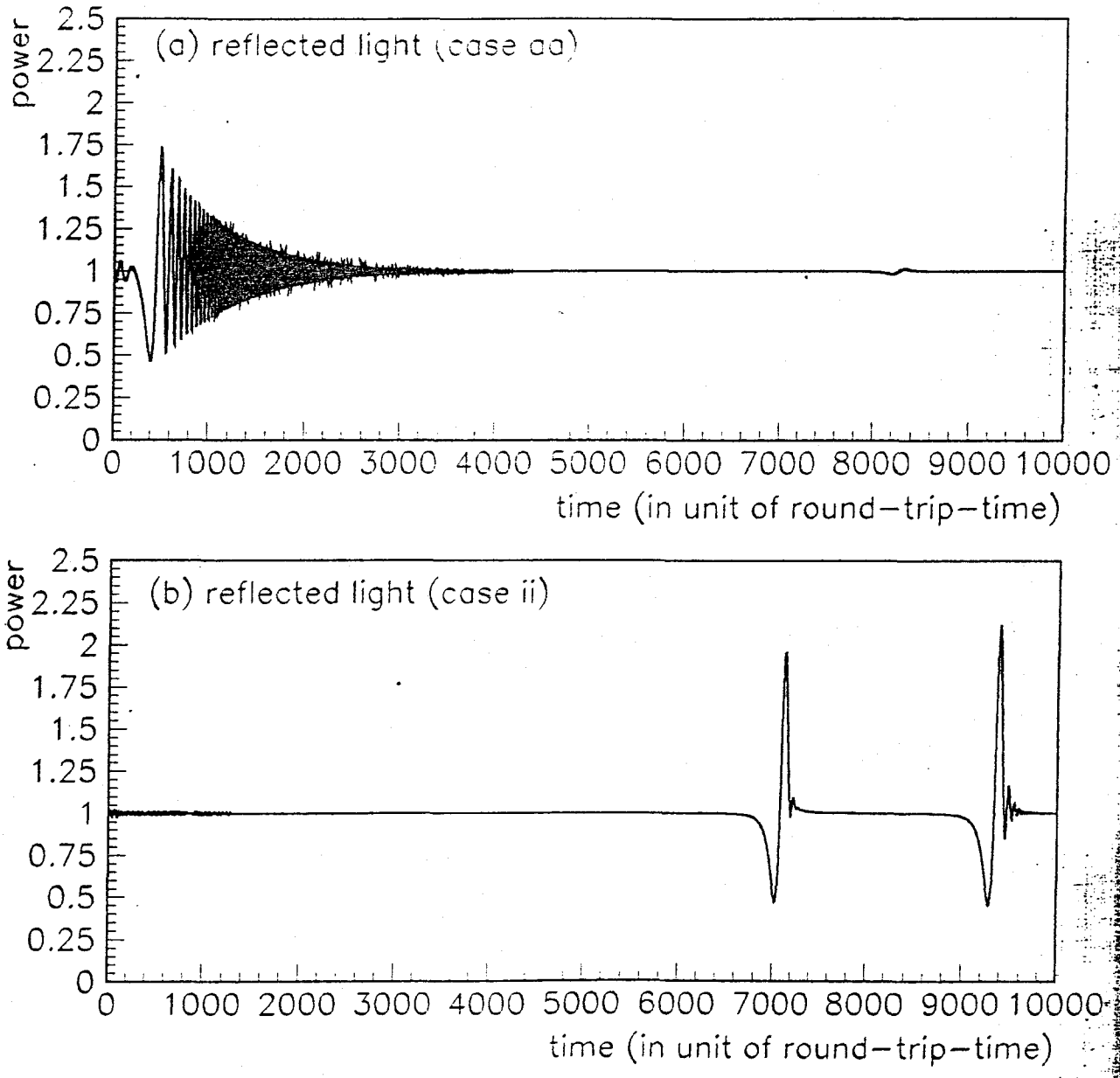

Figure 26: Reflected light in (a) case aa and (b) case ii.

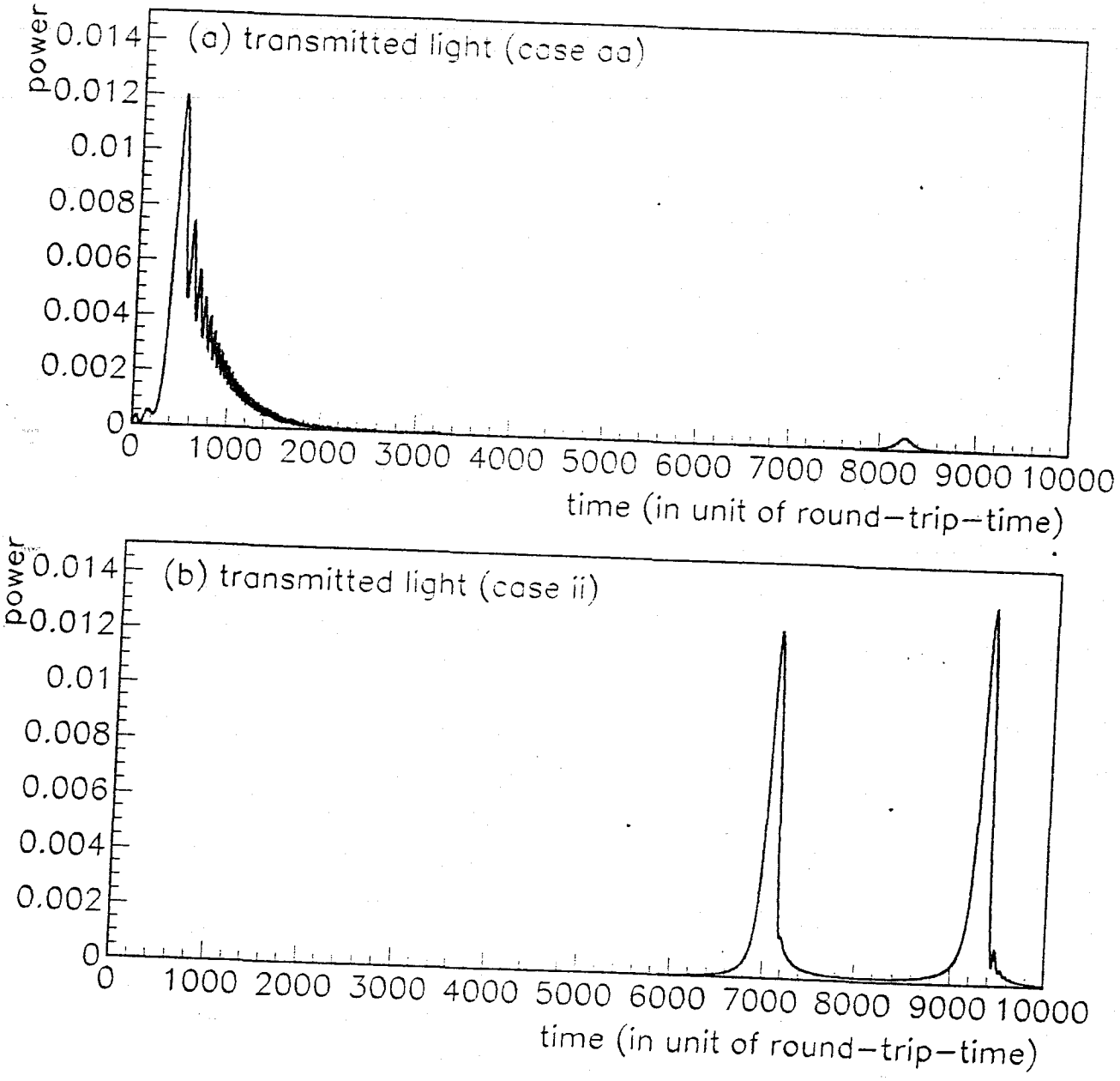

Figure 27: Transmitted light in (a) case aa and (b) case ii.

Let us also express the phase of the reflected light from the arm cavity as

$$\theta_{\rm refl} = (2m-1)\pi + K_r \Delta_i^{\rm refl}, \tag{59}$$

and plot $\Delta_i^{\rm refl}$ as a function of phase offset in the arm cavity (Δ_i^c) in Fig.28. For reasons to be explained soon, $\Delta_i^{\rm refl}$ is expressed in the same unit as that of θ_r as can be noticed above. It should be noticed that the (0,0) point of this plot corresponds to $\theta_c = 2n\pi$ and $\Delta_{\rm refl} = (2m+1)\pi$, representing the fact that the phase on reflection from an undercoupled cavity is an odd multiple of π on resonance.

By inspecting values of different quantities in Table 4 and referring to Fig.28, the following conclusion can be arrived at: In the case of a static 3-mirror cavity, a peak can always be found whenever Δ_i^c (phase offset in the arm cavity) is such that the corresponding value of $\Delta_i^{\rm refl}$ (phase on reflection from the arm cavity in excess of an odd multiple of π) exactly cancels the value of Δ_i^r (phase offset in recycling cavity in excess of an even multiple of π) at that operating condition, thus making the round-trip-phase in the recycling cavity equal to $(2m+1)\pi$, the condition for the individual resonance of the recycling cavity.

The essence of the statement is that a peak always apppears whenever the operating condition fulfills the requirement of the individual resonance condition of the recycling cavity (θ_r + phase on reflection = $(2m+1)\pi$): The arm cavity is individually resonant only at the double resonance condition. In all other cases, the phase offset in the arm cavity should change in a suitable way to ensure that to have a resonance peak.

Notice that a statement like the above was also made at the end of section III of Ref.[15], but their statement bears a restriction equivalent to $K_c \Delta_i^c \ll 1$ (i.e., phase offset in the arm cavity expressed in radian). The fact that the above rule is always true in the static case without any restriction on phase offset, can be tested for each of the cases presented in Table 4.

- *Positioning of peaks in the dynamical cases*: As we have already observed, while on double resonance (first peak of case aa), the gap between the dynamical peak ($j_1(DY) = 450$, Table 2) and the quasistatic peak ($j_1(QS) = 324$, Table 3): this represents the actual double resonance point) is about 126. The value of this gap reduces to almost nil for the case ii, when the operating condition at the point of appearance of the first peak corresponds to a low value of the effective finesse of the system. In conclusion, we can say, that even in the dynamical cases, the peaks try to position themselves in accordance with the rule described above, however, when the effective finesse is quite high, a large number of partial beams get stored for a long time, each of them bearing different phase information about the moving cavity and a combination of all these beams find a maximum point of their combined power at a point somewhat displaced from what would have been their original point of resonance in a static case. This displacement gets reduced if either the velocity or the effective finesse decreases.

In this section, we noted how combinations of peaks may appear in coupled cavities under general conditions of phase evolution in different constituent cavities. A power-recycled FP-type interferometer is rather a combination of two 3-mirror systems which are coupled together by a shared part of their recycling cavities. By observing a handful number of details of such successive peaks in these systems during *start-up* time, one may decide which way to control the cavities to bring them close to the desired operating condition before starting the linear/nonlinear locking procedure, thereby saving time and effort. Development of such an algorithm based on these information is currently under progress.

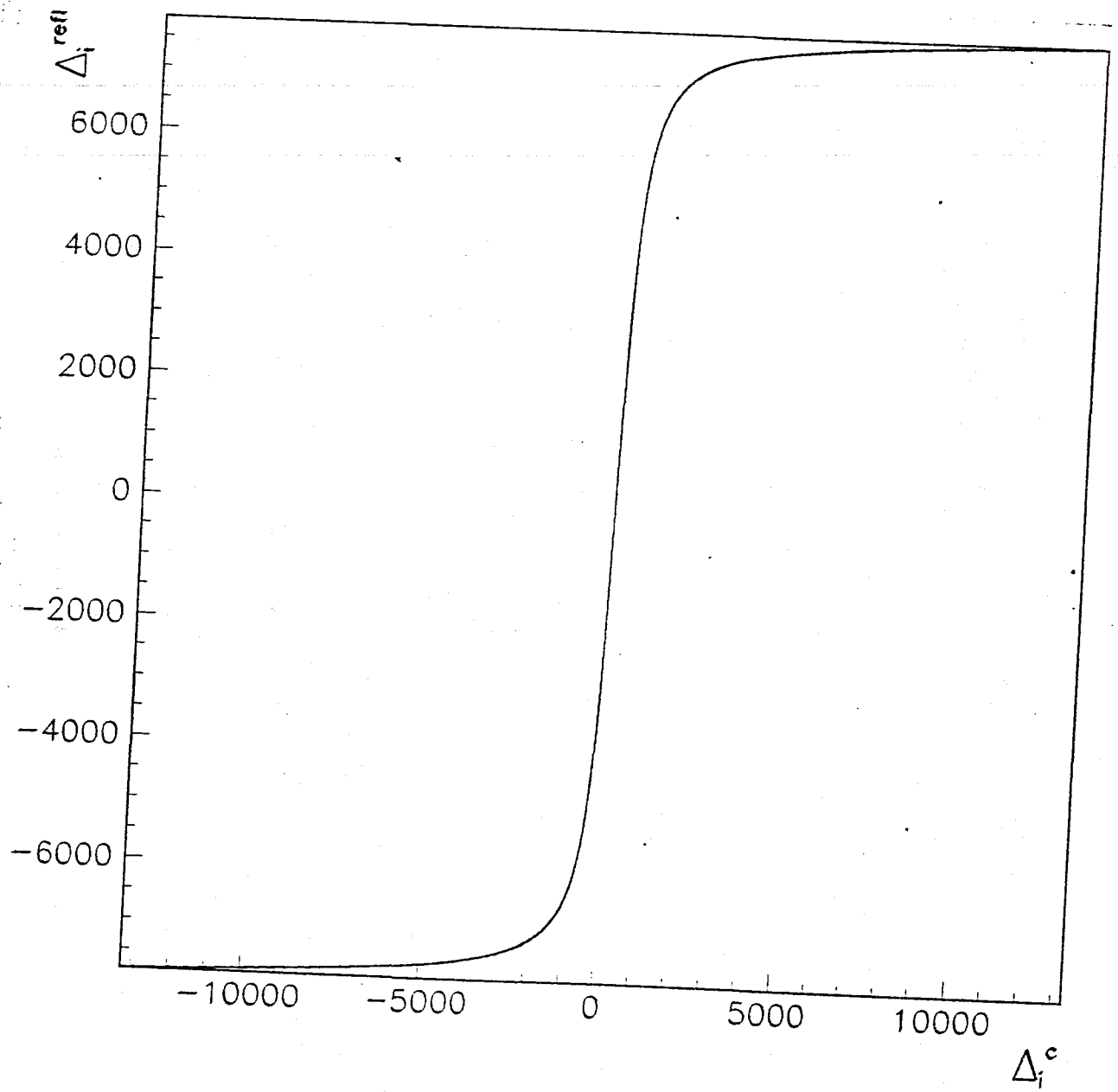

Figure 28: Phase acquired on reflection (in excess of $(2m+1)\pi$) from the arm cavity as a function of the phase offset (in excess of $2n\pi$) in the arm cavity. These are expressed in units of phases acquired by recycling and arm cavities respectively in a round-trip-time of the arm cavity due to mirror motion corresponding to $w_r = 1.7\mu$m/sec. and $w_c = 1\mu$m/sec.

6 Real-time simulation of power-recycled interferometric detectors

In this section, I apply all the techniques developed and applied in previous sections to the case of the full length power-recycled interferometer to develop a fast dynamical simulation code for it. The *in-line* arm cavity (that receives transmitted light through beam-splitter) and the *perpendicular* arm cavity (that receives the reflected light from the beam-splitter) are represented by X and Y respectively; These two letters appear in the subscripts of various quantities to make a differentiation between them.

We may think of the whole interferometer as a combination of two 3-mirror coupled cavity systems, which have a common shared part (that between recycling mirror and beam-splitter) in their recycling cavities. The recycling cavity X is the one between the recycling mirror and the corner mirror of the *in-line* arm cavity, whereas the recycling cavity Y is the one between the recycling mirror and the corner mirror of the *perpendicular* arm cavity. These two 3-mirror systems are coupled to each other through their shared part, so that some amount light always get exchanged between these two 3-mirror systems. In case of a static interferometer this exchange rate remains to be constant, however, in dynamical cases, the rate may vary depending on phase conditions of these systems, as we can see in the equations written in the following subsections.

6.1 Simplified problem : when only the end mirrors move

To investigate into the nature of coupling of fields between the two 3-mirror systems constituting the whole interferometer, let us first study a simple case when only the end mirrors of both the arm cavities move but other mirrors and beam-splitter remain to be static. The reflectivities of corresponding mirrors in both arms are assumed to be perfectly matched with each other and the beam-splitter is assumed to be of 50:50 type (exact). These simplifications are made for the time being to concentrate on only the physical effects due to dynamical coupling between the two 3-mirror systems, while keeping away other effects.

Let us also assume that the round-trip phases, θ_{ry} and θ_{rx}, in both the recycling cavities are set to be integral multiples of 2π, which ensures that whenever a particular arm cavity gets resonant (when θ_{cy} or θ_{cx} gets to a value of integral multiple of 2π), the corresponding recycling cavity also gets resonant (by receiving the extra π phase from reflection) and the corresponding 3-mirror system gets doubly resonant. The aim of locking the whole interferometer is to make both the component 3-mirror systems doubly resonant for the laser carrier frequency.

For such a simple case of dynamical interferometer, let us write down the equations for the intracavity fields with *short-rec-cav* approximation, thereby neglecting lengths l_0, l_x and l_y of parts of the recycling cavities (see Fig. 1) as compared to the full arm length of the interferometer. Both the arm lengths are considered to be same, $L = 3000m$. The intracavity fields at the input mirrors and travelling towards the end mirrors inside the respective arm cavities are represented by D_y and D_x respectively. The field at the recycling mirror and travelling towards the beam-splitter inside the common shared part of the recycling cavities is represented by B_{sh}. The error analysis of the small-rec-cav approximation in sec. 4 gives us the confidence that this should lead to a negligible level of error near resonance for any of the constituent 3-mirror cavities and thus for the whole interferometer:

$$B_{\rm sh}(t) = t_1 A + \frac{1}{\sqrt{2}} r_1 t_2 r_3 D_y(t-\tau) \exp j[\theta_{cy}(t-\tau/2)] + \frac{1}{\sqrt{2}} r_1 t_2 r_3 D_x(t-\tau) \exp j[\theta_{cx}(t-\tau/2)] - r_1 r_2 B(t), \quad (60)$$

$$D_x(t) = \frac{1}{\sqrt{2}} t_2 B(t) - r_2 r_3 D_x(t-\tau) \exp j[\theta_{cx}(t-\tau/2)], \quad (61)$$

$$D_y(t) = \frac{1}{\sqrt{2}} t_2 B(t) - r_2 r_3 D_y(t-\tau) \exp j[\theta_{cy}(t-\tau/2)], \quad (62)$$

Note that the round-trip times in both the arm cavities are assumed to be same and equal to τ. In the actual design of an interferometer, however, the FP cavities in the arms may be physically different in length even by several meters. We can say rightaway that as long as this difference is of the order of 0.4% (the length of recycling cavity as compared to that of the arm in case of VIRGO), the error would remain to be in the same negligible level as that of small-rec-cav approximation. We can reasonably hope that the difference in round-trip-times in actual long-baseline interferometers will not be too much higher than this and thus we can use such an approximation without making much error in our simulation.

These equations can be rearranged and written as

$$B_{\rm sh}(t) = \frac{r_1 t_2 r_3}{\sqrt{2}(1+r_1 r_2)} D_y(t-\tau) \exp j[\theta_{cy}(t-\tau/2)] + \frac{r_1 t_2 r_3}{\sqrt{2}(1+r_1 r_2)} D_x(t-\tau) \exp j[\theta_{cx}(t-\tau/2)] + \frac{t_1 A}{(1+r_1 r_2)} \quad (63)$$

$$D_y(t) = \mathcal{A} + r_3 \beta D_y(t-\tau) \exp j[\theta_{cy}(t-\tau/2)] + r_3 \mathcal{C} D_x(t-\tau) \exp j[\theta_{cx}(t-\tau/2)], \quad (64)$$

$$D_x(t) = \mathcal{A} + r_3 \beta D_x(t-\tau) \exp j[\theta_{cx}(t-\tau/2)] + r_3 \mathcal{C} D_y(t-\tau) \exp j[\theta_{cy}(t-\tau/2)], \quad (65)$$

$$(66)$$

where

$$\mathcal{A} = \frac{t_1 A}{1+r_1 r_2}, \quad (67)$$

$$\beta = r_2 + \mathcal{C} = r_2 + \frac{r_1 t_2^2}{2(1+r_1 r_2)} \quad (68)$$

$$\mathcal{C} = \frac{r_1 t_2^2}{2(1+r_1 r_2)}. \quad (69)$$

The numerical values of β and $\mathcal{C}$ for the chosen parameter-values for VIRGO are about ≈ 0.969367 and 0.029367 respectively. In case both the arm-cavities change in length in the same manner, their fields also evolve in the same way and we can set $D_y = D_x$ and get back the 3-mirror coupled cavity equation. We can then identify

$$r_{\rm rec} = \beta + \mathcal{C} \approx 0.998733. \quad (70)$$

Under such a condition, the nature of the field evolution shows a high finesse behaviour corresponding to $r_c = r_{\rm rec}$ as shown in Fig.29(a) for either D_x or D_y. One may note that the field evolution behaviour is exactly like that in Fig.6 for the field F in a 2-mirror cavity of $r_c = 0.998733$ or the field D in the 3-mirror cavity considered by us in sec.4: the only difference being in power level - a factor of half - originating from the presence of the beam-splitter in the interferometer.

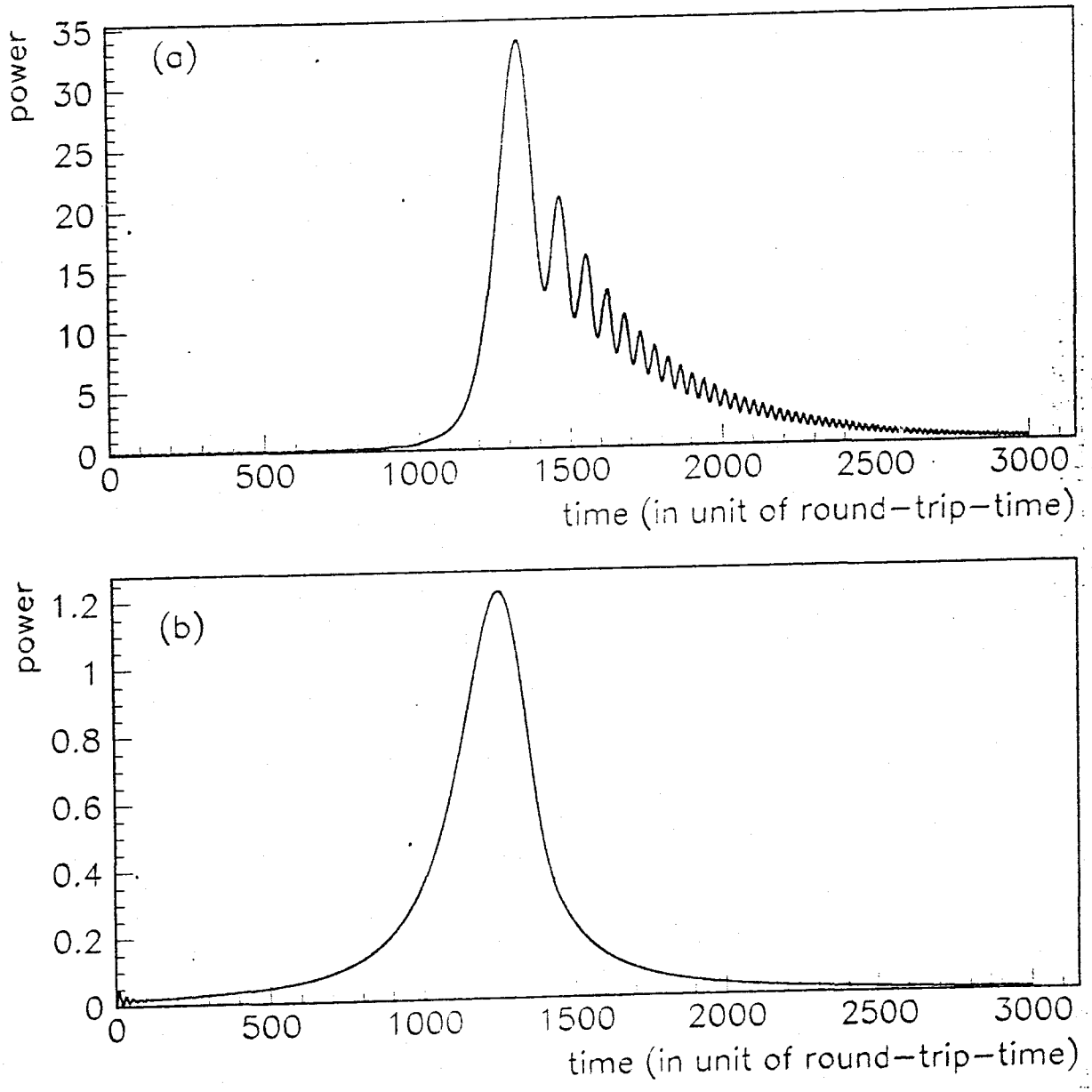

Figure 29: (a) Resonance peak for either of the fields D_y or D_x when both the 3-mirror systems get doubly resonant at the same time, (b) Peak in power of either D_y or D_x when only the corresponding 3-mirror system get doubly resonant but the other 3-mirror system remains far in out-of-resonace. In both the figures, the input power is one unit.

If the motion in the two arm cavities are out of phase with each other, each arm cavity gets resonant on its own at different points in time and this resonance shows a low finesse behaviour corresponding to $r_c = \mathcal{B}$ as shown in Fig.29(b). The contribution of coupling of the nonresonant cavity to the resonant one is negligible in that case. Whenever the values of θ_{cy} and θ_{cx} get close-by together and move towards the resonance point, fields in the arm cavities start getting coupled to each other and the term with the coupling factor $\mathcal{C}$ becomes important.

We may thus conclude that in between the two extreme cases described above, whenever the two sets of 3-mirror coupled cavities cross their individual resonance points (double or others) very close-by in time, the fields strongly couple with each other and their evolution always shows characteristics typical of 2-mirror cavities with a value of r_c in between $\mathcal{B}$ and $\mathcal{B} + \mathcal{C}$. The exact profiles of the resonance peaks in individual arm cavities may, however, differ from each other depending on how close-by in time and with what velocities of their constituent mirrors, the two systems cross their resonant points.

If the finesse of the arm cavities are increased, that leads to an increased value of β but a reduced value for $\mathcal{C}$ (one should ,however, note that if arm cavity finesse is increased, one also has to change r_1 to have optimum recycling of light). But that does not make coupling between the arms on resonance less important than the case of low finesse arm cavities because the power stored is much higher in high finesse arm cavities.

The situation when the fields in the arms couple with each other, is the one which is important for the purpose of locking. To simulate such or other situations, the following algorithm is developed.

6.2 Simulation procedure for the whole interferometer

The simulation procedure to be described here is based on the *state vetor* representation of the intra-cavity fields of the full interferometer. This particular way of solving problems have been utilized in many multi input/output cases in the field of digital filtering and signal processing (see chapter 4 and 12 of Jackson[10]). The method is presented in three parts: first, the equations for the simple case of the previous section is written down utilizing DFA based on JAS. Next the equations are generalised by incorporating dynamical changes in the recycling cavity and also other asymmetries due to differing mirror reflectivities. At the end the simulation procedure for both these cases are discussed together.

6.2.1 Equations for the simple case

In order to express the main points of the simulation procedure in an easier way, let us first consider the simple case when (i) only end mirrors move, (ii) θ_{rx} and θ_{ry} are set to integral multiples of 2π, (iii) corresponding mirror reflectivities in both arms are perfectly matched with each other, and (iv) the beam-splitter is of (exactly) 50:50 type, (v) beam-splitter is static, let us write down Eqs.(65) and (66) with the following state-vector representation:

$$\underline{D}(t+\tau) = \underline{A} + \underline{R}\,\underline{\mathrm{Exp}}(t+\tau/2)\,\underline{D}(t), \qquad (71)$$

where

$$\underline{D}(t) = \begin{pmatrix} D_y(t) \\ D_x(t) \end{pmatrix} \tag{72}$$

$$\underline{A} = A \begin{pmatrix} 1 \\ 1 \end{pmatrix} \tag{73}$$

$$\underline{R} = r_3 \begin{pmatrix} \beta & \mathcal{C} \\ \mathcal{C} & \beta \end{pmatrix} \begin{pmatrix} \exp j[\Phi_{cy}] & 0 \\ 0 & \exp j[\Phi_{cx}] \end{pmatrix} \tag{74}$$

$$\underline{\mathrm{Exp}}(t) = \begin{pmatrix} \exp j[\frac{4\pi}{\lambda} v_{3y} t] & 0 \\ 0 & \exp j[\frac{4\pi}{\lambda} v_{3x} t] \end{pmatrix} \tag{75}$$

where it is assumed that for a short time the end mirrors are moving with velocities v_{3y} and v_{3x} respectively for arms Y and X; Φ_{cy} and Φ_{cx} being initial round-trip phase offsets in arm cavities.

6.2.2 Equations for the generalised case

When all mirrors move, we can write down the coupled equations of the intra-cavity fields in arms by also incorporating all asymetries due to differing mirror reflectivities and moving beam-splitter as:

$$\underline{D}(t+\tau) = \underline{A}(t+\tau) + \underline{R}(t+\tau)\ \underline{\mathrm{Exp}}(t+\tau/2)\ \underline{D}(t). \tag{76}$$

Various quantities in Eq.76 are defined as follows. Note that, in the subscripts of these quantities, letters c and r represent arm cavity and recycling cavity respectively; numbers 1,2,3 and b represent recycling mirror, input mirror, end mirror and beam-splitter respectively; as already stated, x and y refer to recycling or arm cavitities of the 3-mirror systems X and Y respectively :

$$\underline{A}(t) = \frac{t_1 A}{\chi(t)} \begin{pmatrix} r_b t_{2y} \exp j[\theta_{ry\uparrow}(t)] \\ t_b t_{2x} \exp j[\theta_{rx}(t)] \end{pmatrix} \tag{77}$$

$$\chi(t) = 1 + r_1 r_b^2 r_{2y} \exp j[\theta_{ry\uparrow}(t) + \theta_{ry\downarrow}(t)] + r_1 t_b^2 r_{2x} \exp j[2\theta_{rx}(t)] \tag{78}$$

$$\underline{R}(t) = \begin{pmatrix} \beta_y & \mathcal{C}_x \\ \mathcal{C}_y & \beta_x \end{pmatrix} \begin{pmatrix} \exp j[\phi_{cy}] & 0 \\ 0 & \exp j[\phi_{cx}] \end{pmatrix} \tag{79}$$

$$\underline{\mathrm{Exp}}(t) = \begin{pmatrix} \exp j[\frac{4\pi}{\lambda} W_{cy} t] & 0 \\ 0 & \exp j[\frac{4\pi}{\lambda} W_{cx} t] \end{pmatrix} \tag{80}$$

$$\beta_y = r_{2y} r_{3y} + \frac{1}{\chi(t)} r_1 r_b^2 t_{2y}^2 r_{3y} \exp j[\theta_{ry\uparrow}(t) + \theta_{ry\downarrow}(t)] \tag{81}$$

$$\beta_x = r_{2x} r_{3x} + \frac{1}{\chi(t)} r_1 t_b^2 t_{2x}^2 r_{3x} \exp j[2\theta_{rx}(t)] \tag{82}$$

$$\mathcal{C}_x = \frac{1}{\chi(t)} r_1 r_b t_b t_{2y} t_{2x} r_{3x} \exp j[\theta_{rx}(t) + \theta_{ry\uparrow}(t)] \tag{83}$$

$$\mathcal{C}_y = \frac{1}{\chi(t)} r_1 r_b t_b t_{2y} t_{2x} r_{3y} \exp j[\theta_{ry\downarrow}(t) + \theta_{rx}(t)]. \tag{84}$$

The phase factors in the above equations can be expressed in the following form if we assume that for a short span of time, $N\tau$ (where N is some number to be determined numerically) all mirrors are moving with constant velocities (Note: this assumption on arm cavities have been already used in

writing down Eq.76) :

$$\theta_{ry\uparrow}(t) = \phi_{ry}/2 + \frac{2\pi}{\lambda}(W_{ry}t + V_{bx}t) \quad (85)$$

$$\theta_{ry\downarrow}(t) = \phi_{ry}/2 + \frac{2\pi}{\lambda}(W_{ry}t + V_{by}t) \quad (86)$$

$$\theta_{rx}(t) = \phi_{rx}/2 + \frac{2\pi}{\lambda}W_{rx}t \quad (87)$$

$$\theta_{cy}(t) = \phi_{cy}/2 - \frac{2\pi}{\lambda}W_{cy}t \quad (88)$$

$$\theta_{cx}(t) = \phi_{cx}/2 - \frac{2\pi}{\lambda}W_{cx}t \quad (89)$$

where ϕ-s are initial round-trip phase offsets in various cavities and W-s are relative velocities defined as

$$W_{ry} = V_{2y} - V_1 \quad (90)$$

$$W_{rx} = V_{2x} - V_1 \quad (91)$$

$$W_{cy} = V_{3y} - V_{2y} \quad (92)$$

$$W_{cx} = V_{3x} - V_{2x} \quad (93)$$

All the V-s above are magnitudes of velocities of the corresponding mirrors wrt the initial position of the beam-splitter; V_{bx}, V_{by} are components of the velocity of the beam-splitter wrt its initial position, as shown Fig.30. It should be noted that if the beam splitter moves, light beams do not retrace their path while returning to the beam splitter. This may lead to distortion of beams in the transverse direction and thus generation of higher order modes. In this paper, however, we confine our attention only to the longitudinal effects. Investigations related to the transverse effects are going on at present.

6.2.3 steps of simulation

step 1: Time is sliced into equal intervals of width $\Delta = N\tau$, so that any time $t_i = iN\tau$, where i is an integer.

step 2: During the time interval (t_i, t_{i+1}), the rates of the changes of phase offsets in arm cavities, v_{3x} and v_{3y} (simple case) or W_{ry}, W_{rx}, W_{cy}, W_{cx}, V_{by} and V_{bx} (generalised case) are assumed to be constants.

step 3: The phases, Φ_{cx}, Φ_{cy} (simple case) or ϕ_{cx}, ϕ_{cy} (for generalised case) are fixed to the following constant values during (t_i, t_{i+1}):

$$\Phi_{cx} = \Theta_{cx}(t_i) \quad (94)$$

$$\Phi_{cy} = \Theta_{cy}(t_i) \quad (95)$$

$$\phi_{cx} = 2\theta_{cx}(t_i) \quad (96)$$

$$\phi_{cy} = 2\theta_{cy}(t_i) \quad (97)$$

(98)

step 4: (*Freezing-the-finesse* for the generalised case) In the matrix $\underline{R}$ and $\underline{A}$ are set to the following constant matrices during the same time-interval :

$$\underline{R} = \frac{1}{2}\left(\underline{R}(t_i) + \underline{R}(t_{i-1})\right) \quad (99)$$

$$\underline{A} = \underline{A}(t_{i-1}). \quad (100)$$

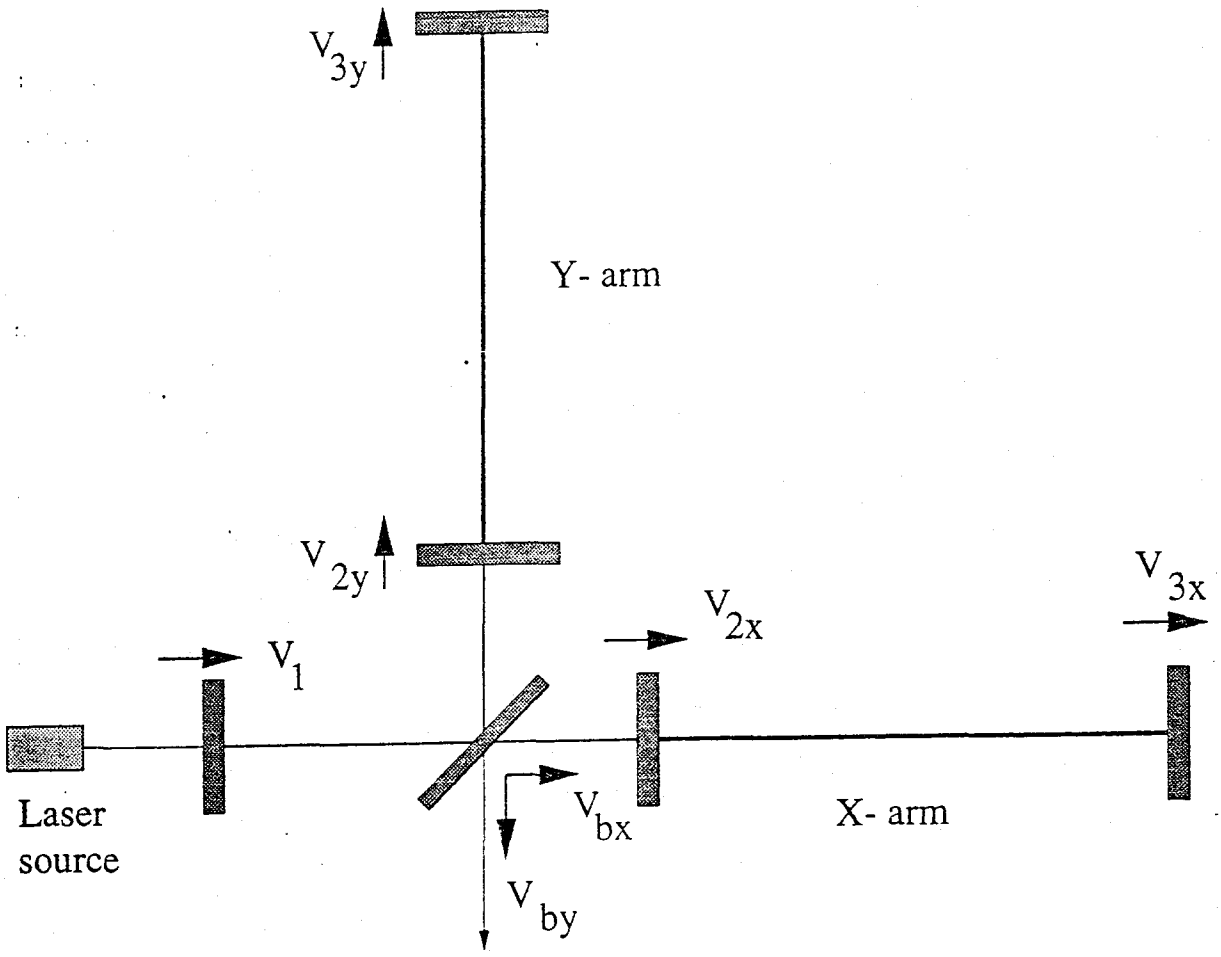

Figure 30: Notation for the mirror velocities wrt the initial position of the beam-splitter. The arrows indicate positive signs for V-s in Eqs.90-93.

step 5: (*Jump-and-sump*) Now by performing the equivalent algebraic operations of JAS as described in section 3 on either Eq.71 (simple case) or Eq.76 (for which $\underline{R}$ and $\underline{A}$ are now constant matrices), we can arrive at the follwing equation equivalent to Eq.27:

$$\underline{D}(t+N\tau) = \underline{R}^N \underline{E}\, \underline{D}(t) + (\underline{U}-\underline{R})^{-1}\left[(\underline{U}-\underline{R}^N) + \underline{R}\,\underline{S}\,\underline{\xi} - \frac{1}{2}(N^2-1)\underline{R}^N\,\underline{\xi}\right]\underline{A} \quad (101)$$

where

$$\underline{U} = \begin{pmatrix} 1 & 0 \\ 0 & 1 \end{pmatrix} \quad (102)$$

$$\underline{E} = \begin{pmatrix} \exp(\xi_y N^2/2) & 0 \\ 0 & \exp(\xi_x N^2/2) \end{pmatrix} \quad (103)$$

$$\underline{\xi} = \begin{pmatrix} \xi_y & 0 \\ 0 & \xi_x \end{pmatrix} \quad (104)$$

$$\underline{S} = (\underline{U}-\underline{R})^{-1}.\left[(N-\frac{1}{2})\underline{U} - 1.5\underline{R}^{N-1}\right] + (\underline{U}-\underline{R})^{-2}\left[\underline{R}^{N-1} - \underline{R}\right] \quad (105)$$

$$\xi_y = j\frac{4\pi v_{3y}\tau}{\lambda} \quad (106)$$

$$\xi_x = j\frac{4\pi v_{3x}\tau}{\lambda} \quad (107)$$

The Eq.101 is now applied to calculate the value of the field inside the arm cavities.

step 6: In the next step, the same procedure is performed by replacing $i \leftarrow i+1$ and with changed (if these change) mirror velocities.

The error levels are found to be almost at the same levels as these are in 3-mirror cavities (section IVC) when both cavities achieve either the highest (Fig.14) or the lowest finesse (Fig.15) conditions at the same time.

Fig.31(a) shows dynamical curve for the field D_y for the case when the 3-mirror system Y gets doubly resonant ahead of system X with a time-gap corresponding to a phase difference of $\pi/100$, while $W_{ry} = W_{cy} = W_{rx} = W_{cx} = 1\mu$m/sec and the beam-splitter is assumed to be static. The relative error by DFA as compared to equations based on only *small-rec-cav* approximation is shown in Fig.31(b). The difference between power levels of D_y and D_x is shown in Fig.32.

Fig.33(a) shows the peak in field D_y when the 3-mirror system Y gets to the lowest finesse condition of 'antiresonant in arm cavity but resonant in the recycling cavity' ahead of system X with a time-gap corresponding to a phase difference of $\pi/100$, while $W_{ry} = W_{cy} = W_{rx} = W_{cx} = 1\mu$m/sec and the beam-splitter is assumed to be static. The relative error by DFA as compared to equations based on only *small-rec-cav* approximation is shown in Fig.33(b). Note that in this case there is no difference between power levels of D_x and D_y could be found even at a level of 10^{-4} unit of power. This is another manifestation of the low-finesse characteristics of the operating condition for the beam when partial beams do not get stored for a long time to make any difference between two coupled cavities.

6.3 Proposal for a relatively easier start-up procedure for long baseline power-recycled interferometers

One problem with the power-recycled interferometer with suspended mirrors is to bring all of its constituent cavities near to the operating condition starting from time zero. As already noted, the

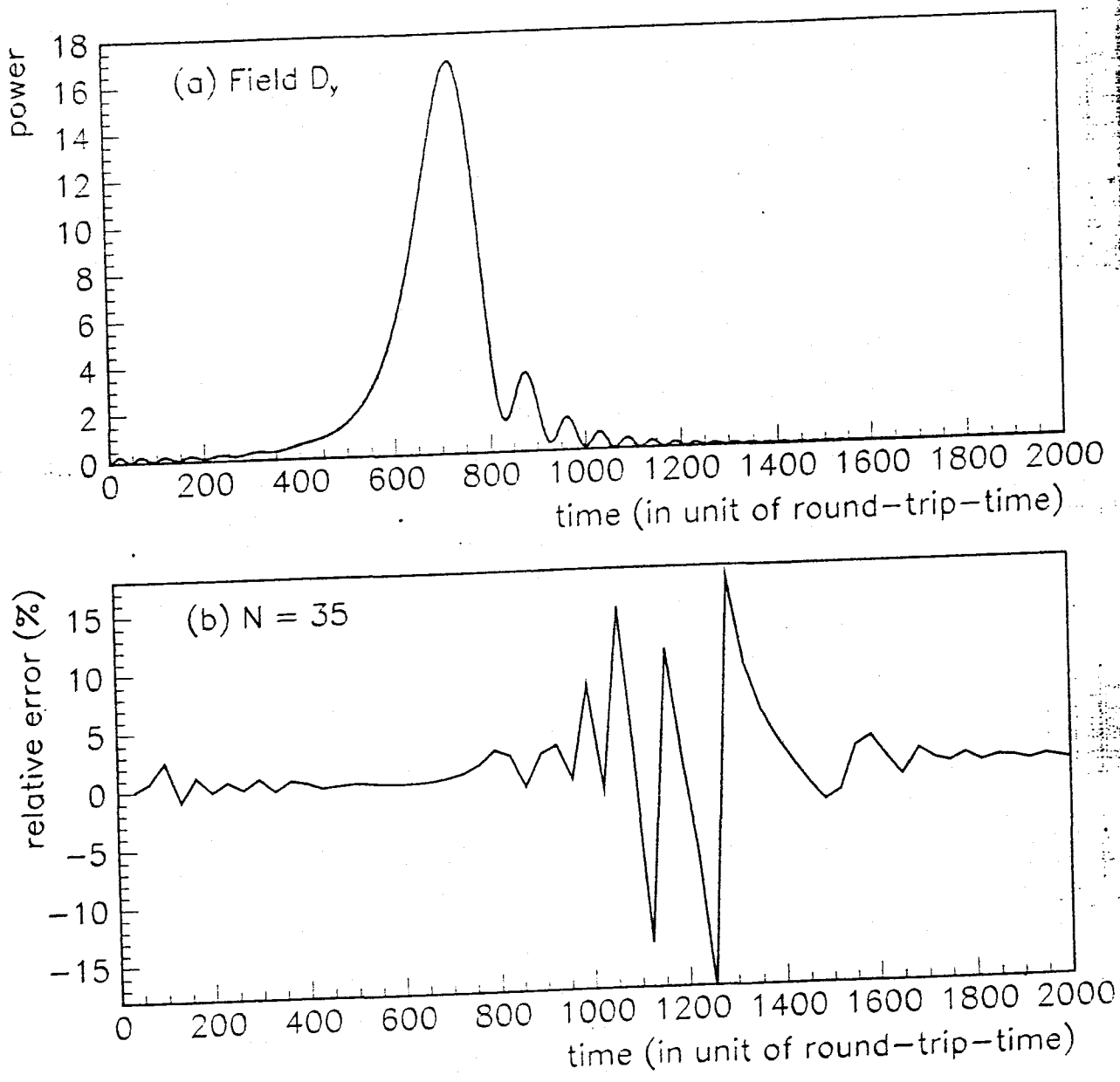

Figure 31: (a) Resonance peak for the field D_y when 3-mirror system Y gets doubly resonant ahead of system X with a time gap equivalent to a phase difference of $\pi/100$, while mirrors move such that $W_{ry} = W_{rx} = W_{cx} = W_{cy} = 1\mu$m/sec and beam-splitter is assumed to be static. Input power is one unit. (b) Relative error by DFA based on JAS and FTF wrt only *small-rec-cav* approximation in computing such a peak. The relative error increases for a short time while the field amplitude is very small; This 'increase' is thus unimportant.

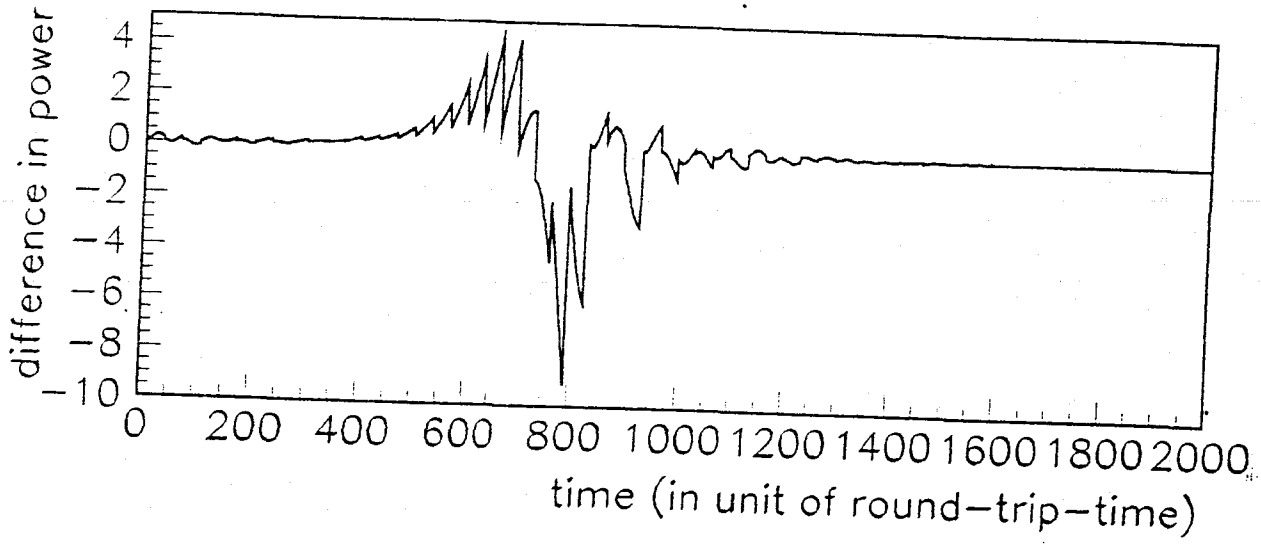

Figure 32: The difference between resonant power levels of fields D_y and D_x under the condition described for Fig.31.

mirrors, by getting excited by the residual seismic noise, may oscillate around their equilibrium points at very low frequency with an amplitude of some tens of wavelength. A local damping system may reduce this amplitude to a fraction of a wavelength, but that is not sufficient when we consider changes in the relative positions of the mirrors which may also be caused by slow thermal drifts. To maintain the appropriate operating condition of the interferometer, it thus requires an active global control of relative changes of the mirror distances in various cavities.

Sensing schemes based on the phase modulation of light [23, 24] have thus been devised in order to produce signals corresponding to small deviations from perfect interference and then to use these signals to feed back to the laser frequency and/or the mirror control system to bring back the system to the perfect operating condition. Under these schemes, the phase of the laser light is modulated at a radio frequency, typically of the order of 10MHz. The effect of this modulation is to impose effectively two sidebands on the laser, $\omega_0 \pm \omega_m$; ω_0, ω_m are the carrier and modulation frequencies respectively. The lengths, l_0, l_y and l_x (in Fig.1) are so chosen that both the carrier and sidebands are resonant in the recycling cavity. The operating condition of the sidebands in the arm cavity is generally chosen to be somewhere out of resonance; The best condition seems to be the exact antiresonance. The difference between l_y and l_x should be suitably chosen so that it allows sideband light to be transmitted to the output port while that port remains to be dark for the carrier. If, for some reason, the arm-lengths of the interferometer get distorted, some amount of carrier light exit the outport port where it beats against the sidebands. This light is detected and demodulated with a mixer. The signal thus generated is called the Pound-Drever signal[25]. This signal is linear wrt either frequency or length deviation in a small range around the perfect resonance condition. This range is wider for a system of lower effective finesse and thus controlling is relatively easier in such a case.

It should, however, be noted that these schemes work only when the interferometer is very close to its desired resonant condition and a Pound-Drever signal gets generated. It is, therefore, also important to plan a method which, starting from time zero, can act on all of the coupled cavities

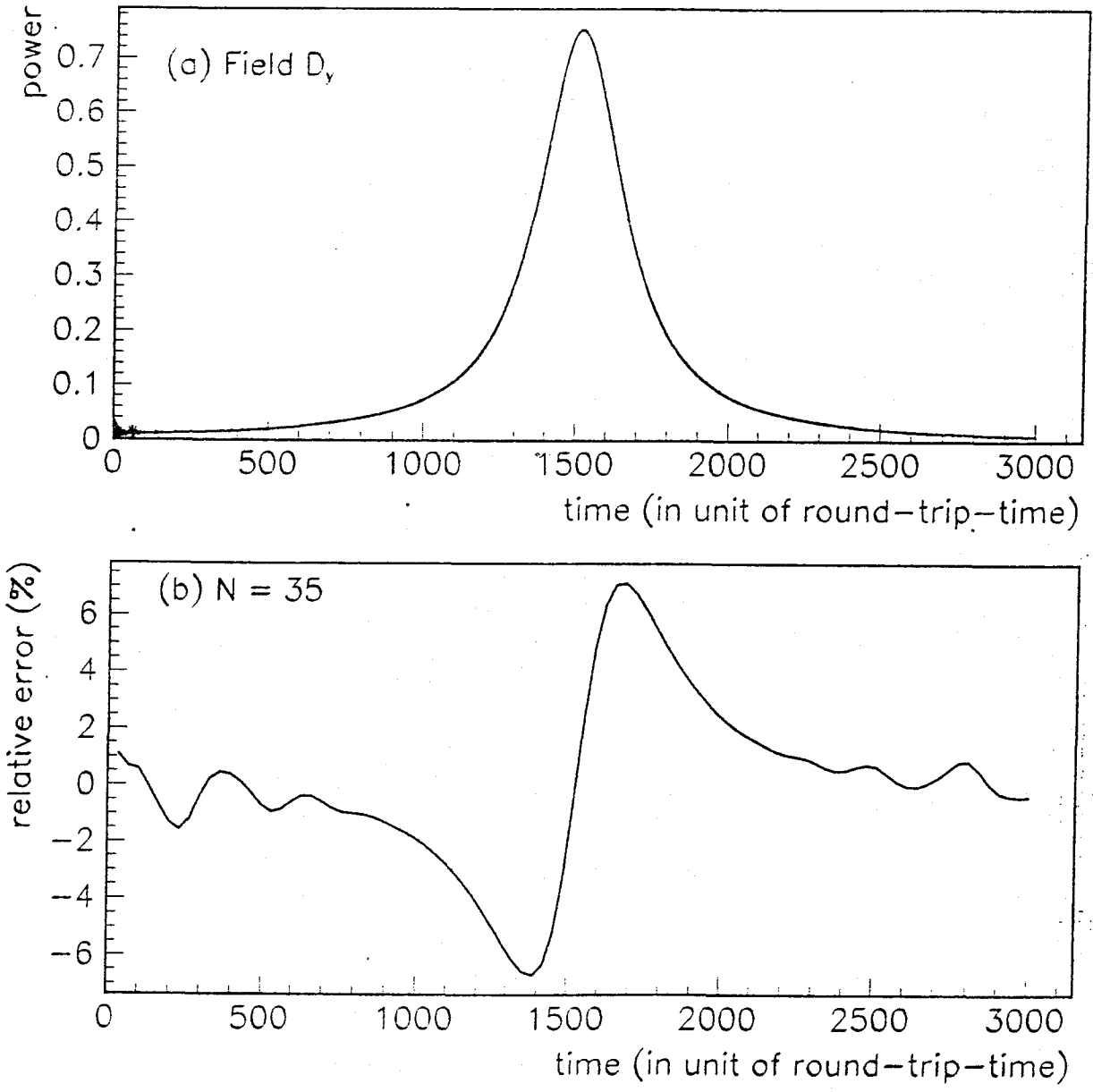

Figure 33: (a) Peak in power of the field D_y when 3-mirror system Y gets to a condition of resonance in recycling cavity but exact antiresonance in arm cavity ahead of system X with a time gap equivalent to a phase difference of $\pi/100$, while mirrors move such that $W_{ry} = W_{rx} = W_{cx} = W_{cy} = 1\mu$m/sec and beam-splitter is assumed to be static. Input power is one unit. (b) Relative error by DFA based on JAS and FTF wrt only *small-rec-cav* approximation in computing such a peak.

to bring them very near to this condition so that the Pound-Drever signal gets generated and the above-mentioned locking scheme can start its operation. A lot of time and effort can be saved if we are able to develop an efficient procedure to do that.

The power-recycled interferometer with FP arm cavities can be thought to be a combination of two 3-mirror cavity systems sharing a common part in their recycling cavity. Right in the beginning, when all mirrors are moving arbitrarily, one may encounter resonance peaks under a variety of conditions. One needs to recognise and try to get near the right peak (double resonance) among many others, in both of these 3-mirror components. Dynamical situation makes the job difficult. One needs to know if some odd-looking resonance peak gets its shape out of mirror motion or a bad operating condition. An algorithm can be developed on the basis of the physical points described in section 5 and can be utilized for this purpose. For example, by observing time difference between two successive peaks and their profiles, one may decide which way to control the cavities to get to the desired goal.

If we assume that corresponding mirror reflectivities are matched with each other, then most of the time under the *starting-up* condition, the field evolution in arm-cavities obeys Eqs.(65) and (66). The nature of field-evolution deviates much from these two equations only when the beam is very near to the individual resonance point (i.e., about $\pm 0.2\pi$ around θ_{rx} and/or $\theta_{ry} = (2m+1)\pi$) of the recycling cavity while the finesse changes quite rapidly. So, we can expect that in a long range of time near the desired operating condition, we can use Eqs.(65) and (66) to describe the evolution of fields without making much error. So, on the basis of our discussion in section 6.1, we can divide the start-up procedure into two steps [26] which can make the job relatively easier to perform.

Step 1 : *Locking first the 3-mirror cavity Y* : In this step, one needs to keep *in-line* arm cavity out-of-resonance and try to bring the system Y near to its double-resonance condition (using an algorithm based on section 5). The locking procedure based on Pound-Drever technique can be started thereafter. While locked, the *perpendicular* arm cavity will have a constant power corresponding to a 2-mirror cavity with input mirror ampli-reflectivity, $r_c = \beta \approx 0.96937\ldots$ for VIRGO. The 3-mir system Y is chosen to be locked in step 1 to take care of the extra 2-degrees of freedom of beam-splitter movement right in the beginning and avoid these in the *relatively tougher* Step 2.

Step 2 : *Locking the in-line 3-mirror cavity X* : Since other 3-mirror cav is already locked, *in-line* cavity now has a level of power always higher than its own antiresonance level. Various peaks will appear in this system from time to time due to the movement of two mirrors of the in-line arm-cavity. One has to try to get to the desired condition again by observing (for example) the successive peaks. The variation of power in **X** cavity will cause the same variation in **Y** arm cavity above the constant level of power it has obtained due to its already-achieved resonance condition. However, this is like varying the input power of the resonant 3-mirror system Y and can not take it out-of-resonance.

The advantages of this procedure can be described as follows: From Eqs.66 and 65, we can see that trying to lock the whole interferometer together is like trying to lock a high finesse 2-mirror cavity with $r_c = \beta + \mathcal{C} = 0.998733\ldots$ (for VIRGO), while keeping control over 4 cavities coupled together. Now step 1 is like locking a 2-mir cav with $r_c = \beta = 0.96937\ldots$ (a lower finesse one), while keeping control over 2 cavities coupled together. Also, step 2 is like locking a 2-mir cav with $r_c = 0.998733\ldots$ but keeping control on only 2 mirrors of the *in-line* arm cavity. Effectively, we can take advantage of the reduced number of degrees of freedom and increased linear region in the Pound-Drever signal in step 1 due to the reduced finesse of the system. In step 2 the linear region get reduced to what the full interferometer originally has, but the task becomes relatively easier because most of the degrees of freedom have already been taken care of in step 1.

Of course, such an advantage can also be obtained in the case of interferometers with arm cavities that may have finesse higher than that of VIRGO: only the values of β and $\mathcal{C}$ will be different.

7 Concluding remarks

A digital filtering approach of simulating a power-recycled interferometer has been developed in this paper and successfully applied to study various dynamical conditions of an interferometer with tolerable error level. Here I write down a number of important conclusions:

7.1 Physical effects

(a) A power recycled interferometer with FP arm cavities can be thought to be a combination of two 3-mirror systems which are coupled to each other through a shared part of their recycling cavities. Field evolution in the arm cavity of any of these dynamical 3-mirror systems can be shown to be equivalent to that in a 2-mirror cavity with changing finesse. An interesting analogy has thus been established between the evolution of field in a dynamical 2-mirror cavity and that of the arm cavity fields in a full interferometer, when the latter are given an analytical representation with state-vectors.

(b) We may give a quantitative representation of the response of a 3-mirror system by the finesse or, equivalently, by the amplitude reflectivity of the input mirror, r_c of an equivalent 2-mirror cavity whose end mirror has a fixed value of high reflectivity. In an interferometer, the r_c of any of the two coupled 3-mirror systems can be divided into two parts : $r_c \approx \beta + \mathcal{C}$ in a long range around the desired operating condition of double resonance. The quantities, β and $\mathcal{C}$ depend on various parameters of the mirrors and depend on time only through the evolution of the phase offsets in the corresponding recycling cavity. The quantity, $\mathcal{C}$ is always very small but is very important in terms of making that little contribution in r_c which might change the response of a 3-mirror system from a lower finesse to a higher finesse one.

(d) In case the two 3-mirror systems are achieving double resonance at well-separated points in time, the evolution of fields in each system is similar to that of an equivalent 2-mirror cavity with $r_c = \beta$ and thus shows a lower finesse behaviour. However, if both the systems achieve their double resonance at the same point of time (which is the desired operating condition for the carrier), the evolution shows a high finesse behaviour corresponding to $r_c = \beta + \mathcal{C}$ in both the cavities.

(e) A 3-mirror system may show peaks under various dynamical conditions of its two constituent cavities. These peaks have been studied in Sec. 5 and a rule has been established. It is shown that such peaks appear whenever the recycling cavity gets resonant; Double resonance condition is just one of the various possibilities that may ensure this. On the other hand, the individual resonance point of the arm cavity may not correspond to a resonance peak for the whole system. Only at the double-resonance condition, both the arm and recycling cavities get to their individual resonant points together.

In a power-recycled interferometer, the evolution of fields due to coupling between a double resonance peak and a wrong peak or between two wrong peaks from the two 3-mirror systems shows a behaviour corresponding to r_c in between $\beta < r_c < \beta + \mathcal{C}$.

(h) Based on the above-mentioned points a proposal for an easy *start-up* procedure for such interferometers have been made in sec. 6. Development of an algorithm for deciding which way to control the mirrors during *start-up* time is now in progress.

(i) Finally, we should note why and how the digital filtering approach has been successful in developing a fast dynamical simulation. It is true that the response of the whole interferometer is highly

nonlinear towards mirror movement especially near the desired operating condition of double resonance. However, if we divide time into small fragments then within such an interval, the response can be well approximated to be linear one, provided we properly take into account *the feedback* in the form of the field at the beginning of the interval. The JAS method of analytical calculation is based on this idea. The Digital filtering approach thus could be applied to the full interferometer by suitably modifying the analytical procedure in various cases, but applying the same idea.

7.2 Computational speed

The simulation programme developed here is quite fast and is applicable to a full length interferometer under general dynamical conditions of its various cavities with tolerable error level.

(a) We may write a code for the whole interferometer with the following considerations : (1) It should work under a general operating condition of the interferometer and not just for the case when it is very near to the locking condition, (2) The operating condition for sidebands can be chosen to be anywhere. (3) Rates of changes in cavity-lengths are of the order of 1 $\mu m/sec$.

Such a code written in C-language using DFA based on JAS and FTF with $N = 50$ runs faster than real time in a DEC ALPHA work-station; The computational time is about 80% of real-time for calculating the dynamical evolution of fields at various locations of the VIRGO interferometer.

(b) The code can be made about 2.5 times faster than this if (1) the operating condition for the sidebands are chosen to be the lowest finesse condition (i.e., resonant in recycling cavities, but anti-resonant in arm cavities) or some other point well inside $\pm 0.2\pi$ around this (most probably this will be the choice for all long-baseline detectors), and (2) we are interested in calculating dynamical field-evolution *only* near the desired operating condition while the Pound-Drever signal can be generated.

In sec. 4 and 6, investigations have been made for a beam near a operating condition of the lowest finesse. Since near such a condition, the field evolution shows a low finesse behaviour, we can write the part of the code for the sidebands by using computationally much inexpensive DFA with perturbative approach (sec.2) rather than DFA with JAS. We just need to apply the equivalent matrix equations corresponding to Eqs.(13) and (18) instead of Eq.(101) in step 5 in section 6.2.3. Although error consideration remains to be same, two-third of the code can be made about 3 times more efficient in such a way, so that the full programme runs at a speed about 2.5 times faster than the general code described in item (a).

(c) While achieving locking, if we are sure that the system will not go very far away from the operating condition, we may switch over to a programme somewhat faster than the codes described above by getting rid of the step of *freezing-the-finesse* in the part of the code for the carrier, since we know that near the double-resonance the finesse of the system for the carrier changes very little and very slowly.

(d) If the speeds of the mirror can be slowed down much, we can go somewhat faster by increasing the length of our *jump* in time, i.e., increasing the value of N to certain extent.

(e) These codes have been studied specifically for the VIRGO interferometer whose arm cavities are of low finesse (≈ 50). It may be noted that there will be very little change in the error consideration and thus the computational speed of the codes, if cavities with higher finesse are

incorporated in the arms. Numerical investigation shows that the method of DFA based on JAS works quite well when applied to interferometers with arm cavities of much higher finesse.

(e) One should, however, note that all these codes do not address the transverse effects on the laser beam. If these higher order effects due to mirror misalignments are also incorporated in such a programme, the codes will be somewhat slower. Works on incorporating higher order effects are going on at present.

7.3 Further works

Works on testing computational speed and error of another method of simulating the full interferometer based on DFA with JAS but summing-up the most significant partial beams [27] coupled between two arm cavities (instead of using algebra of state-vector representation) are currently under progress and will be communicated in future.

It needs to be seen how this method works for other potential optical configurations for interferometric gravitational wave detectors: dual recycled [28], doubly-resonant signal recycled [29], resonant sideband detection [16] etc. However, what may be a really interesting problem is to try this method in Sagnac interferometers [30] incorporating dynamical FP cavities in both arms. The completely different nature of coupling between fields in two arms of such an interferometer may shed newer lights on the dynamical nature of coupled cavities. Thoughts and calculations are currently under progress in these directions.

8 acknowledgements

I am especially thankful to P.Hello and J.-Y. Vinet for the initial motivation they provided me and for many useful discussions and critical comments. It is also my pleasure to thank M. Barsuglia, F. Bondu, A. Brillet, F. Cavalier, R. Chiche, H. Heitmann, F. Lediberder, C.N. Man, M. Pham Tu and E. Tournie for comments and clarifications. This work is supported by C.I.E.S., France.

References

[1] A. Abramovici, W.E. Althouse, R.W.P. Drever, Y. Gürsel, S. Kawamura, F.J. Raab, D. Shoemaker, L. Sievers, R.W. Spero, K.S. Thorne, R.E. Vogt, R. Weiss, S.E. Whitcomb, and M.E. Zucker, Science, **256**, 325 (1992).

[2] A. Brillet, A. Giazotto *et al*, *The VIRGO project* (INFN, 1989); *VIRGO: Final design* (1995).

[3] J. Hough *et al*, *Proposal for a Joint German-British Interferometric Gravitational Wave Detector* (1989).

[4] K. Tsubono, in *Gravitational wave experiments*, proc. of the Edoardo Amaldi Conference (World Sc., 1995).

[5] R.W.P. Drever, in: Gravitational Radiation, ed. N. Deruelle and T. Piran (North-Holland, Amsterdam, 1983);

[6] J. Camp, L. Sievers, R. Bork, J. Heefner, Op. Lett., **20**, 2463 (1995).

[7] B. Bhawal, *Global Control Document: dynamical simulation of cavity using a digital filtering approach*, VIRGO report no. VIR-NTS95-016 (March, 1996).

[8] S. Song, *Recycling and squeezing in high-precision optical measurements*, Ph.D Theses (Univ. of Southern California, 1994).

[9] Harry Y-F. Lam, *Analog and Digital Filters*, (Prentice Hall, NJ, 1979); A. Bateman and W. Yates. *Digital Signal Processing Design*, (Pitman Publishing, London, 1988)

[10] L.B. Jackson, *Digital filters and signal processing*, (Kluwer Academic Pub., Boston, 1996).

[11] I.S. Gradshteyn and I.M. Ryzhik. *Tables of integrals, series and products*, 4th ed., Academic Press, NY, USA (1980).

[12] F. Cavalier, P. Hello, J.-Y. Vinet, *Global Control Document: dynamical simulation of cavities* VIRGO report no. VIR-NTS95-037 (November, 1995).

[13] B. Bhawal, *Global Control Document: Dynamical simulation of 3-mirror coupled cavity using a digital filtering approach*, VIRGO report no. VIR-NTS96-033 (July, 1996)

[14] A.E. Seigmann, *Lasers*, pp524-530 (University Science, Mill Valley, California, 1986).

[15] P.Fritschel, D. Shoemaker and R. Weiss. Ap. Optics, **31**, 1412 (1992).

[16] J. Mizuno, *Comparison of optical configurations for laser-interferometric gravitational-wave detectors*, Ch.4, PhD theses (Max-Planck Institut für Quantenoptik, 1995).

[17] P.K. Fritschel, *Techniques for laser interferometric gravitational wave detectors*, sec.5.2-5.3, PhD theses (MIT, 1992).

[18] M.W. Regehr, *Signal extraction and control for an interferometric gravitational wave detector*, sec.5.4, PhD theses (Caltech, 1995).

[19] D. Redding, *Mathematical Description of the LIGO Single-Mode Acquisition Code*, LIGO internal note no. T-960171-00-D (January, 1996).

[20] F. Marion, in *Minutes of the electronics and software meeting* at Anncey, France, ed. B. Mours, VIRGO report no. VIR-NTS96-037 (June, 1996); B. Bhawal, *ibid.*

[21] B. Bhawal, *Global Control Document: Freezing-the-Finesse - A technique used for fast simulation of 3-mirror coupled cavity*, VIRGO report no. VIR-NOT-LAL-1390-049 (Sept., 1996)

[22] B. Bhawal, *What happens when all mirrors move in a 3-mirror coupled cavity*, VIRGO report no. VIR-NOT-LAL-1390-057 (Oct., 1996).

[23] R. Weiss, Q. Prog. Rep. Res. Lab. Electron. MIT, **105**, 54 (1972); C.N. Man, D. Shoemaker, M. Pham Tu, D. Dewey, Phys. Lett., **A148**, 8 (1990); M.W. Regehr, F.J. Raab, S.E. Whitcomb, Opt. Lett., **20**, 1507 (1995).

[24] R. Flaminio, H. Heitmann, Phys. Lett., **A214**, 112 (1996); H. Heitmann, *Modulation and interferometer geometry*, VIRGO report no. VIR-NTS94-007 (March, 1994).

[25] R.V. Pound, The Rev. of Sc. Instru., **17**, 490 (1946); R.W.P. Drever, J.L. Hall, F.V. Kowalski, J. Hough, G.M. Ford, A.J. Munley, H. Ward, Appl. Phys., **B31**, 97 (1983).

[26] B.Bhawal, in *Minutes of the control workshop* at Rome, Italy, ed. B. Caron, VIRGO report no. VIR-LIS-LAP-1320-058 (Sept., 1996).

[27] B. Bhawal, Appl. Opt., **35**, 1041 (1996).

[28] B.J. Meers, Phys. Rev., D **38**, 2317 (1988); *ibid* Phys. Lett., A **142**, 465 (1989); K.A. Strain and B.J. Meers, Phys. Rev. Lett., **66**, 1391 (1991).

[29] B.J. Meers, R.W.P. Drever, *Doubly-resonant signal recycling for interferometric gravitational-wave detectors* (unpublished, 1991)

[30] K.-X. Sun, M.M. Fejer, E. Gustafson, R.L. Byer, Phys. Rev. Lett., **76**, 3053 (1996).